**ADDIS ABABA UNIVERSITY**

**SCHOOL OF GRADUATE STUDIES**

**DEPARTMENT OF CIVIL AND ENVIRMONATLA ENGINEERIN**

# Structural Deformation Monitoring In Urban Area Using INSAR

**By:**

**Wossila Nassir**

**By the supervision of: Dr Tulu Besha (PhD)**

A THESIS TOPIC SUBMITTED TO THE SCHOOL OF GRADUATE STUDIES OF ADDIS ABABA UNIVERSITY IN PARTIAL FULFILLMENT OF THESIS REQUIREMENTS FOR THE DEGREE OF MASTERS OF SCIENCE IN GEODESY AND GEOMATICS

**June, 2019**

**ADDIS ABABA, ETHIOPIA**

**ADDIS ABABA UNIVERSITY**

**SCHOOL OF GRADUATE STUDIES**

**DEPARTMENT OF CIVIL AND ENVIRMONATLA ENGINEERIN**

# Structural Deformation Monitoring In Urban Area Using INSAR

**By:**

**Wossila Nassir**

**Approved by board of examiners:**

| | | |
|---|---|---|
| _____ | _____ | _____ |
| Advisor | Signature | Date |
| _____ | _____ | _____ |
| Internal Examiner | Signature | Date |
| _____ | _____ | _____ |
| External Examiner | Signature | Date |
| _____ | _____ | _____ |
| Chairman | Signature | Date |

## DECALATION

I hereby declare that the thesis entitled "Structural Deformation Monitoring In Urban Area Using InSAR: A Case of Addis Ababa" has be carried out by me under the supervision of Tulu Besha Bedada (PhD), School of Civil and Environmental Engineering, Addis Ababa Institute of Technology, Addis Ababa University during the year 2016 to 2018 as a part of Master of Science programed in Geodesy and Geomatics. I declare that this work has not been submitted to any other

| _____ | _____ | _____ |
|---|---|---|
| Name | Signature | Date |

Place: Addis Ababa

This thesis has been submitted for examination with my approval as a university advisor

| _____ | _____ | _____ |
|---|---|---|
| Name | Signature | Date |

## CERTIFICATION

This is certified that the dissertation entitled "Structural Deformation Monitoring in Urban Area Using InSAR" is a work carried out by Wossila Nassir under my guidance and supervision. This is the actual work done by Wossila Nassir for the partial fulfillment of the award of the Degree of Master of Science in Geodesy and Geomatics specialized in Geomatics.

**Tulu Besha Bedada (PhD)**

**School of Civil and Environmental Engineering**

**Addis Ababa**

## Acknowledgements

All my praises and worship for the Almighty ALLAH, by his name the knowing everything to give me patience, strength he bestows on me to start and finish this work successfully.

I would like to thank all the people without their support; this task work would not have been successful.

Firstly, I would like to express my deepest gratitude to my parents and my family for their unfailing humor, warm wishes, their endless support and their day to day encouragement during my study without reservation.

I would like to express my heart felt and warmest gratitude to my advisor, Dr. Tulu Besha Bedada for his close guidance, encouragements and comments to improve the quality of my thesis. His scientific ideas and suggestions were a constant source of guidance during my research.

I express my sincere thanks to Ato Daniel Bahiru for his constant encouragement and friendly support that added a new dimension to my knowledge in SAR technology for detecting & delineating ground deformation. His continuous support and assistance have indeed proved to be the guiding force in all my activities. He patiently tolerated my endless questions and always had confidence in me.

I like to thanks Ato Andenet Ashagere for his continuous help and providing materials software and data.

My elder brother Muhaba Hussen the networking department(electrical) in ethio telecom for his kind downloading and providing senteniel data set from 2014-2016.

My friend Mohamed Ahmed from the earth science department of in GIS and Remote sensing in 4 kilo campus for permitting me to use his office internet access and downloading 2 years of sentinel data set from 2017-2018.

Additional thanks go to Daniele Perissin and sarproz team (SARROZ.COM) for providing Sarproz licenses and tutorial manual

Finally I would like to thanks to my best friends specially Alem seid ,Amina Jemal ,Hiwot Alemu Amelework Yemata ,Mohammed Habtamu , Mohammed Tarekegh,Mulualem sheferaw and Sisay Walelegh for their moral and technical support throughout my project work.

## ABSTRACT

In recent years, space-borne InSAR (interferometric synthetic aperture radar) techniques have shown their capabilities to provide precise measurements of Earth surface displacements for monitoring urban infrastructure. The methodology described in this paper aims at detecting ground motions and structural deformations at the whole city and local scale, In this research, present two test sites studies on how space geodetic tools, especially Radar Interferometry (InSAR), can be used to monitor structural deformation. First, investigate the land subside and uplifting extent and severity area of deformation in the city of Addis Ababa using InSAR. Short wavelength C-band data are explored in this study. The integrated use of interferometric synthetic aperture radar technology for monitoring structural deformation offers several perspectives for investigation of new and aging infrastructure around the city. Spanning almost 12 years space born of observation, and the interferograms produced from the raw ENVISAT and SENTENIEL data to perform classical PS-INSAR analysis in corporate measurement those satellite data. and can be detect a long term maximum land subsidence rate of about -36.78mm/yr measuring at PSINSAR , and minimum 3mm of uplifting are detected. The quantitative validation results of the InSAR-derived deformation trend during the five observation periods are stable with the ADIS GPS station data measured from 2014 to 2018. Overall, the adopted methodology can be used successfully for detection, mapping and monitoring of the subsiding areas vulnerable to future collapse. This will facilitate efficient planning and designing of surface infrastructures and other developmental structures in the urban areas and mitigation management of subsidence induced hazards.

# Contents

LIST OF TABLE

## LIST OF FIGURE

## LISTOF ABBREEVATION

| | |
|---|---|
| ALOS | Advanced Land Observation Satellite |
| APS | Atmospheric Phase Screen |
| ASI | Amplitude Stability Index |
| DEM | Digital Elevation Mode |
| ENVISAT | Environmental Satellite |
| ESA | European Space Agency |
| FBD | Fine Beam Double |
| FBS | Fine Beam Single |
| GNSS | Global Navigation Satellite System |
| InSAR | Interferometric Synthetic Aperture Radar |
| LOS | Line of sight |
| MT-InSAR | Multi Temporal InSAR |
| MST | minimum spanning tree |
| PS | Persistent Scatter |
| PSC | Persistent Scatter Candidate |
| PSI | Persistent Scatterer Interferometry |
| PSInSAR | Persistent Scatterer Interferometric Synthetic Aperture Radar |
| RCS | Radar Cross Section |
| SAR | Syntethic Aperture Radar |
| SLC | Single Look Complex |
| SRTM | Shuttle Radar Topography Mission |
| STAR | Star graph |
| TOPS | Terrain Observation with Progressive Scans |
| OLS | Ordinary least square |
| VV | Vertical /Vertical |
| VH | Vertical/ Horizontal |
| HH | Horizontal/Horizontal |

# CHAPTER ONE

# 1. ITNRODUCTON

## 1.1 Background of the study

Urban areas are densely populated areas having complex infrastructure for a well-functioning economic activity. Rapid urbanization coupled with population growth accelerates the development of key socio-economic infrastructure. More specifically; an ever increasing demand for housing and business has resulted in the development of condominium and high rising buildings. Buildings and other key urban infrastructures are sensitive to movements caused by ground deformation (Ciampalini et al., 2014) as a consequence; cities have been suffering different kinds of land subsidence (Perissin D et al., 2009,). Subtle deformation of infrastructures and ground surface can be detected at millimetric level using interferometric synthetic aperture radar technique. Deformation analysis can be used for investigate the stability of slopes, bridges, roads, railways, buildings. The exploitation of subsurface resources (e.g. groundwater, oil and gas, minerals) has resulted in many collapses during the last century that caused a large number of subsidences in various parts of the world (Majumdar 2007). Ground subsidence and deformation of buildings and other urban infrastructures can be monitored by using InSAR technique. With clever processing methods, InSAR can detect and measure subtle vertical displacements (cm to sub-centimeter level) of ground surface, buildings and other key infrastructures (Ferretti et al., 2010) .These techniques are considered to be the most efficient way for measuring spatially-continuous ground deformation with higher precision. The precision and feasibility of InSAR technique is largely controlled by the quality of data pairs, in terms of baseline and wavelength of the Synthetic Aperture Radar (SAR) signal. Most of the monitoring activities are concentrated in urban and downtown areas. This study aims to investigate the capability of remote sensing satellite technologies; specifically InSAR satellite data for use in assess deformation of urban landscape with millimetric accuracy. However, impacts of urban development such as subsidence are rarely studied in this field. Synthetic aperture radar interferometry (InSAR) allows us measuring the terrain movement with radar observations acquired by satellites (Hooper 2009). Permanent Scatters technique (PS-InSAR) was invented and developed at the Politecnico di Milano (POLIMI) in the late 1990s to overcome some uncertainties related InSAR in order to provide reliable and accurate solutions.PS-InSAR exploits long temporal series of acquisitions to identify point-like stable reflectors (PS) instead of extracting information from the whole SAR image. The electromagnetic Stability of PSs allows obtaining an accurate

DEMs and millimetric estimates of terrain motion (Perissin 2010). PS help us to interpret the patterns of deformation of the target area (Perissin. et al., 2011). The association of each coherent pixel to an actual target is achieved by exploiting all the measures with time series of InSAR images. Target motion causes phases that strongly correlated in time exhibiting different degrees of spatial correlation (Ferretti et al., 2001). PSs represent stable artificial targets and are instrumental to investigate spatial and temporal deformation of buildings and infrastructures deformation can be studied on a regular revisiting cycle. Now days in Ethiopia there are great changes due to several building construction works taking place throughout the country mainly in urban areas. Especially in the capital city, Addis Ababa infrastructures are growths rapidly. In Addis Ababa city there are enormous governmental offices, private buildings, roads, railways, airport, and houses. These infrastructures are built from different construction materials, with different quality as well as geographically situated across different geological formation. This study aims to investigate potential site of land subsidence and detect subtle deformation of infrastructures across the whole city of Addis Ababa. The study also investigates landslides across specific landfill sites (named Koshe) that collapsed in 2017.

## 1.2 Statement of the Problem

Excessive withdrawal of groundwater, underground work and massive construction of high-rising buildings can cause ground subsidence as well as cracking and subsidence of infrastructures. Monitoring subsidence of urban landscape in space and time scale is important for protecting human life and properties. The major challenges in infrastructure management are timely detection of problems for applying preventive measures and early analysis. Many studies and experiences of agencies show that there are no deformation monitoring practice that helps to detect early symptoms of problems and treat them with preventive measures. Hence, this potentially reduces expected service year of buildings, results in an unexpected cost as well as endangers human beings. Therefore, there is a growing need for implementing appropriate monitoring tools that facilitate the detection of the problems, and enable detection of slow-moving settlements within the city. Such deformation monitoring techniques and tools will benefit the agencies to manage buildings and other key socio-economic infrastructures. The last pervious major land subsidence in this area happened in 2017 at koshe site about covered 36ha to the western part of Addis Ababa city and consequently the area has never been studied using space geodesy techniques. In spite of a huge damage to the city of Addis the land slide has provided good opportunity for researchers to study the active subsidence area and provide information for the decision makers to prevent human life and un expected coast.

## 1.3 Objective

### 1.3.1 General objectives

To investigate structural deformation on at Bole airport and Koshe site in Addis Ababa by using InSAR technology.

### 1.3.2 Specific objective

The specific objectives of the research are:

1. To monitor and delineate ground subsidence using InSAR technique
2. To detect sub-centimeter deformation of buildings and infrastructures.
3. To evaluate if the processing chain can be applied for an early warning service.

## 1.4 Scope of the study

In the light of the current infrastructure and structural monitoring practices, this study aims to investigate the capability of remote sensing satellite technologies, specifically application of InSAR

satellite data for infrastructure monitoring. The InSAR technique allows us to determine deformation with a millimetric level of accuracy.

Scope of this research is limited to the evaluation of the possibility of using InSAR based systems for infrastructure monitoring in general and include the effectiveness of such systems for detecting different type and severity of structural surface distresses. However, all recent efforts on InSAR-based infrastructure monitoring are briefly included in the literature review section.

## 1.5 Significance of the study

This thesis uses InSAR technology to monitor structural deformation across Addis Ababa city. The scientific contributions of this work can be put in three categories. The first is contribution to structural deformation research in general where we observe, explain, and simulate many ground deformation phenomena to learn about various geophysical processes, some of which have not been observed or realized before. The second is contribution to the ongoing research activity in the study location. And third one is contribution to the methodology on how to use InSAR observations in crustal deformation studies, which are of interest to scientists who use InSAR data to study various geophysical problems. The other major thing regarding subsidence is an issue that involves many policies, complex technical aspects and governance embedment. Thus, early warning system is important for alerting the local authorities, industry, and governmental agencies before major subsidence of the ground surface, buildings and infrastructures take place. There is a need for an integrated approach in order to manage subsidence and to develop appropriate strategies and measures that are effective and efficient in both short and long term. Urban (ground) water and rock management, adaptive flood risk management and related spatial planning strategies are just examples of the options available.

## 1.6 Limitation of the study

For applying InSAR in this study, some limitations were encountered, which are listed as follows:

- ✓ Unavailability of more ALOS PALSAR image data set for all over the study area.
- ✓ Unavailability of both ascending and descending in those data sets, which leads to one dimensional measurement, which gives deformation projected on the satellite LOS direction.
- ✓ More sensitivity to vertical displacement, rather than to horizontal.
- ✓ Sensitivity to phase decorrelation, specifically near and on the rupture, where usually Spatial decorrelation is too much.
- ✓ No unique solution for phase unwrapping (different algorithms with different initial Values, give different results)

## 1.7 Structure of Thesis

This thesis is divided into 6 chapters. Chapter two is an extensive review of literature pertaining to the need for ground surface deformation measurement and the available ground surface and monitoring structural techniques, includes a few major applications of SAR Interferometer to monitor different natural disasters and measure displacement, as well as past results using the similar techniques and methods for different periods. Chapter three It is a description of the introduction of the study area; this research presents some information about the background, the geology and the geography of the study area for in the city of Addis Ababa Ethiopia. Chapter four It presents the research design and methodology. It is focusing on data acquisition Processing and presentation, the details about the amount, type and basic information about the satellite data that were used. Additionally, it describes the general idea of SAR Interferometry and how it is applied as well as the methodology on which the processing was based on. Chapter five it presents interferometric SAR processing results with their geological interpretation, and points out two test site areas. The results produced by the processing of the data in the form of maps and time series graphs. Also, it includes the comparison of InSAR results with GPS measurements. Chapter 6 presents extracted conclusions and recommendation made to develop the key points and the outcomes of the project.

# CHAPTER TWO

## 2. LITERATURE REVIEW

This chapter outlines of the importance of mapping surface deformation for better understanding of the subsurface structural behavior. This is followed by a discussion of the methods for monitoring of surface deformation, particularly the methods focused on using observations from microwave SAR remote sensing data.

## 2.1 Background

The configuration of the Earth's surface reflects to some degree virtually all of the processes that take place at or close to the surface as well as those that occur deep in the crust, and that governing the external shape of that changes due to subsidence and uplifting. Surface deformation depends on the nature of local geology, soil property and thickness. Extent of ground deformation is dependent on the depth and thickness of the layer that experienced depression, and the properties of the overlying formations (Nelson S 2015).Surface deformation can be measured by using several geodetic techniques such as leveling and InSAR. InSAR is the most efficient method for monitoring ground deformation with the required spatial and temporal completeness; providing consistent deformation map of the Earth's surface with sub-centimeter accuracy (IESC, 2014). It is also cost effective technique. Collecting optical and microwave satellite images to observe, analyze, and assess natural resources globally has been done for more than two decades. Compared to optical satellites, microwave satellites do not rely on sunlight to collect the images. Moreover, they use a specific portion of the electromagnetic spectrum that can penetrate thick clouds, fog and dust during any weather conditions due to lower levels of atmospheric attenuation. Synthetic Aperture Radar (SAR) is one of the microwave remote sensing tools used widely for measuring regional-scale land subsidence, SAR in general and interferometric SAR in particular have been used to quantify the surface response to ground deformation in different locations. Land surface deformation in order to mitigate or prevent the associated risk is one objective of using the surface deformation observations. High-resolution mapping of spatio-temporal deformation fields can provide important information about source geometries and associated physical processes (Anderssohn et al., 2009). This is followed by a review of different Surface deformation monitoring techniques. These include the space-borne SAR remote sensing capabilities and the InSAR processing techniques.

## 2.2 Surface Deformation

Active underground mining and subsurface coal fire are the main causes of land subsidence. Additionally, subsidence can occur at any time over old mine workings, regardless how long it has been deserted due to the existence of voids and weak supporting pillars (Lokhande, et al., 2009). Surface deformation can be caused by a natural or anthropogenic source, and occur over a wide range of temporal scales, from almost instantaneous settlement (i.e. earthquake, volcanic, and glacier movement) to a gradual gentle displacement resource extraction It can be induced from mining, ground water and oil and gas extraction. Moreover, it can be localized or large-scale. These can cause a great deal of serious environmental hazards, such as collapse of infrastructures, damage of bridges and changes of river and groundwater flow path. These hazards not only threaten individuals' everyday lives and properties, but also lead to massive impacts on the national economy. The most immediate impact of local surface deformation may involve crucial surface infrastructure and their sustainable development (Bakon et al., 2014; Hooper et al., 2004; Normand and Heggy, 2015; Poland and Davis, 1969). However, regional ground settlement contributes to an increased risk of flooding in coastal areas; seawater intrusion; changes in groundwater systems or regional faults reactivation (Nagel, 2001; Zektser et al., 2005). Therefore, measuring and monitoring ground surface deformation is crucial for current and future planning of developments. Various techniques are used to assess and predict the surface deformation, its magnitude, direction, and causes (Galloway and Burbey, 2011). Mapping relative changes in the elevation or inclination of the ground surface are usually conducted through either ground-based or remotely-sensed geodetic surveys such as tilt meter, GPS, levelling, InSAR and LIDAR (Densmore et al., 2010; King et al., 2007; Leva et al., 2003; Massonnet and Feigl, 1998).

## 2.3 Causes of land subsidence and surface deformation

Active ground water extraction, underground mining and subsurface coal fire are the main causes of land subsidence. Additionally, load of buildings and structures is also considered to be one of the causes of land subsidence but also it can occur at any time over active volcanic areas and extraction of natural gas (Donaldson and Chilingarian, 1997).

In mining several types of sub surface mining and specific methods which intentionally cause the extracted void to collapse such as pillar extraction, long wall mining and any metalliferous mining method will result in surface subsidence. Surface compressive and tensile strains, curvature, tilts and horizontal displacement those are the cause of the worst damage to the natural environment, buildings and infrastructure. The other cause is Extraction of natural gas if natural

gas is extracted from a natural gas field the initial pressure (up to 60 MPa (600 bar)) in the field will drop over the years. Subsidence due to fluid withdrawal occurs when: (1) reservoir fluid pressures are lowered, (2) reservoir rocks are compactable and/or are unable to effectively resist deformation upon the transfer of load from the fluid phase to the grain-to-grain contacts, and (3) the overburden lacks internal self-support and the formations can easily deform downward (Donaldson and Chilingarian, 1997). Also an Earth quake Land subsidence can occur in various ways during an earthquake. Large areas of land can subside drastically during an earthquake because of balance along fault lines. Land subsidence can also occur as a result of settling and compacting of unconsolidated sediment from the shaking of an earthquake. The Geospatial Information Authority of Japan reported immediate subsidence caused by the 2011 Tohoku earthquake. In Northern Japan, subsidence of 0.50 m (1.64 ft.) was observed on the coast of the pacific Ocean in Miyako, Tohoku while Rikuzentakata, Iwate measured 0.84 m (2.75 ft.). In the south at Soma, Fukushima, 0.29 m (0.95 ft.) was observed. The maximum amount of subsidence was 1.2 m (3.93 ft.), coupled with horizontal diastrophism of up to 5.3 m (17.3 ft.) on the Oshika Peninsula in Miyagi Prefecture. Ground water exploitation is one of the major causes of land subsidence in many coastal cities, such as in Jakarta, Bangkok and Shanghai, (Yusupujiang Aimaiti, Fumio Yamazaki Wen Liu2018).Groundwater-related subsidence is the subsidence (or the sinking) of land resulting from groundwater extraction. The habitation of lowlands, such as coastal or delta plains, requires drainage. The resulting aeration of the soil leads to the oxidation of its organic components, such as peat, and this decomposition process may cause significant land subsidence. Many soils contain significant proportions of clay. If building foundations are above the level reached by seasonal drying, they move, possibly resulting in damage to the building in the form of tapering cracks.

## 2.4 Monitoring surface deformation

Ground surface deformation refers to any change in shape, dimension and position of a deformable body, and might include natural or man-made features. Moreover, these ground movements could be the result of natural processes or anthropogenic activities and measuring them is crucial for safety assessments and future disaster prevention. Either shallow impacts such as swelling and shrinkage of clay soils or landslides, or deeper features such as earthquakes, fluid abstraction, and mining operations or can be the cause of ground surface deformation (Duncan et al., 2010). In situ geodetic measurements such as leveling, or remote surveys (e.g. digital photogrammetry and remote sensing techniques) are two types of monitoring techniques that can be used for the establishment of a ground control network and the measurement of deformation in different epochs that cover the

desired time span are required for monitoring the ground behavior and for determining the vertical displacement using in situ techniques. Combining both geodetic and geotechnical observations could also be used to obtain a detailed pattern of the ground displacement (Telioni, 2006).

### 2.4.1 In situ Monitoring

Conventionally, mapping of earth surface deformation can be achieved by using field-survey techniques, such as Global Positioning Systems (static and real-time kinematic GPS), total stations and digital levels. However, these methods have their limitations. They could be labor-intensive and time-consuming once the measurement regions become large. Soil under expansion or compression can cause significant economic damage. Using traditional laboratory testing is difficult to accurately measure the in situ behavior of a clay deposit, because it will depend on both environmental factors such as hydrological cycle, and the soil properties(Zheyuan Du) .In addition, these point wise historical measurements show limited spatial coverage (Lu and Likos, 2004, Garner and Coffman, 2014). Multiple types of static deformation monitoring for the surface such as tilt meter, optical leveling and differential GPS (or GNSS), ground-based radar interferometry and LIDAR, or combinations of these four can be used to define the dislocation vectors. Tilt meters provide continuous and precise local mapping of deformation gradients with two vertical derivatives, but long-term drift and its installation (i.e. at least 3-4m below the surface) significantly impact on its set-up0 and operationa0l costs. GPS stations can measure ground motion in three dimensions with relatively low accuracy in the vertical direction.

Comparable to tilt meters, a large network of GPS receiver stations can cover the entire monitoring area providing point measurements, but this would be an extremely expensive solution for obtaining accurate displacement observations. Contrary to GPS, optical leveling provides high vertical accuracy for surface deformation of a set of distributed benchmarks. In leveling, the measurement accuracy relies on the height differences between each observation point and the reference point that can be affected by temperature variation over long time periods (Ferretti, 2014).

### 2.4.2 Remote Sensing Monitoring

Frequent and large-scale observations of surface deformation with centimetre-scale vertical accuracy have been achieved using air-borne or space-borne interferometric SAR to retrieve valuable information about the ground surface behavior and its long-term analysis (Amelung et al., 1999; Baer et al., 2002; Carnec and Delacourt, 2000; Cigna et al., 2012; Galloway et al., 1998; Liu, 2012; Wright and Stow, 1999). Having access to adequate SAR dataset acquisitions, processing, and analysis for surface deformation consists of two complementary stages which will also reduce

the time and cost of analysis: stage one is low-cost screening over large areas with high spatial extent but low spatial resolution SAR images such as C-band to detect unknown deformation spots. Following this primary observation, the next stage is a more localized interferometric analysis by using a higher resolution SAR dataset such as X-band (Crosetto et al., 2005). Moving from low spatial resolution C-band towards high spatial resolution X-band, L-band SAR satellite offers a medium resolution with greater penetration in vegetation. Accordingly, using a two-stage screening strategy is common for interferometric monitoring of areas for different application purposes or challenging surface conditions, such as densely vegetated areas or non-urban and mountainous regions. Implementing advanced processing algorithms provides more reliable results because of their reduced sensitivity to foliage (Colesanti et al., 2005; Perski et al., 2009). Recent investigations by NASA's airborne interferometric SAR (UAVSAR) team also raised the possibility that InSAR could provide a way to predict the location of sinkholes by detecting horizontal surface deformation as an early-warning signature (Buis and Harrington, 2014).

### 2.4.2.1 SAR for Surface Deformation

Space-borne imaging Synthetic Aperture Radar (SAR) systems are active sensors operating at microwave wavelengths, which can monitor the surface under any weather conditions with no need for solar illumination. They can measure amplitude and phase simultaneously, from which phase values are related to the sensor-target distance. SAR images over topographically rough terrains are distorted by atmospheric artefacts or geometric effects; the latter can be improved by looking at the same location from different acquisition geometries. The following section presents the fundamental concepts of SAR as an imaging tool, and interferometric SAR as a technology to extract ground surface deformation rate from SAR images.

#### 2.4.2.1.1 Principles of SAR and Interferometric SAR

SAR is a specific form of imaging radar that measures the return of an actively emitted microwave signal from a target. Due to the nature of microwave energy as an illuminating source in radar sensors, this imaging technology does not rely on solar irradiation, making it more versatile than traditional passive optical and spectral sensor technologies. The radar signals are unaffected by darkness or by clouds in terms of visibility of the land surface, and are therefore capable of obtaining information largely irrespective of the surface and atmospheric conditions. Imaging radar sensors emit signals over a specific portion of the electromagnetic spectrum that is generally based on their mission purposes. They operate in different microwave frequencies and wavelengths including X-band (9.6GHz, ~ 3cm), C-band (5.3GHz, ~5.6cm), L-band (1.3GHz, 23.6cm), and P-

band (0. 4GHz, 74cm) with typically higher spatial resolution in X-band and greater penetration power in P-band (Ferretti et al., 2011a). Accordingly, X-band operating systems are suitable for surveillance purposes while P-band is the preferred choice for biomass mapping and hydrological monitoring due to its potential to recover the forest height and its resistance to temporal de correlation (Le Toan et al., 2011; Neeff et al., 2005). SAR can generate an electromagnetic field with a fixed phase relationship between the electric field values at different locations and at different times. It also has the potential to record amplitude and phase information simultaneously for a ground target (Ferretti, 2014). The on-board integration of backscattered signals is represented by a matrix of complex numbers containing both the amplitude and phase information of ground scattering elements illuminated by the radar pulse. While the amplitude data depends on the amount of returned energy from each resolution cell or image pixel, the phase information depends on the distance between the phase centres of the radar antenna to the terrestrial target. SAR data can be recorded in different polarizations (i.e. temporal variation or oscillation) of the electric field associated with each radar pulse in a specific plane. The polarization can be in linear-single or dual-pol modes, or more sophisticated full-polarimetric modes. While single polarization SAR transmits and receives polarized radiation vertically (VV) or horizontally (HH), the dual polarization is designed to generate two linear polarization combinations (HH, HV) or (VH, VV). Recently available full-polarization systems have been designed to transmit two orthogonal polarizations and record both received polarizations (HH, HV, VH, and VV) (Cloude, 2009; Van Zyl and Kim, 2010). In comparison with classical single or dual polarization, SAR systems that are equipped with full-polarization can provide a complete scattering matrix to extract substantial information from the image and to separate surface scattering from dihedral scattering in more vegetated areas (Shirvany, 2012).The coordinates of each pixel in a SAR image according to range and azimuth directions are related to the acquisition geometry. While range direction is orthogonal to the moving platform path, azimuth direction refers to the path. The inclination of the radar antenna with respect to the nadir is called off-nadir or look-angle ($\theta$) which is never zero but ranges from about 20 to 50 degrees. The ability of SAR systems to change the off-nadir angle is important for their adjustment to mountainous terrain, which is a potential barrier to InSAR. The direction along the sensor Line of Sight (LOS) is usually called slant-range direction and SAR acquisitions are collected in this direction (Ferretti, 2014). Over rough topography, SAR images can be geometrically distorted due to three types of effects: foreshortening, layover and shadow effects. Slopes facing the sensor are affected by foreshortening and layover. In foreshortening, a radar beam reaches the base of a tall feature before it reaches the top, while for the layover case a radar beam touches the top of feature

before its base. When a radar beam is not able to illuminate the ground surface, the image is distorted by the so-called shadow effect and spatial sampling is shrunk to a few meters (Lillesand et al., 2008). This normally occurs behind vertical features or steep slopes. In SAR imagery brighter pixels represent stronger backscatter with high amplitude values, whereas the phase value for each pixel is related to the sensor-target distance and the signal-target interaction. Conversely, variations in imaging conditions such as acquisition geometry, surface roughness and orientation, dielectric constant (in particular moisture content), wavelength and polarization can affect the visibility of the ground scattered by changing its Radar Cross Section (RCS) values and backscatter coefficient (Ferretti, 2014). The near-polar orbit of SAR satellites - in combination with the Earth's east-west rotation -theoretically allows observing the same area from two different looking angles on satellite orbits i.e. ascending (S-N) and descending (N-S), or left and right-looking geometries with different incidence angles. This observation is conducted based on the orbiting schedule of each individual satellite, which varies from 46 days down to 11 days. Combining these observations not only mitigates the problems due to the acquisition geometry and the uneven sampling on hilly terrain areas, but can also distinguish between vertical and east-west motions (Ferretti et al., 2007). In other words, the use of data acquired by satellites in both ascending and descending orbits makes it possible to compute the true vertical movement and the east-west component of horizontal movement. Since phase varies in SAR image acquisitions over the same area at different times, this can be used to retrieve ground motion over large remote regions with little or no regular access for ground-based observations (Bürgmann et al., 2000). For this purpose, InSAR, as one of the major applications of SAR imagery, is based on the superposition of two images to generate a new image which shows topography and changes in ground levels with precision to the millimetre, as well as random orbital error, and weather and background noise interferences (Duro et al., 2013; Massonnet and Feigl, 1998).

#### 2.4.2.1.2 PS (Persistent Scatterers)

PS technique is very useful and suitable for analysis of urban areas, where it is producing angular structures and efficient reflectors that dominate background scattering. Persistent Scatterer Interferometry (PSI) technique was developed by Ferretti in 1999. PSI approach helps us to measure deformation with uncertainties of one millimeter per year, interpreting time-series of interferometric phases at coherent point scattered (Ruiz, et al., 2008). The PS method uses large stacks of images to generate differential interferograms with respect to one common master. The PSI approach relies on identifying pixels whose scattering properties vary little with time and look

angle (Ferretti, et al., 1999, 2000, 2001). Pixels that are dominated by a singular scattered best meet these criteria; therefore images are processed at full resolution to increase the chance of being only one dominant scattered present, and also to reduce the contribution from other scattered within each pixel (Ruiz, et al., 2008). The electromagnetic stability of PSs allows obtaining around 1-m accuracy DEMs (Perissin2008) and millimetric estimates of terrain motion (Ferretti 2007) recently, by considering different interferometric combinations, the Quasi-PS (QPS) technique was presented (Perissin 2008) to extract information also from distributed and decorrelating targets. Since a good knowledge of the PS physical nature is a key step for the correct interpretation of the measured deformation mechanism, the physical nature of the targets has been investigated in (D. Perissin and F. Rocca, 2006). The association of each coherent pixel to an actual target is achieved by exploiting all the measures with time series of InSAR images. Since PSs are the stable artificial targets, which can be usually found in urban areas, their lifetime and density can be used to describe the urban development with spatial and temporal context. With a regular revisiting cycle, the benefits that can be gained from time series of InSAR images are in two aspects: 1) since the PS is related to artificial targets, different PS birth time that represents the urban growth can be obtained with the ground displacement and 2) each PS can be related to the physical characteristics of the single target.In images where most pixels contain multiple scattered of similar strength, PS approach is less optimal because scattering characteristics of these pixels vary substantially with look angle. Although PS-InSAR deformation measurements may be very precise, but the limitation is that it does not necessarily imply a reliable estimation of the parameters of interest. PS-InSAR deformation measurements may be caused by different types of deformation such as gas extraction, shallow compaction or structural instabilities making unambiguous interpretation very difficult (Ferretti, et al., 2001).

# 3. CHAPTER THREE

## 3. Description of the study area

### 3.1 Location and Climate

Geographically, Addis Ababa is the capital of city of Ethiopia covers an area from at 9°01′29″ N between 38°44′48″ E, The landform of Addis Ababa city corresponds to hilly at the north and flat terrain at the south of the city. This region is located in the plateau of mountain ranges at a height of 2405 m = 7890 ft. above mean sea level. Its topography ranges from rolling to hilly area relatively steep gradients and numerous rivers stream valleys. Addis Ababa has a subtropical highland climate (Köppen: Cwb). The city has a complex mix of highland climate zones, with temperature differences of up to 10 °C (18 °F), depending on elevation and prevailing wind patterns. The high elevation moderates temperatures year-round, and the city's position near the equator means that temperatures are very constant from month to month. Mid-November to January is a season for occasional rain. The highland climate regions are characterized by dry winters, and this is the dry season in Addis Ababa. During this season the daily maximum temperatures are usually not more than 23 °C (73 °F), and the night-time minimum temperatures can drop to freezing. The short rainy season is from February to May. During this period, the difference between the daytime maximum temperatures and the night-time minimum temperatures is not as great as during other times of the year, with minimum temperatures in the range of 10–15 °C (50–59 °F). At this time of the year, the city experiences warm temperatures and a pleasant rainfall. The long wet season is from June to mid-September; it is the major winter season of the country. This period coincides with summer, but the temperatures are much lower than at other times of year because of the frequent rain and hail and the abundance of cloud cover and fewer hours of sunshine. The city is located in the central part the country and its well developing city compare to other city. So people move from different part of the country to Addis Ababa for it is suitable for job opportunity and life status to live in. The land area of Addis Ababa city is over 540 Sq.kms and divided with 10 sub-cities for administrative purpose. The city has experienced spatial spread mostly towards the southern, eastern and south western of the main city. The spatial spread is mainly guided by topography construction investment and road development. After the construction of the ring road and condominium site are built up new settlements were observe in the city. And the recorded population is from the end of 2007 is with a total population of 3,384,569 according to the 2007 census. However, it is believed that this number was inaccurate when recorded and underestimated the city’s population. The city has through recent years seen a strong annual growth rate, and population counts as of 2017 are

growing closer to 6.6 Million (population 2018). Now days the city is the largest populated area in Ethiopia. See Figure (1)

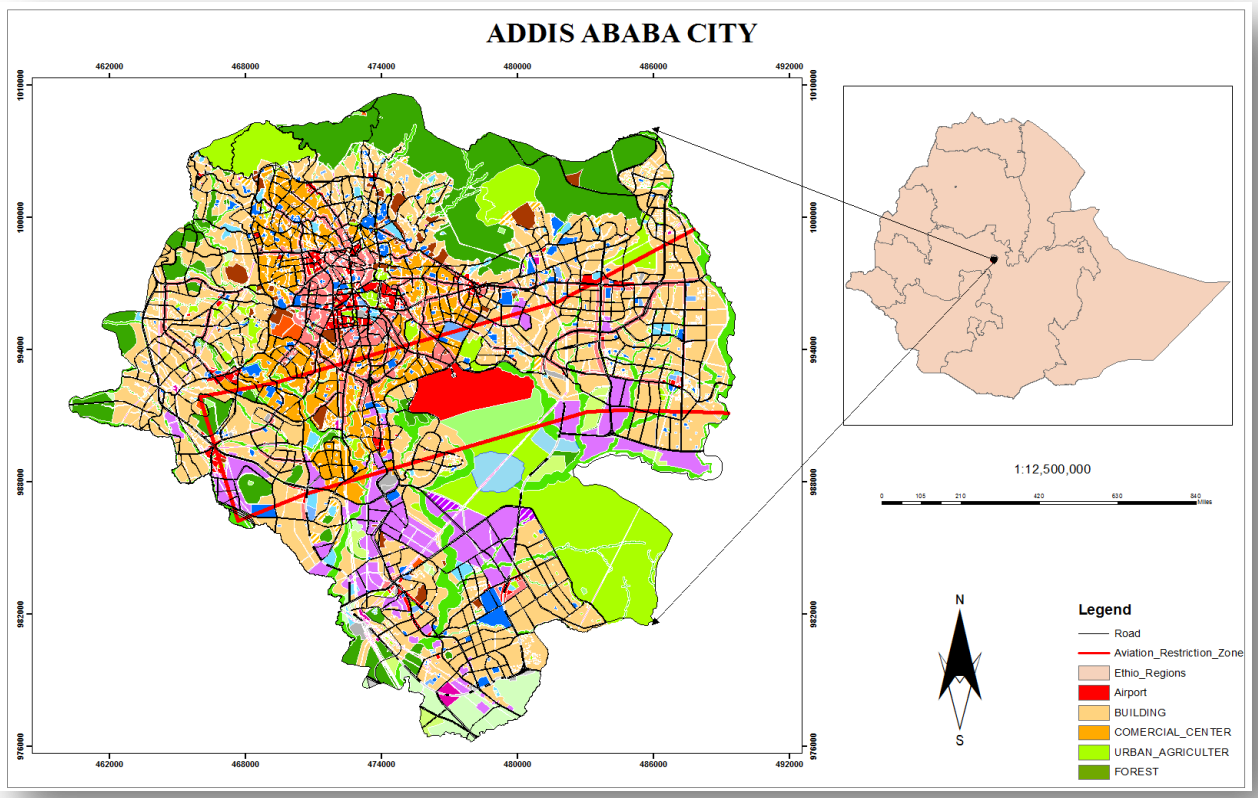


Fig 3.1.STUDY AREA OF ADDIS ABABA LAND USE

## 3.2 GEOLOGICAL BACKGROUND

In the city of Addis Ababa Many researchers systematically proposed the geology and volcanic stratigraphic sequences of area. Proposed the stratigraphy of the area starting from Sululta to Nazareth, based on Morton's geological map, unpublished student reports (Haileselassie Girmay and Getaneh Assefa 1989), they redefine the lithostratigraphic units and modified the existing stratigraphic sequence. The suggested Miocene-Pleistocene volcanic succession in the Addis Ababa area from bottom to top are: Alaji basalts, Entoto silicics, Addis Ababa basalts, Nazareth group, and Bofa basalts (Tamiru et al., 2005). The Alaji group volcanic rocks (Alaji rhyolite and Basalt) in this part of the escarpment were outpoured from the end of Oligocene until middle Miocene (Zanettin et al., 1974 in Tamiru et al., 2005). This unit is composed of basalts, which show variation in texture from highly pophyric to aphyric. Within this unit there is an intercalation of gray and glassy welded tuff. The researchers (Haileselassie Girmay and Getaneh Assefa, 1989), discussed that The outcrop of Alaji basalt extends from the crest of Entoto (ridge bordering the northern parts of Addis Ababa)

towards the north. The other one is the ENTOTO SILICICS These early Miocene age silicic volcanics could represent localized terminal episodes to massive Oligocene fissure-basalt activity in the Addis Ababa region (Morton et.al. 1979 in Tamiru et al., 2005). The thickness of the flow become maximum on the top of Entoto ridge and thin both towards the plateau and the plain east of Addis Ababa. This basalt covers the southern part of the town, especially the areas of Bole International Airport and Lideta Airfield. The rock body shows vertical curved columnar jointing together with sub-horizontal sheet jointing. The age of the basalt in Addis Ababa ranges from 3.4 to 3.6 million years (Morton, 1974). Young Trachyitic Flow This rock is predominating in the southwest part of the town, from Dama hotel towards Furi and Repi along the hills and foothills of Hana Mariama and Tulu Iyou. It is porphyritic with phenocrysts of plagioclase (albite-oligoclase) sandine, biotite within a groundmass of microlities of feldspar. Moreover, it is underlain by the tuff that covers the young ignimbrite and overlaying by alternating flows of plagioclase porphyritic basalt and rhyolite especially in the Repi hill.

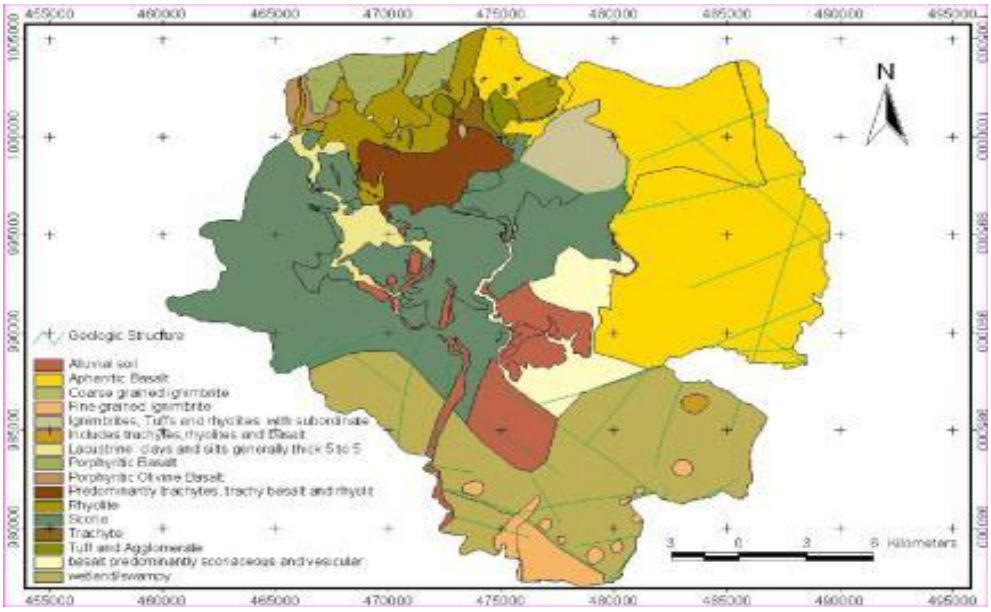


Fig 3.2 Geological map of the study area (Source: Tamiru et al., 2005)

## 3.3 ECONOMY

Addis Ababa is the economic center of Ethiopia. Addis Ababa's economy is growing annually by 14%. The city alone currently contributes approximately 50% towards the national GDP, highlighting its strategic role within the overall economic development of the country(Resilient city program).Thus, thousands of construction projects are currently underway or in the planning stages. Recognizing the strategic importance of Addis Ababa, the government is taking steps to address important urban issues such as improved land-use and transportation planning, the development of

low income housing, expansion of wastewater collection and treatment facilities, efficiency enhancements to the water supply system, and establishment of an urban safety net(Resilient city program).

## 3.4 URBAN PLANNING AND DEVELOPMENT

Addis Ababa is urbanizing at an exponential rate and it is transform into a megacity of almost 10million people by 2037(World Bank 2015). Recent growth has been sprawling low density with the rate of spatial expansion out spacing the rate of population growth. This has implication for the cost of infrastructure and service delivery, traffic congestion, land management, social inclusion and over all liability. Addis Ababa city governance institutional capacity and resource are also being stretched thin by the pressure of rapid urban growth and the city is struggling to provide basic service all the residence. At the same time the city core has extremely high density from around 15,000-30,000 people per Km concentrating around 30% of the population on 8% of the land in Addis Ababa generally with poor living condition .this high density of population ,poor quality of construction material and inaccessibility of emergency service contribute to urban fire vulnerability.

## 3.5 DISASTER RISK MANAGEMENT AND CLIMATE CHANGE ADAPTATION

The climate of Addis Ababa is forecasted to have an increase in precipitation variability and temperature. This will likely induce a wide range of hazards in the city including flooding and landslides in addition to drought and fire which have been the most common hazards in rural and urban areas. The geographic location and topographic features of Addis Ababa compounded by the existing state of the drainage system, road network and sewerage system expose the city to street and river rain flooding as well as landslides. However the degree of sensitivity to anticipated climate change varies from community to community within the city due to variation in topography, poverty level access to basic services, quality of housing and settlement patterns. Landslides are become a major threat in some parts of the city due to frequent digging to the construction explosion. Addis Ababa is only 75-100 Km away from the western edge of the main Ethiopian rift valley which is hotbed of earthquake and active volcanoes. According to a risk assessment project focusing on seismic activities in urban areas including Addis Ababa the city could be severely impacted by earthquakes. If an earthquake was to occur at about 27Km away from the city (at similar magnitude of historic earthquake events in 20$^{th}$ century), it was estimated that 15% of buildings could suffer collapse as well as a high number of fatalities (UNISDR, 1999).[1]

[1] UNISDR,:https://gprs.unops.org/pages/viewvacancy/VADetails.aspx?id=6060

# CHAPTER FOUR

# 4. Data source and research methods

## 4.1 Radar image data sets for interferometry

The area of interest to investigate the application of InSAR method for detection of deformation phenomena is located in city Addis Ababa covers an area of 540 km2.Most of the area is without vegetation and covered with man-made structures, except the south-west region where the little expansion begins in the city territory. SAR images including ENVISAT, and SENTENIEL has been provided by ESA as a data set package .This data set is composed of SAR Level 0 as well as SLC products but in the case of our study uses the SLC data set formats and is available from ESA virtual archive website[2].

### 4.1.1 ENVISAT

The dataset analyzed in this work consists of 22 SLC image with acquisition date 14-Jan-2009 is selected as the master image of Envisat (Image Mode, I2 incidence angle, VV polarization) the time between 2003-2010 along descending orbit and track No.321 of Envisat. The Envisat satellite was launched into orbit by European Space Agency on 1$^{st}$ of March, 2002 as the largest civilian Earth observation spacecraft ever built. Equipped with advanced C-band synthetic aperture radar (ASAR), Envisat provides continuity to the observations started with ERS satellites. In Image Mode, the ASAR generates high spatial resolution products of approximately ~ 30 m and 100 km swath coverage. Envisat is in a 98.54$^0$ sun-synchronous polar orbit at 800 km altitude, with a 35-day repeat cycle data set.

### 4.1.2 SENTENIEL_1A

Sentinel-1A data are provided via the online Sentinel-1A Scientific Data Hub in Alaska Satellite Facility center in Interferometric Wide-swath (IW) focused Single Look Complex (SLC) format. Each SLC is split into three sub-swaths that are subsequently subdivided into ~ 10 bursts. In total, the IW SLCs are ~ 150 km in the along-track direction and ~ 250 km across-track, with a spatial resolution (pixel size) of ~ 14 m. We use swath1 and 2, which covers the Addis Ababa area. The dataset analyzed in this work consists of 180 SLC images acquired by sentinel (Image Mode, IWS incidence angle, VV polarization and VH polarization), the time between 2014-2018 along an ascending and descending orbit and track No. 229.

[2] http://earth.esa.int/services/auxiliary_data/asar/

Table 4.1 Characteristics of Sentinel 1A. Information retrieved from (Sentinel-1Team, 2013)

| Characteristics | Description |
|---|---|
| Launch | Sentinel 1A 2014 |
| Orbit | Near-polar, sun-synchronous |
| Orbital Hight | 693 km |
| Repeat period | 12 days repeat cycle (1 satellite); 6 days when both satellites (A and B) operating |
| Spatial resolution | (5-20) x (5-40) m (depends on acquisition mode) |
| Flight Attitude | Right looking |
| Incident Angel | 20° - 46° (depends on acquisition mode) |
| Polarization | Single and dual polarization (depends on acquisition mode) |
| Frequency | 5.405 GHz (C band) |

Table 4.2 Acquisition modes of Sentinel 1(Sentinel-1Team, 2013)

| Mode | Wave mode(WM) | Strip map (SM) | Interferometric Wide Swath (IW) | Extra Wide Swath(EW) |
|---|---|---|---|---|
| Swath(KmxKm) | 20 | 80 | 250 | 400 |
| Geometric Resolution(range X azimuth) | 5X5 | 5X5 | 5X20 | 20X40 |
| Polarization | single | Double | double | double |

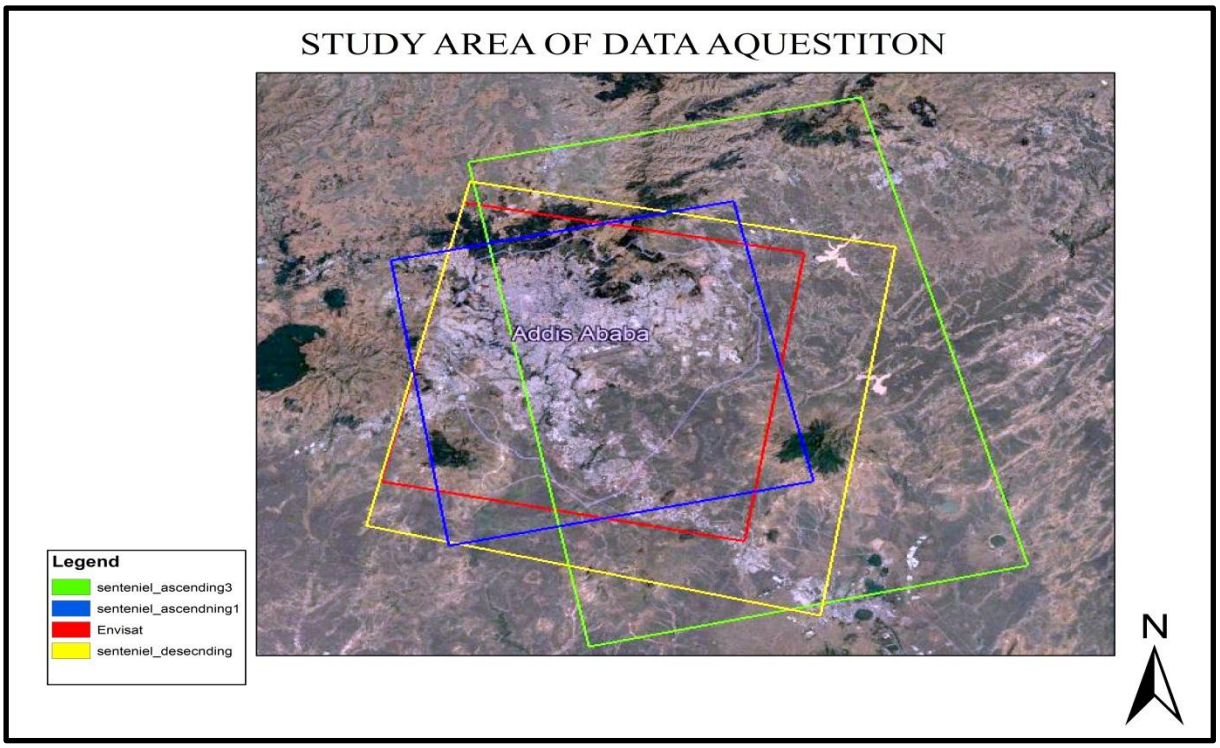


Fig 4.1 Study area data set acquisition on google earth

## 4.2 Auxiliary data sets

### 4.2.1 DEM

Topographic phase signature is removed from interferograms using a precise DEM of the study Area (Hooper et al., 2004). Such a DEM can be either generated indirectly by three pass interferometry (e.g. Graham, 1974; Massonnet and Feigl, 1998) or obtained from other sources or methods such as photogrammetry. Before June 29, 2009, a DEM generated by Shuttle Radar Topography Mission (SRTM) was the most complete and homogeneous available DEM with highest resolution for the whole globe (Farr et al., 2007). SRTM DEM is available in one arc sec (about 30 m spatial resolution) for United States and its territory and three arc sec (about 90 m and also one kilometer spatial resolution) globally.

### 4.2.2 Orbital parameter

Orbital parameters of SAR satellites for repeat pass interferometry or so called orbit files are provided by relevant agencies or universities in preliminary precise processing and accuracy levels. For ENVISAT satellite, there are two sources of obtaining orbit files: Department of Earth Observation and Space Systems (DEOS) of Delft University of Technology and ESA. Both of these institutes are providing preliminary and precise orbit files, but in different formats. In this research, precise orbit files produced by ESA using Doppler Orbitography and Radio positioning Integrated by Satellite (DORIS) method are used to remove orbital phase signature from interferograms. For

ALOS satellite, precise orbits are delivered with the leader file of L1.0 products, as 28 state vectors with accuracy of better than one meter, and they are available three days after data acquisition (Sandwell and Wei, 2006).

## 4.3 Material and software used

By reviewing the characteristics and requirements of the interferometric processing techniques and the satellite observations in the previous section while two methods are used in this study, for two same satellite data acquisitions in both C-band microwaves. Details of each processing technique are described in the following sections. The Processing involves in sarproz software solutions for obtaining single interferograms and performing PS method. PS derived time series of deformations were compared to ADIS GPS data. The GNSS data includes time series from at one stations ADIS, which is located at Addis Ababa 4 kilo university that is registered by unavco. Then result is shown on google earth that the sarproze software geocode the intefrogram and PS map. The validation analyses were done by Mathcad and top cat software to find correlation coefficient and RMSE. Finally we used ArcGis and smart GIS software to integrate the result and display a better visualization.

## 4.4 Method and Stack Formation

The first step of the processing is to import the raw Envisat and Sentinel-1A data. An extra step which is not always necessary (depending on the SAR satellite) is the correction of the orbit data which include the instant position and velocity of the satellite. The next step of the processing is to import a Digital Elevation Model (DEM). It is worth mentioning that the DEM is a very important part of the processing chain because it is used in the crucial step of co-registration as well as in the interferogram generation step. The processing strategy of the co-registration of a pair of S1 TOPS SLC is crucial (Prats Iraola et al. 2015) since interferometry with Sentinel 1 SLC data requires a high quality and precise co-registration of the SLC pairs. In order to achieve very high coregistration accuracy, the method that is used in sarprozz software, the selected image (master) which was used as basis to coregister the rest of images is slave image in the ascending and the descending datasets, respectively the pixel offsets between the master and the slave images that occurred from the coregistration process for the ascending and the descending dataset respectively. Generally, the miss-registration errors are very low and thus are good for an interferometric processing with reliable results. Subsequently, the initial differential interferograms were formed, 26 ascending and 71 descending image 22 and 18 interferograms were formed in total, by using a

multi-reference interferogram generation method. Another important result from this step is the generation of the coherence for each interferometric pair. Topography phase parameter was also removed from the differential interferograms using the imported DEM. Next, an adaptive phase filtering method (Goldstein and Werner 1998) was applied to all differential interferograms, in order to improve the quality of the phase unwrapping step. Concerning the phase unwrapping, Phase unwrapping is the process of restoring the correct multiple of $2\pi$ to each point of the interferometric phase image. The unwrapped phase can be evaluated by a simple path-independent integration of the phase differences of adjacent wrapped phases, starting from a reference location and using the assumption that all phase differences are in the interval $(-\pi, \pi)$. However, in actual interferograms, phase unwrapping is more difficult because of phase steps which are outside of the interval $(-\pi, \pi)$. Causes for local phase gradients larger than $\pi$ are: i) Phase Noise (temporal decorrelation, shadow and low SNR) ii) Phase Under-sampling iii) Phase Discontinuities (layover and discontinuous surface deformation) (Werner et al. 2002).

After completing the phase unwrapping, in order to achieve better accuracy on the values of perpendicular baseline between all interferometric pairs, a baseline refinement step is required, which re-calculates the initial baselines based on the wrapped and unwrapped differential interferograms already formed. After the execution of the refinement process, the interferograms are reformed, additionally, to complete the processing chain; the phase was converted to displacement with knowledge of the topography from the DEM. Finally, it is important to mention that the differential interferometric phase corresponds to the displacement along the SAR look vector.

### 4.4.1 Inteferometric Stacking (IS)

The stacking of differential interferograms is based on calculating the average phase of two or more interferograms in a certain time scale in order to reduce the decorrelation factors which cause the phase fluctuations and to extract common information. The most basic procedure of the technique is to compute linear combinations (generally sums or averages) of interferograms. The stacking technique is substantially useful in overcoming shortcomings of conventional InSAR which arise from the negative contribution of two decorrelation factors: Low coherency over long temporal separations and Atmospheric influences (Zebker and Rosen 1997; Parcharidis et al. 2006; Raucoules et al. 2008). When applying this method, a reference point on the scene needs to be specified. The reference point works as a point with a phase of zero and based on it, the relative change rate of differential phase for the whole image is calculated. The selection of the location of

the point is based on two criteria: a) placing the point on areas with high coherence values and b) placing the point on areas where we already know that the relative deformation is very low.

## 4.5 Data Analysis

### 4.5.1 Processing with Sarproz Interferogram Resampled Displacement

InSAR technique uses the main principle of InSAR interferometry is to compare the phase of two or more radar images which are typically acquired from the same flight track but at different times. This is used to determine displacements of the Earth's surface at wavelength scale. SAR satellites observe the ground in a non-vertical LOS direction. In zero-baseline condition, the phase information would only be related to the LOS displacement while in reality a certain baseline is always present making the interferogram sensitive to the topography. By using an external DEM, the topographic phase contribution will be subtracted from the interferogram, leading to a Differential SAR interferogram that can be used to detect subtle changes (e.g. deformation) in the range distance between two acquisitions (Goldstein, 1995; Zebker et al., 1997).SAR interferometry phase component and phase unwrapping INSAR analysis and deformation detection required determination of phase difference therefore accurately obtaining phase difference and evaluating the component affection the overall phase change is essential. Five components have contribution to the phase difference of SAR image as presented below:

$$\Delta\varphi = \Delta\varphi displacement + \Delta\varphi elevation + \Delta\varphi flat + \Delta\varphi atmosphere + \Delta\varphi noise \quad (1)$$

$\Delta\varphi$displacement: Contribution of surface deformation to the interferometric phase and the change will be measured.

$\Delta\varphi$elevation : Contribution of topographic effects to the interferometric phase

$\Delta\varphi$flat : Effect of earth curvature to the phase this effect can be estimated and subtracted

$\Delta\varphi$atmosphere : Atmospheric contribution to the interferometric phase due to temperature humidity and atmospheric pressure change between acquisitions

$\Delta\varphi$noise : The phase noise due to temporal change of the scatters and look angel.

After removing the phase contributions from the elevation, curvature of the Earth, noise, and atmospheric effect, the remaining signal is mainly the range change due to surface deformation, and this can be written as following by giving range change (Elliott, 2009).

$$\varphi def = \frac{4\pi\Delta R}{\lambda} \qquad (2)$$

In this work only Interferometric Stacking Module were done where the SLC file are extracted and provides un orbital parameter in order to select input files for master and slave image to create coherence image for processing single inteferogram image. Interferogram calculation were done by Using the sarproz software package and generated 22 coherent interferograms in both sentinel and Envisat including phase unwrapping and topographic phase removal based on the SRTM-1 digital elevation model (DEM) using equation 1 and 2 . In order to improve fringe visibility resulted from reduction of noises, adaptive radar interferogram filter of Goldstein filtering technique were applied. Unwrapped interferometric phases were transformed from radar to geographic coordinate system (geodetic projection on WGS 84 datum). The final product of this step is a set of unwrapped filtered interferograms showing phase changes due to ground motion level changes. So below in figure 4.2 and 4.3 shows the generation of interferogram starting from one single master image connected with each individual image to create a best coherence according to their spatial and temporal base line.

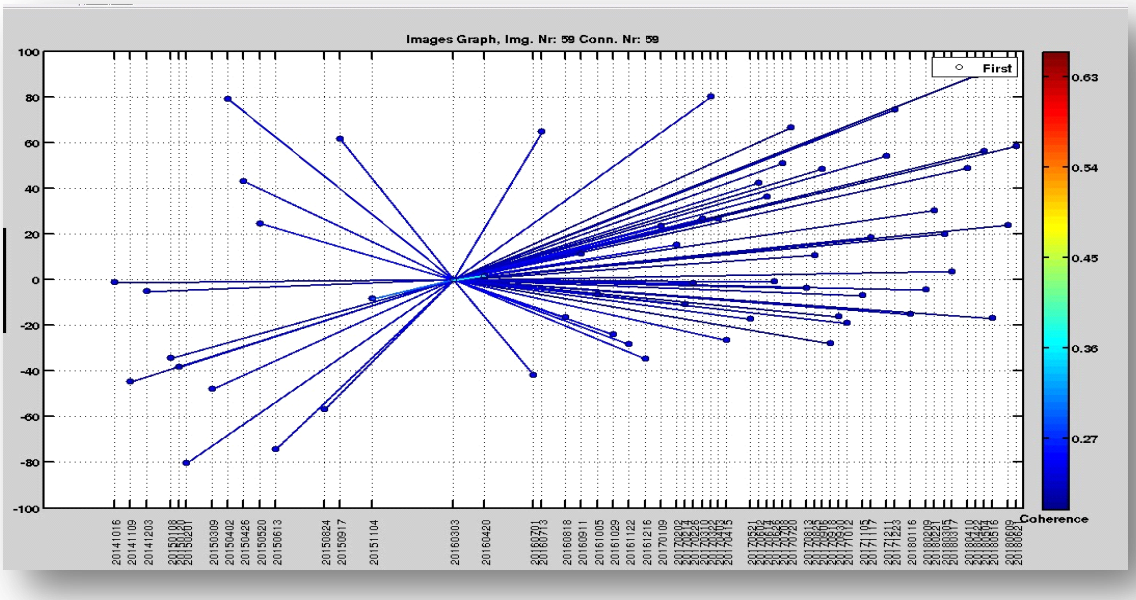


Fig 4.2 Interferometric configurations for descending sentinel dataset On the Y axis the perpendicular baseline expressed in meters, on the X axis the acquisition dates of the images in format yymmdd.

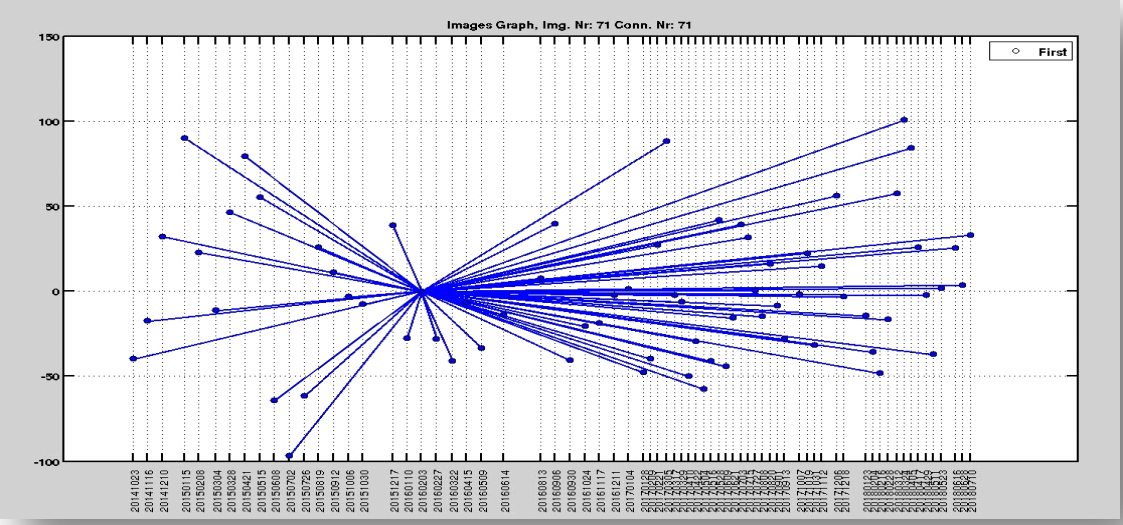


Fig 4.3 Interferometric configurations for descending sentinel dataset On the Y axis the perpendicular baseline expressed in meters, on the X axis the acquisition dates of the images 71 in format yymmdd.

### 4.5.2 Processing with Sarproz PS-INSAR

The techniques that use interferograms with a single master and exploit only coherent pixel with stable phase or amplitude are called Persistent Scatter (PS-InSAR) approaches (Ferretti,et al 2001; Hooper, et al 2004; Kampes, 2006).

In order to overcome decorrelation and atmospheric in homogeneities, PSI is used to estimate the displacement without sacrificing accuracy and resolution (Crosetto et al., 2016).The approach gives the spatiotemporal evolution of an instability phenomenon When the response to the radar is characterized by a strong signal coming from a principal reflecting object and it is constant over time, then these pixels are called Persistent Scatters (PS); when the response is constant over time, but the signal comes from different small objects, then the pixels are Distributed Scatters ( Crosetto et al., 2016).The PSI approach uses a spatial subset of the data with most reliable phase information for detecting displacement changes with time. The method uses a large number of scenes acquired over the same area greater than 11 pair of to make an interferogram image with the same acquisition parameters. After all interferograms are adjusted to the reference region, and then perform stacking and time series analysis was done. Firstly, interferogram displacements at each pixel create deformation rate-maps for each dataset that are scaled to give annual rates of vertical displacement. Thanks to the high level of urbanization of the area under analysis, it was possible to identify a huge number of Permanent Scatters with a high coherence value. About 98000 PS in envisat data and above 10,000 PS have been identified in sentinel data with coherence greater than 0.8 on a single

pixel. Radar targets exhibiting high phase stability over the entire observation in the time period. Because not all data points (pixels) show consistent phase changes, PSI relies on a subset of reliable pixels, termed Persistent Scatters (PS). The criterion for data selection is high scattering value pixels consistent in all scenes. The phase values of these scatters are estimated in all interferograms, which are calculated from all scenes with respect to a master image, even for interferometric pairs with very long geometrical baselines (larger than critical baseline). The scatters distribution density plays an important role in determining the quality of the displacement analysis. PSI was found to work well in urban areas with strong structural reflectors, where the scatters distribution density is high. However, the method is less effective in open areas, because the PS targets density is relatively low. For the full-site analyses, PS candidates (PSC) were selected based on a combination of several quality parameters related to radar signal stability, such as reflectivity, Amplitude Stability Index (ASI, i.e., the amplitude coefficient of variation) and the spatial coherence. A network of PSC was created to estimate the preliminary height and velocity parameters to retrieve and remove the Atmospheric Phase Screen (APS).

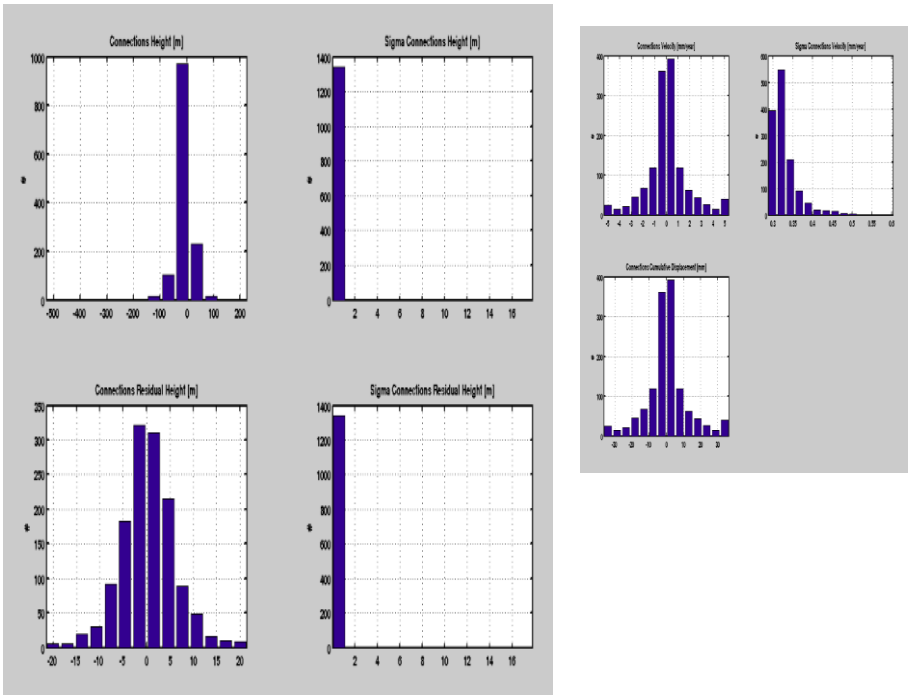




ASP OF A REFERENCE POINT

1. Connection VELOCITY
2. Sigma connection velocity
3. Connection cumulative displacement
4. Connection height
5. Sigma connection height
6. Connection residual height
7. Sigma connection residual height

These all are show stable remain at zero

Fig 4.4 ENVISAT ASP Graph for a reference station

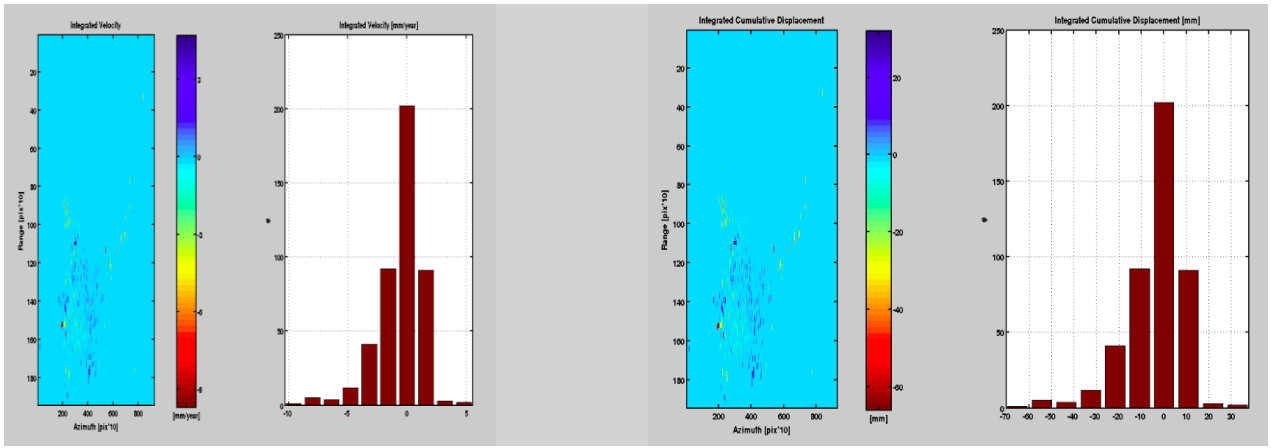


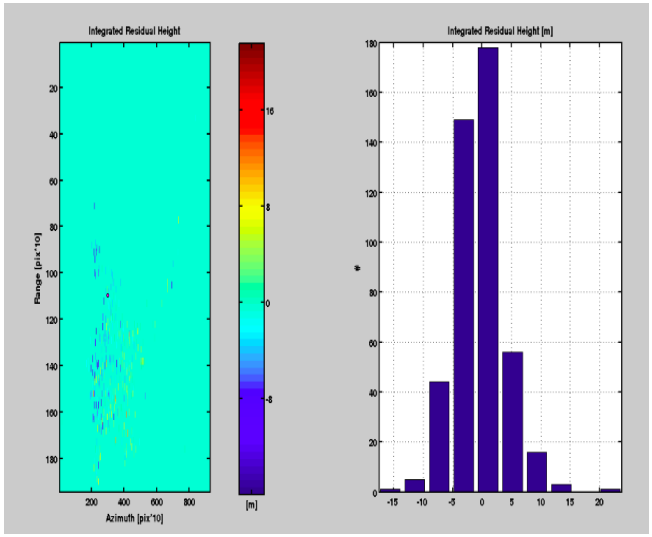


ENVISAT ASP GRAPH FOR REFRENCE POINT (stable point at zero)

4. Integrated velocity
5. Integrated residual velocity
6. Integrated cumulative velocity

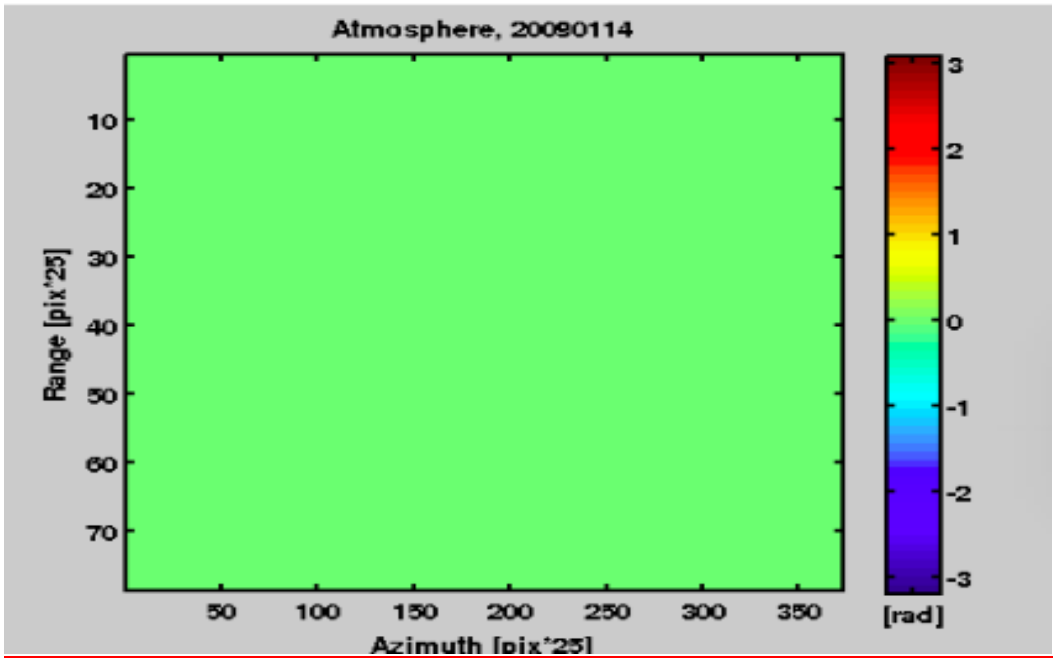


Fig 4.5 Atmosphere of reference point.

After the APS removal, a second estimation of parameters was performed on a wider set of points, selected based on a spatial coherence and ASI combination criterion. At the end of the PS analyses, all PSs with temporal coherence above a reliable threshold (primarily dependent on the number of images analyzed in the data-stack) were selected. For each PS, the LOS velocity, displacement time series and heights have been computed using a linear deformation trend model. Linear deformation modeling means that it is assumed that the target is moving at constant rate. However, the best is to look at the time series for each individual point and see how velocities vary over time. In doing so a reference point among the candidates expected to be stable is chosen, the ground velocities that will be calculated will be relative to this assumed stable point. However, the selection of the reference point depends on the user opinion so it is subjective. The stable point can have some initial velocities, but they are assumed to be zero, because its function is just to define a reference velocity for other points. Therefore, deformation maps generated by different users may look different but expected to be equal in a relative sense. Time series, since atmospheric and noise are reduced because of the spatial closeness of the points (Hooper et al., 2012). Deformation is both spatially and temporally correlated, at the same time as atmospheric artifacts are spatially but not temporally correlated. This information is discouraged to apply a filter to estimate the atmospheric effects and this is the main advantage of this MT-InSAR technique. The final result is the average annual motion for each PS candidate, assuming the deformations are linear.

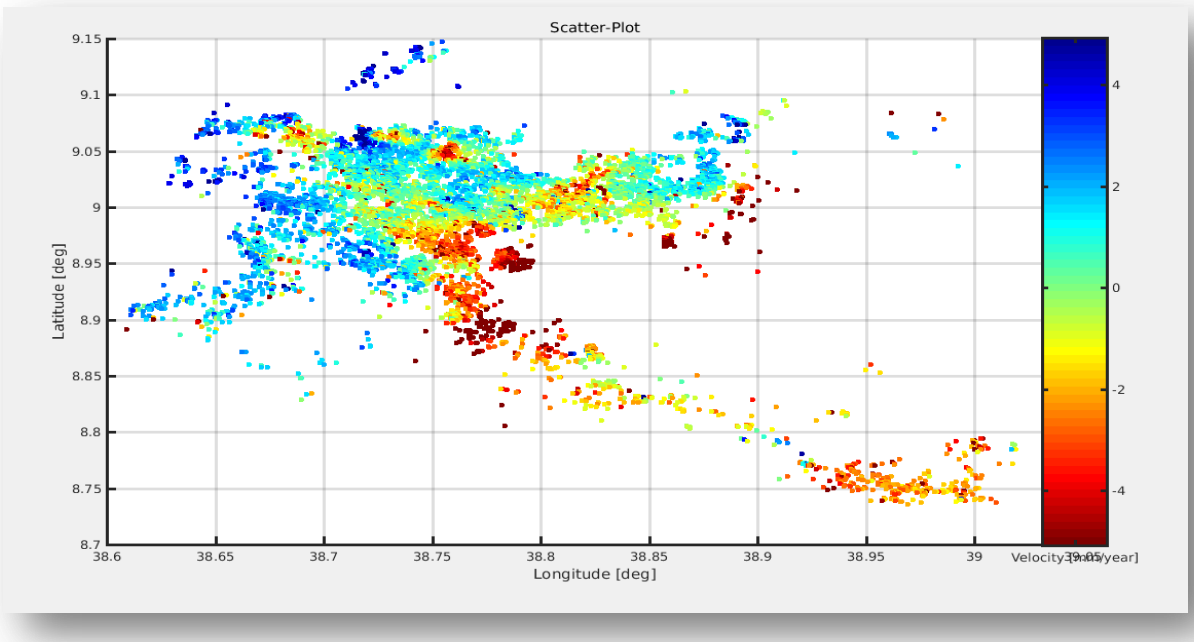


Fig 4.6 Scatter plot of PS candidate Addis Ababa city sentinel descending image

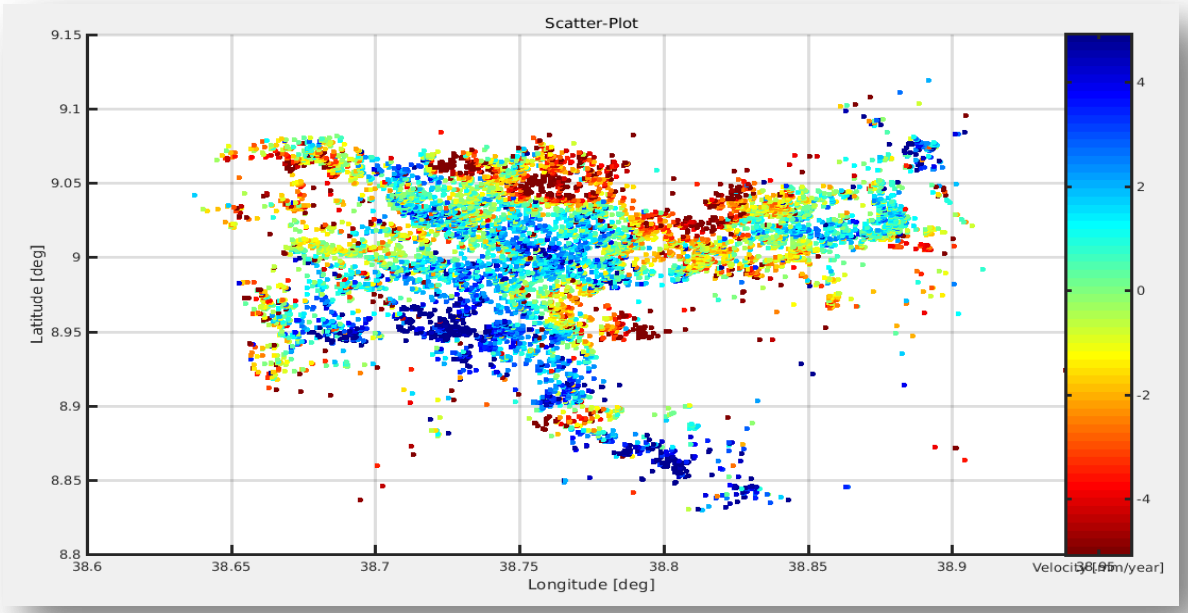


Fig 4.7 Scatter plot of PS candidate Addis Ababa city sentinel ascending image

## 4.7 Validation method

### 4.7.1 Regression Analysis

The Regression method is used in regression analysis to identify a connection between these two interdependent variables from the observation of many points. The most common model is linear regression, which is defined as: $y= mx+c$ …… (3).

So According to (yang et al 2016) also used this regression method to validate the building deformation between Insar and leveling measurement. Where x and y are two variables, and m and c are the unknown parameters. In our case x is the displacement value in ADIS GPS station, and y is the displacement value extracted from InSAR. There are two parameters using to evaluate the quality of the regression analysis, the correlation coefficient and the RMSE. The correlation coefficient describes the degree of fit between the regression model and the observations, where a value near 1 indicates that the degree of fit is closer. The regression analysis of Root Mean Square Error (RMSE), a smaller value always corresponds to regression analysis results that more closely fit the model. For these validation of the two variables select five measurements throughout the validation site, which means in every year of GPS data select one displacement value per year according to the Insar measurement with the same year and month.

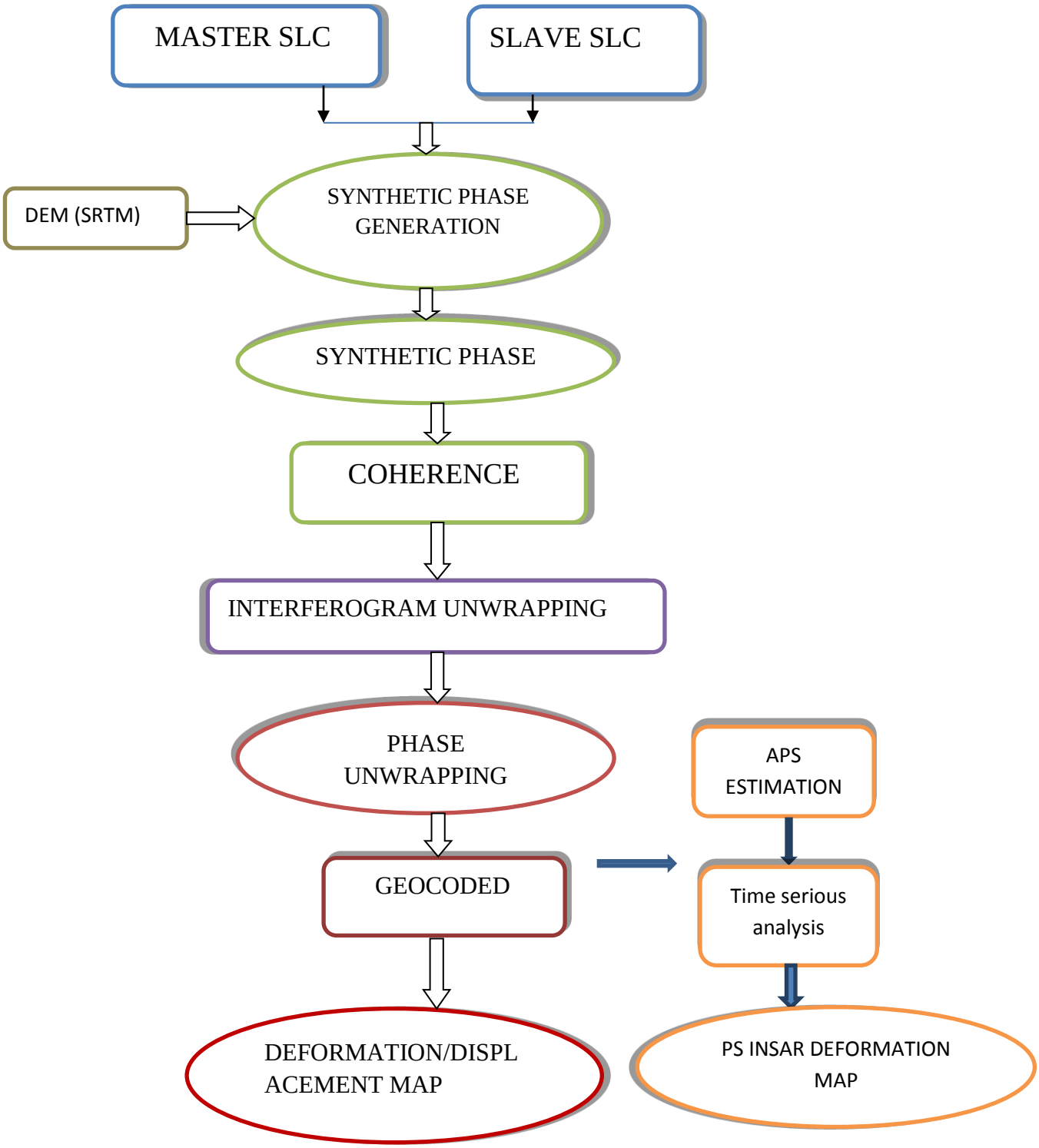


Fig 4.8 Conceptual frame work of data processing

# CHAPTER FIVE
# 5. RESULT AND DISCUSSION

The displacement velocity map is extracted using the interferogram and InSAR time-series results to highlight the major deformation features in the area. The displacement velocity map contains the subsidence rate along the LOS direction. Use the one band of SAR data, namely C-band Envisat and Sentinel dataset. Have a number of dataset of C-band Envisat data 23 acquisitions taken during a period of 2003- 2010,180 of sentinel data period gathered over the period ranging from 2014 to 2018. These datasets were evaluated using Persistent Scatters and single interferogram methods developed in sarproz software to investigate deformation of the ground surface and key infrastructures. Results of Envisat and senteniel dataset illustrated deformation patterns of the study area. Besides, vertical deformations of the infrastructures were determined using InSAR method using both Envisat and sentinel datasets. The subsidence rate was estimated as several millimeters per year using the stacking method. First, SLC SAR datasets were processed using Sarproz. The SLC dataset were extracted to our study area of 20 km to 16km. The second step was co-registration; Co-registration means that for each image, the resolution cells of the same geographic place are overlaid. This is done using orbital information. After co-registration of slave images to their respective masters, a multi-look ratio finished of 5:5 (final pixel size 20 m by 20 m) was used to generate raw interferograms and subsequent products. The mean displacement velocity map is extracted under the assumption of infinite flattening. Therefore, any non-linear deformation, including atmospheric artefacts, has been damped out. Deformation sequences obtained by the time series analysis are used to generate the displacement maps spanning the same time intervals as the interferograms. In the generated subsidence maps, the artefacts generally considered to be atmospheric, are significantly decreased, which shows the effect of smoothing. The velocity map allows for the identification of the long term subsidence. However, the main strength of the time series analysis is its potential to detect deformation signals that are not steady in time, including seasonal effects (Lanari et al.2004). During this period, 2017 subsidence has its maximum rate, as shown in Figs 5.8, 5.9. Finally, the last period 2018 corresponds to continuing the subsidence. The accelerated subsidence is clearly observed during this period in Figs 5.9. To evaluate the results of the time-series analysis, continuous GPS measurements were used a continuously recording GPS station at Addis Ababa University. The location of the ADDIS GPS station is shown in Fig. 5.14 This station has recorded data continuously since 2007.

The phase of the interferogram contains orbital errors, topographic effects, target displacements and atmospheric noise (Ferretti 2014). In order to obtain the ground surface displacement over a time interval, orbital errors, topographic effects and atmospheric noise must be removed from the interferogram. For the topographic effect removal the SRTM DEM with the spatial resolution of 30 m were used. Refer to an appendix part that Figures A-1, A-2, A-3 and A-4 show the interferometric configuration of both the dataset as a graph describing the relationship between the images in function of time and perpendicular baseline. Each image is connected to the chosen Master image, forming an interferometric pair.

## 5.1 Resampled Displacement by Interferogram in city of Addis Ababa

The interferograms were then unwrapped, and adaptive filter was applied to each differential interferograms (Goldstein and Werner, 1998) to reduce phase noise and improve subsequent 2D phase unwrapping. These interferograms provide the relative displacement along the radar line of sight (LOS) direction. Further processing of the InSAR data allows us to estimate deformation velocity for each interferogram derived from different satellite missions: envisat (2003-2010) and Sentinel (2014-2018). The deformation rates in the Line of Sight of the Persistent Scatter points determined by processing the ascending and descending datasets are shown in Figures 5.2 and 5.3, respectively. The rate value in descending sentinel data set maximum -9mm/yr and minimum -3mm/yr subsidence and 9mm/yr maximum and minimum 3 mm/yr uplift as shown in Figure 5.2 while for Figure 5.3 in ascending dataset in both swath the deformation rate value at maximum subsidence -8mm/yr and maximum -4mm/yr and the uplift rate at maximum 8mm/yr and minimum value also 4mm/yr .Positive values indicate a movement of the object toward the sensor (uplift), while negative values indicate the opposite (subsidence).

According to (Parker et al., 2017) InSAR data showed deformation rate across larger geographic area (>5km wide) accounting for 15mm/yr (low magnitude) relative subsidence as well as 20mm/yr relative subsidence at a localized scale (<2km wide); consistent with estimates determined across wetland areas.

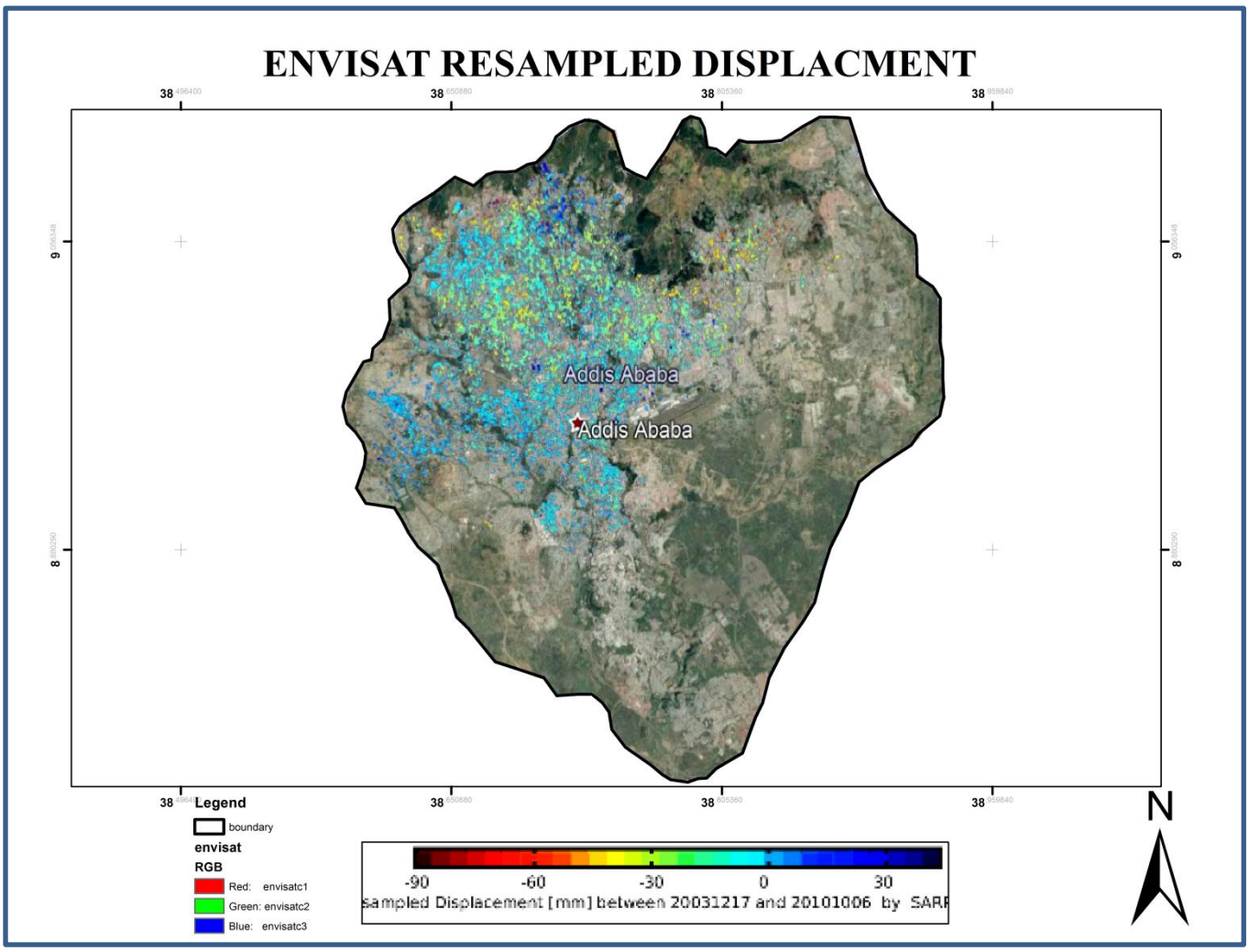


Fig. 5.1 ENVISAT interferogram Descending pair of 2003-2010

Addis Ababa city subsidence in the direction away from the satellite LOS at a rate ranging from -30 mm to -90 mm (Figure 5.1); as computed from envisat data. The same data also showed the subsidence of the study area towards the satellite at a rate of 0 mm to 30 mm (Figure 5.1). Zero rate of displacement represents an almost stable area; where deformation is not significantly going on. To evaluate the second dataset, another interferometric pair of Sentinel images, was chosen, the vertical displacement rates of a few millimeters per year was observed in small areas of the stacked interferogram that are contrasted by broader regions of several centimeters of displacement observed in some short term single pair interferograms (Wisely and Schmidt 2010).

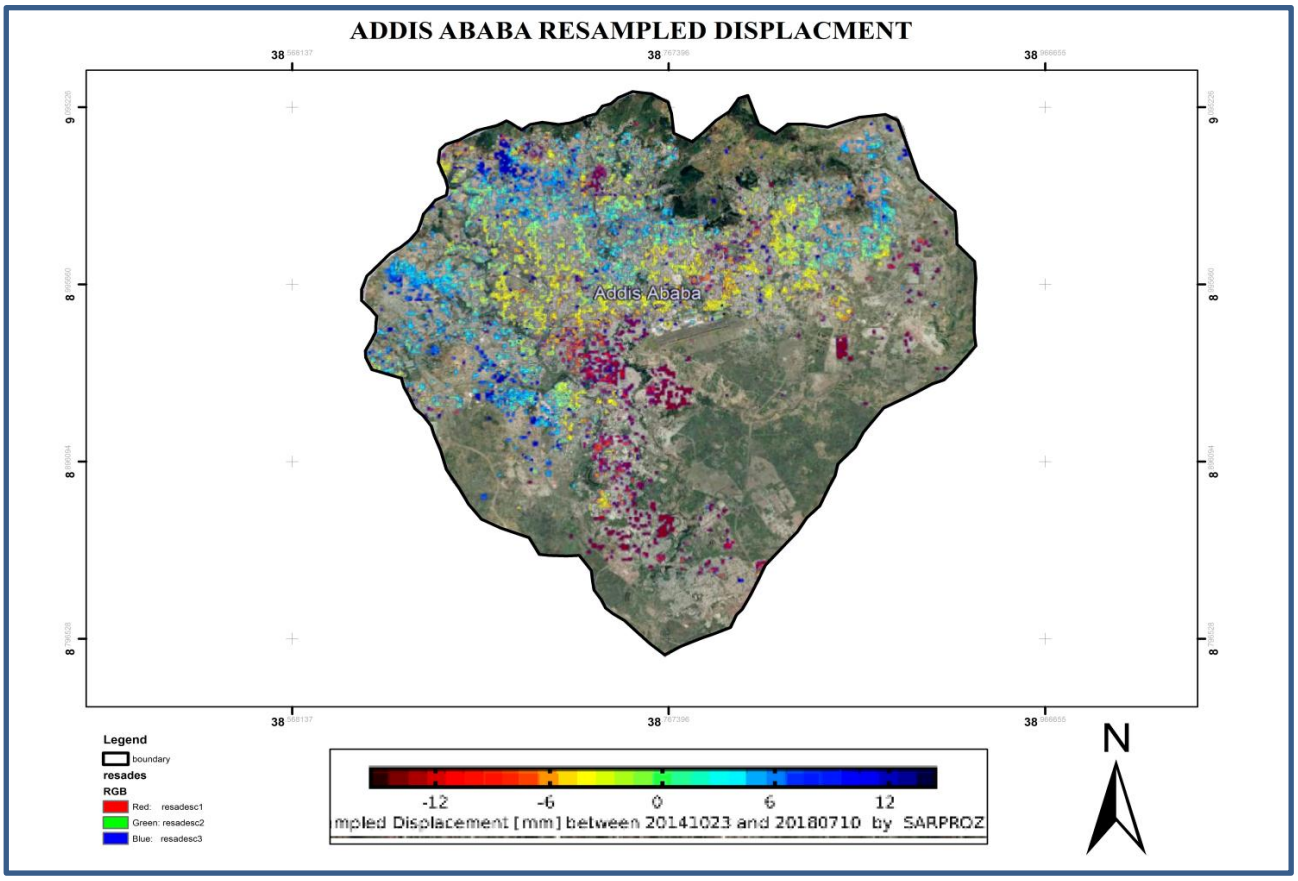


Fig. 5.2 Sentinel descending pair inteferogram approach resampled displacement 2014-2018

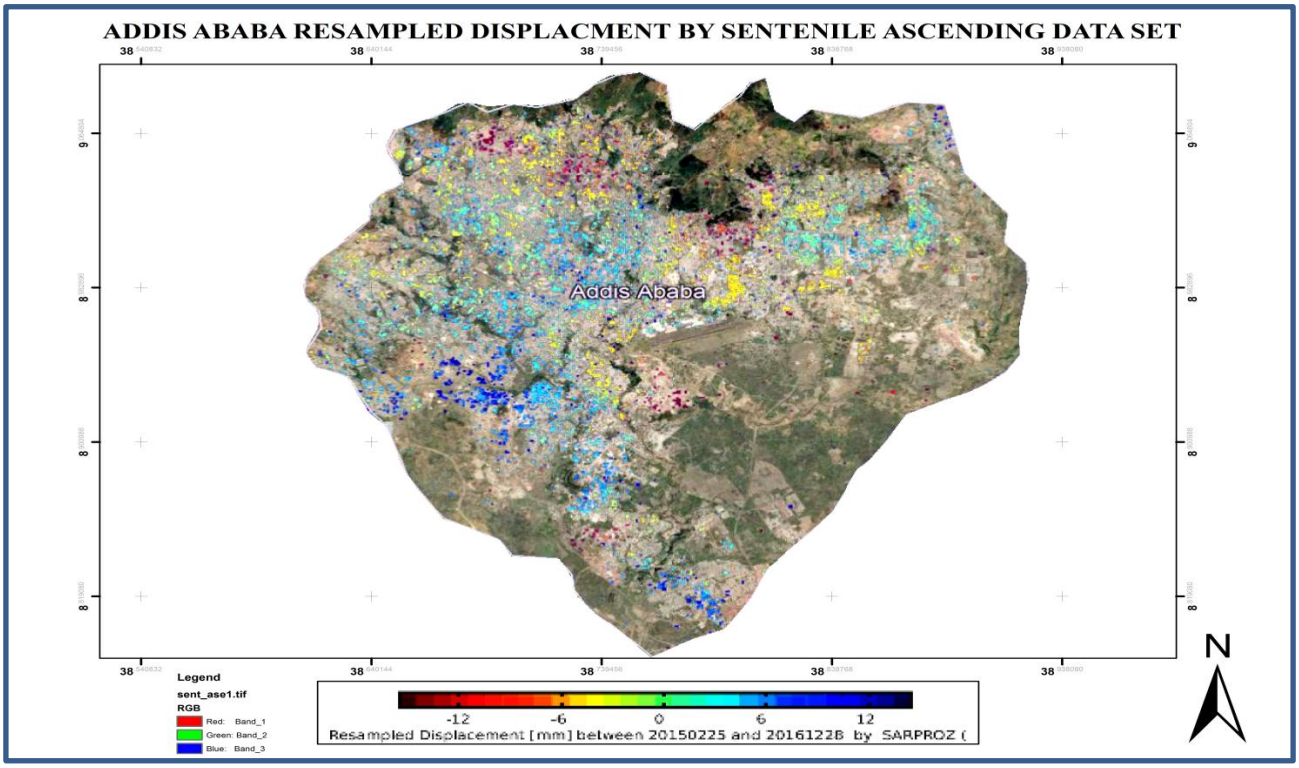


Fig. 5.3 Sentinel ascending pair inteferogram approach resample displacement 2014-2018

Due to the difference in temporal resolutions among different radar datasets, the rate of subsidence determined from each data source across the study area showed slight variability. The maximum rates of observed deformations are: -30 mm from envisat data and -12 mm and -4 mm from sentinel descending and ascending data (Figures 5.1, 5.2 and 5.3). The velocity map shows the spatial variability of deformation across the study area. Large descending interferograms detected ground subsidence, with observed some uplift (Fig. 5.2). For example, significant subsidence (maximum -12 mm) and uplift (maximum 12 mm) are observed in the satellite LOS direction as recovered from the descending image. The ascending imageries showed uplift (maximum 4 mm) and subsidence (maximum -4 mm) in the LOS direction. From the deformation rate-maps, we identify features of the deformation field that are evident in both InSAR datasets. The descending interferogram shows larger values for subsidence in the satellite LOS direction than the ascending interferogram. This is due to the looking direction and the incidence angle of the sensitivity vector and the geometry of the fault which means displacement vector. Verifying the application of Sentinel-1A with independent evidence from ENVISAT and also providing more information about a greater spatial extent of the deformation field in the Addis city, we classify the observed displacements into two categories according to the magnitude and spatial extent of the deformation. These are: (1) whole city of coverage low magnitude (up to -12 mm) relative subsidence (labelled in Figure 5.4 and 5.5); (2) relative cumulative subsidence of -36 mm/yr was observed at the test site.

### 5.2 PS INSAR of Addis Ababa city

The PS value of envisat data almost covers the central, northern and western parts of Addis Ababa, showing less availability of infrastructure. The rate of deformation relative to the resample displacement of envisat data is almost the same across the study area. However, it exhibits slight spatial variability red, light blue and blue points indicating subsidence, stable targets and uplift, respectively.

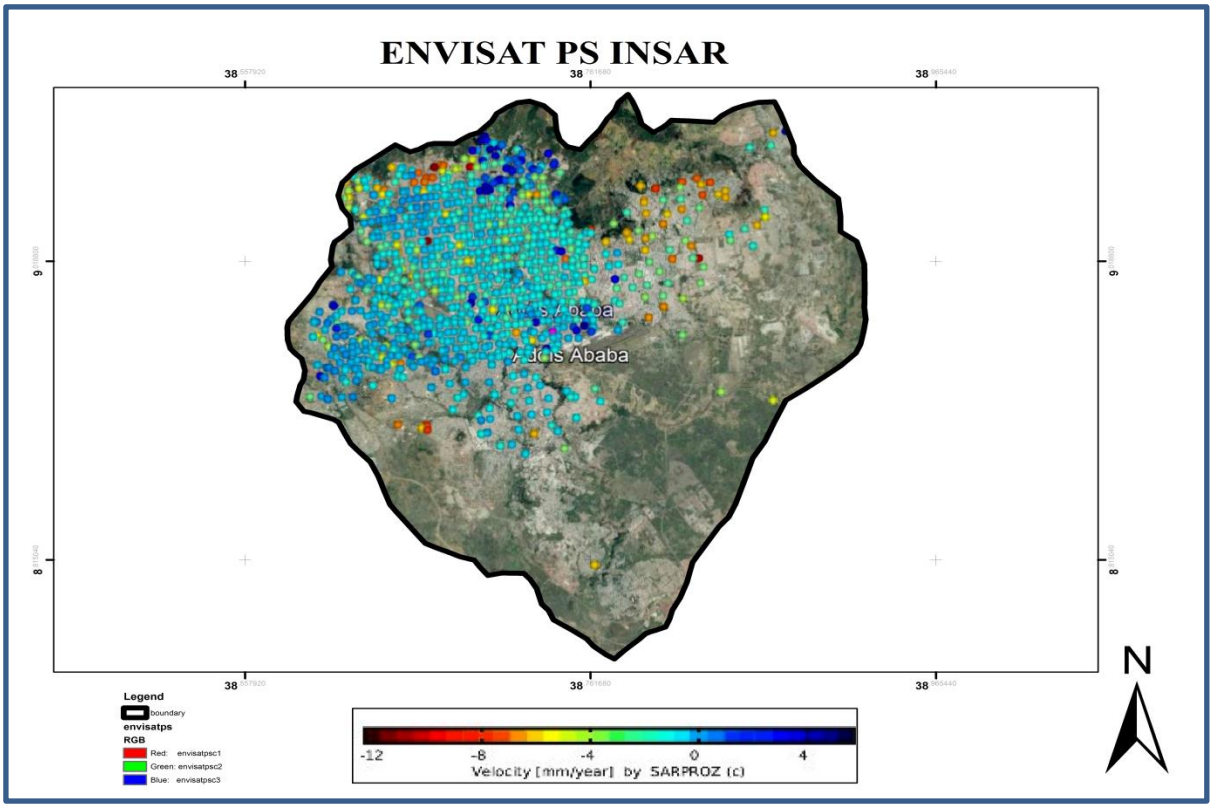


Fig. 5.4 PS INSAR RESULTS OF ADDSI ABABA CITY ENVISAT DATA

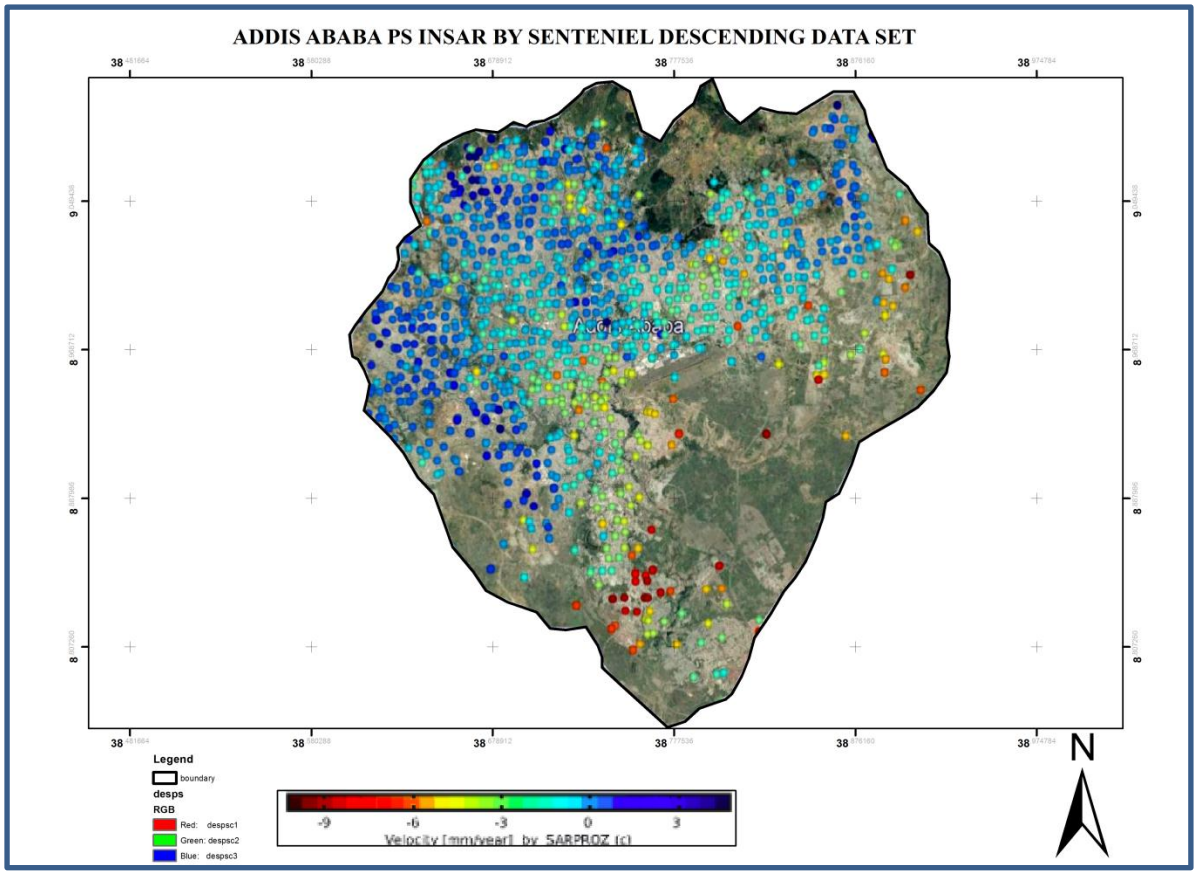


Fig. 5.5 PS INSAR RESULT OF ADDIS SENTENIEL DATA SET FROM DESCENDING

In sentinel dataset the PS value covers all infrastructure areas. PS numbers derived from recent sentinel data are greater than envisat, indicating further infrastructural development within the city. Each point of the PS method indicates deformation rate of specific building, road, stone and any other man made future. So the PS rate shows more blue and light blue color it means light blue is zero or no deformation at the central and eastern part of the city and red color at southern part indicating maximum deformation, the light red shows minimum rate deformation at the southern, south-west and some western part of Addis Ababa.

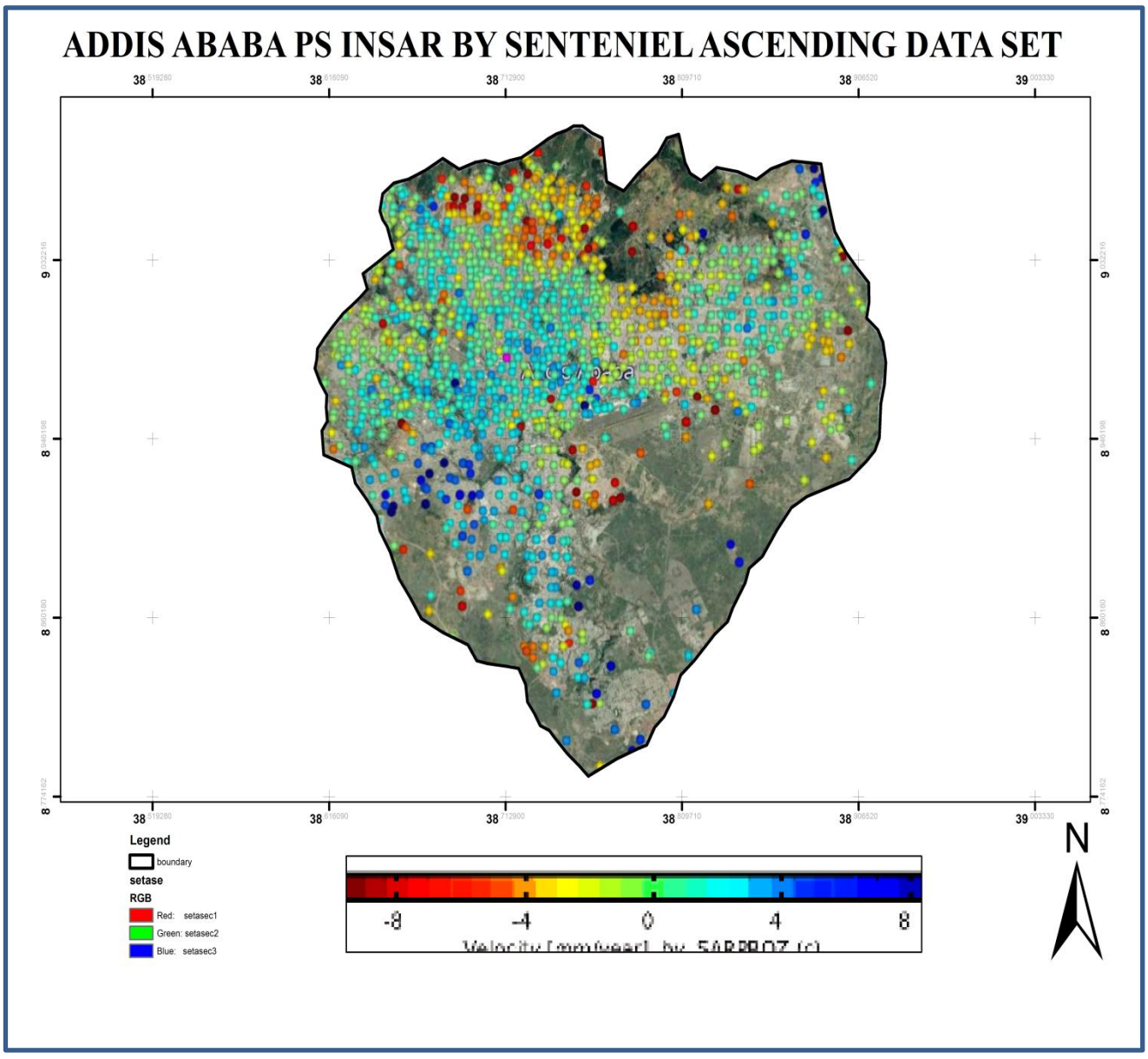


Fig. 5.6 PS INSAR RESULT OF ADDIS SENTENIEL DATA SET FROM ASCENDING

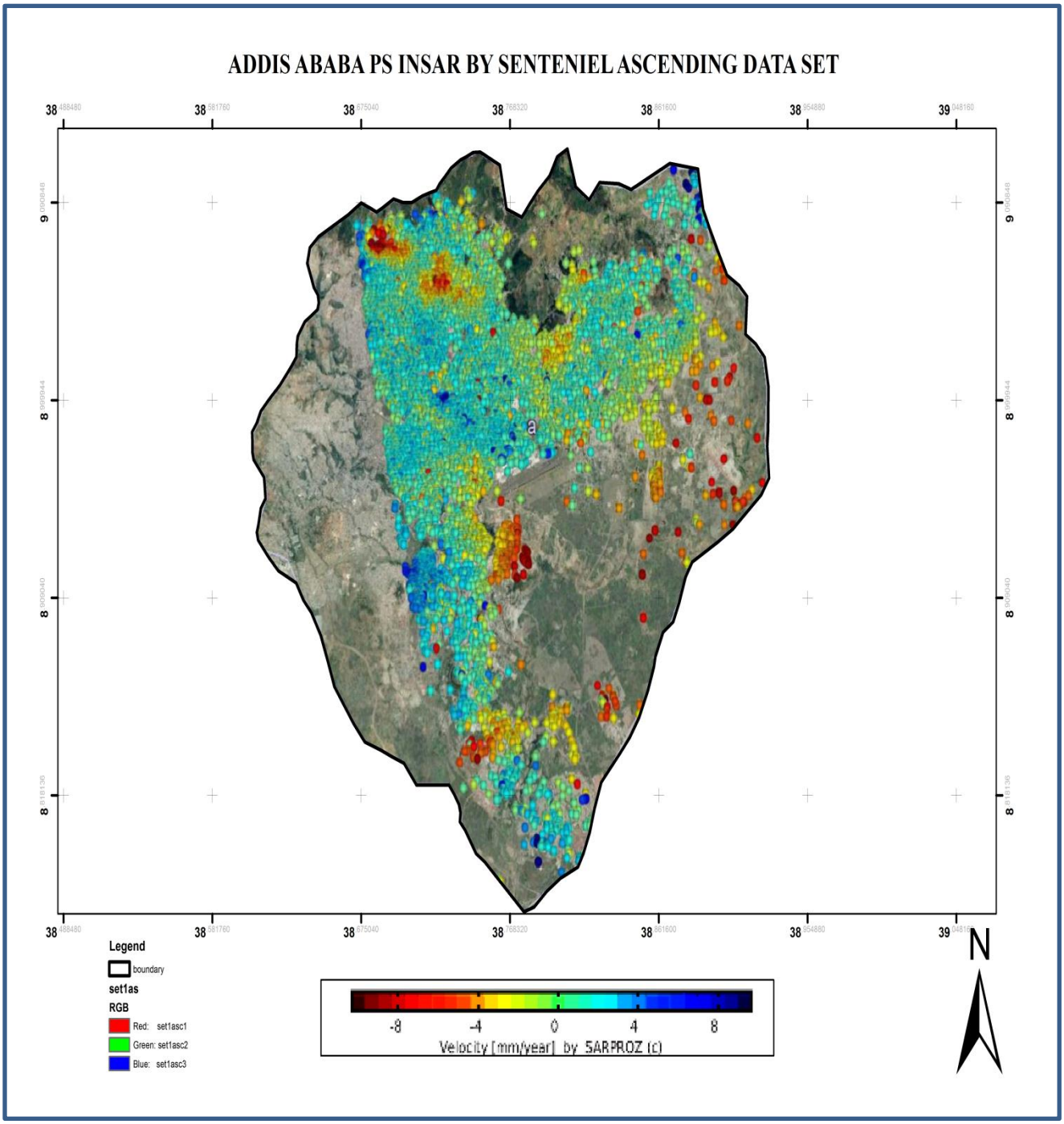


Fig. 5.7 Deformation maps of Addis Ababa derived from PS of sentinel data (from ascending swath 3)

Regional scale monitoring of urban area shows large subsidence (-40mm/yr) and uplifting (+15mm/yr); walls of the ancient city are relatively stable (-10mm/yr to +5mm/yr) (Chen et al., 2017) Sentinel data should different results for ascending data with varying swath. For example, Figures 5.6 and 5.7 showed different results compared to Figure 5.5. But these ascending data sets

also have different swath and area coverage, in Figure 5.6 the PS values are very disperse all over the study area. More stable areas are described by light blue color and deformation is larger in the northern and western parts of the city (as indicated by red points). Figure 5.7 covers almost eastern, north eastern and south eastern parts of the city. PS value colored by light blue showed more stable areas while red and light red values reflect deformation in northern and south eastern region of the city. The study compared displacement in interferogram and time-series approach by PS across the two test sites. For the two test sites, time-series analyses were computed using one master scene for each dataset, and temporal reference (i.e. Master date). To combine the vertical displacement of the three datasets, we have to account for relative ground displacement between the master dates in the two time series. For this, we fitted a linear trend to each of the time-series and calculated the shifts between datasets. The results of those areas as it can be seen, picks randomly and they are at different location in the city. The test site 1 is located in western part of Addis Ababa and it is suffering land subsiding the cumulative displacement of approximately -36.78 mm during 2017 (Fig. 5.9). This area is the large rubbish dump site and has been filled by different kinds of building and infrastructure. The test site 2, which is a well build up infrastructure areas that are located in the south eastern region of Addis Ababa, and it is subsided approximately at a rate of -3.2mm/yr and subjected to cumulative displacement of -12.0mm. Analytical results indicate that test site 2 is relatively stable than test site 1. InSAR derived ground motion rates and displacements are also validated using an independent estimates derived from GPS data, located at Addis Ababa University (ADIS station). InSAR based PS displacements and time series GPS measurements are the same (zero level displacement). This indicates that the GPS is located in more stable area.

## 5.1 TEST SITE 1 KOSHE

The above-mentioned methodology was applied to the western part of Addis Ababa. This area was chosen as the test site, since it is partially landslide affected and characterized by a middle urban fabric density between the city center and the rural area. Moreover, this test site, which extends up to 36 hectares (ha), includes different building typologies, such as stone structures and concrete buildings, with different infrastructure types are built realized in recent years. The landslide occurred on Saturday when a section of the dump collapsed onto a slum built at the toe of the slope. Addis Ababa's construction boom didn't leave Koshe untouched; a biogas plant is being built on top of the rubbish dump. In March 2017, a landslide at the site killed more than 113 people, as recovery continues the death ring is expected to rise.

### 5.1.1 RESULT

In this work, PSI analysis showed that Koshe dump fill is the most critical and unstable area. Besides, extensive dormant mass movements and consequently characterized by the highest PSI ground motion rates were observed across the study area (Fig 5.8 and 5.9).

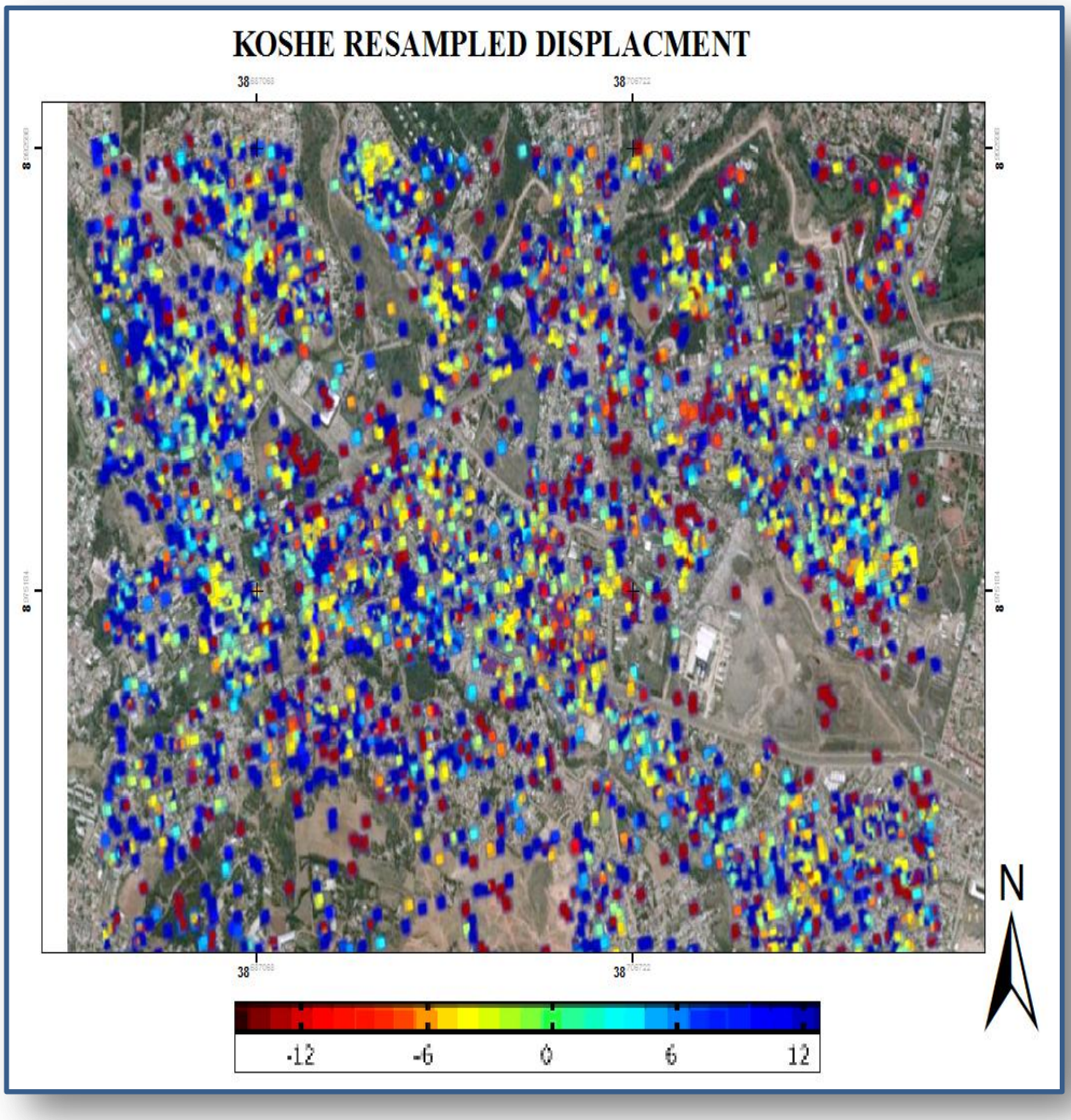


Fig. 5.8 Test site 1 deformation map by interferogram approach the resample displacement of at koshe site

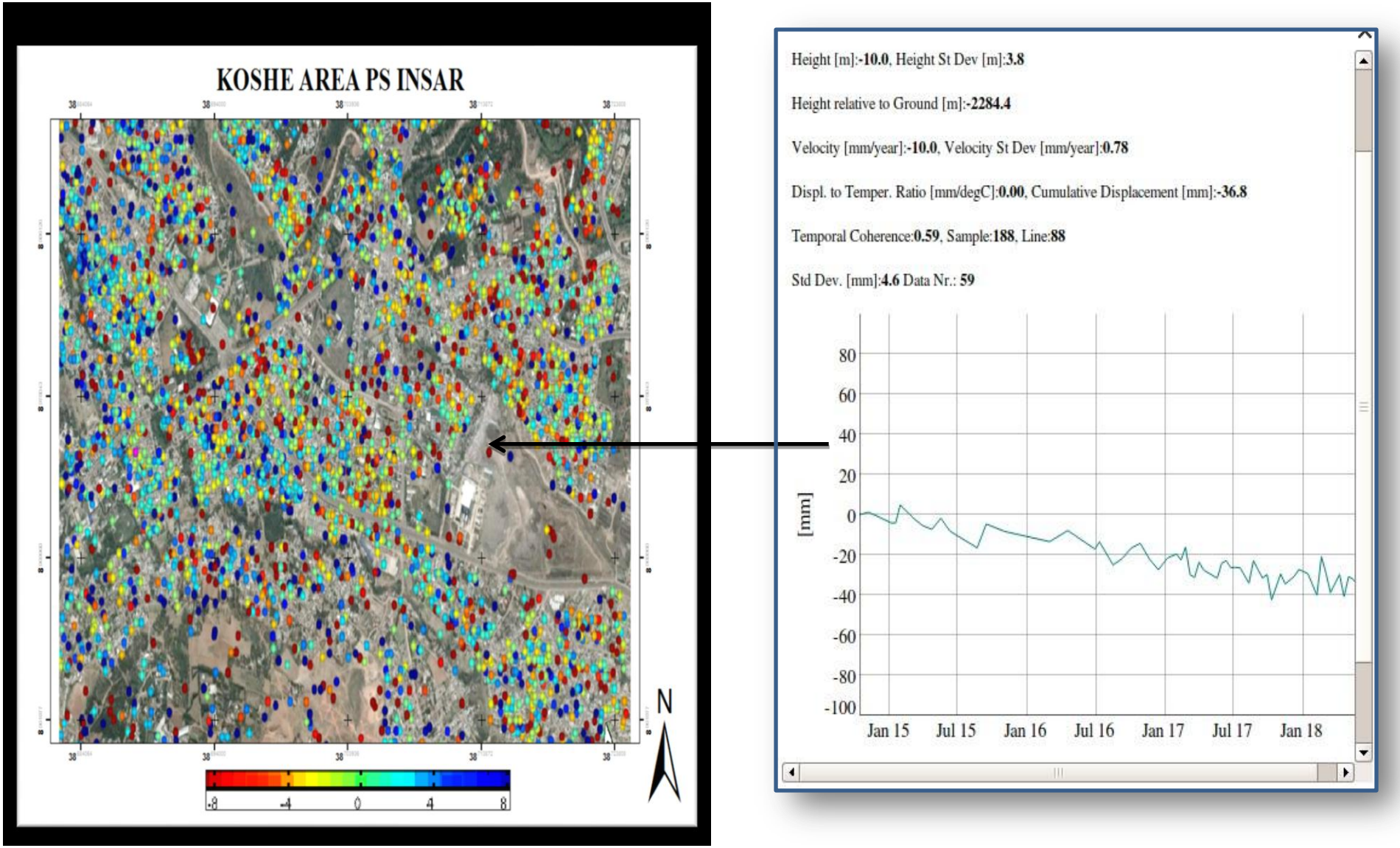


Fig. 5.9 Test Site 1 deformation map and graph by PS approach of at koshe site

The spatial distributions of PSI LOS velocities are shown in Figure 5.9. The negative sign stands for an increasing distance of the away from the satellite sensor, while a positive sign means a movement towards the satellite. Within the PSI velocity, stability thresholds are fixed at -36.8 mm/yr and +10 mm/year in descending and ascending orbits, respectively, for distinguishing stable targets (displayed in a green color) from moving ones. Large magnitudes of PS are indicated in red color, showing subsiding deformation rate. Highest rates of deformation are indicated in the Fig. 5.9; PS velocity -10mm/yr and cumulative displacement -36.8mm/yr in subsidence. Also in uplifting way PS velocity 10mm/yr and 36.8 mm/yr are observed. But in the case of the surrounding area to the west region, PS points are sparse with blue and light blue color. The blue colors indicate that the area is uplifting at a rate of approximately 12mm/yr

## 5.2 TEST SITE 2 AIR LINES

Addis Ababa Bole International Airport is located in the city of Addis Ababa, Ethiopia. It is located in the Bole area, 6 km (3.7 mi) southeast of the city Centre. The national airline that provide flight in Ethiopia and throughout the African continent, in addition to nonstop service to Asia, Europe, North America and South America. The airport is also the base of the Ethiopian Aviation Academy. As of June 2018, nearly 350 flights per day were departing from and arriving at the airport.

In any airways runways are among the key infrastructures that are most critical to airport services. Runways at major airports handle hundreds of thousands of takeoffs and landings per year, with aircraft weighing hundreds of tons moving on and off the asphalt on a daily basis. Given the circumstances, these asphalt need to provide a secure, stable and durable surface through all weather conditions that can adequately support the heavy loads imposed by the airplanes that use them. The length, width and strength is dependent on the type of airport (such as a general aviation field or a major commercial airport), the size of aircraft most commonly served and the current volume of traffic on an annual basis, as well as forecast traffic volumes for future years. The next consideration is the material used. At most airports, runways are constructed of man-made material, usually asphalt, concrete or a combination of both. The choice of pavement material comes down to local ground conditions, the type of aircraft using the facility and cost. Hence bole airport have runway dimension 3,800m x 60m new runway, runway surface is asphalt concrete with the access road asphalt and aerodrome elevation 2325m and the temperature of 25 degree centigrade.

### 5.1.2 RESULT

The selected structures are characterized by different construction typologies, age and foundations, as well as by different foundation ground, since they are located on stone formations of (terminal)

or covered by asphalt and concrete with very different thicknesses. Considering the geological setting, the sensitive anthropogenic context and the logistic importance of this infrastructure, the analysis of surface deformation is a priority. Ge et al. (2009), potential damages of such infrastructures are not only loss of money but also loss of significant landmark in the world.

Detect deformation pattern along infrastructures such as airports, characterized by large linear extent, a monitoring technique combination wide coverage and high precision is required. In the last years, interest and attention on these problems increased, and analysis of linear infrastructures stability has been successfully carried out with PSI technique (Pigorini et al., 2010). Subsidence of about −0.2 to −15mm has been observed in the airport area, with several points exceeding−10mm along the two runway areas. Observed subsidence is without any doubt related to the terrain compaction accompanying the excessive underground rock withdrawal occurred in the near bole at bulbula site.

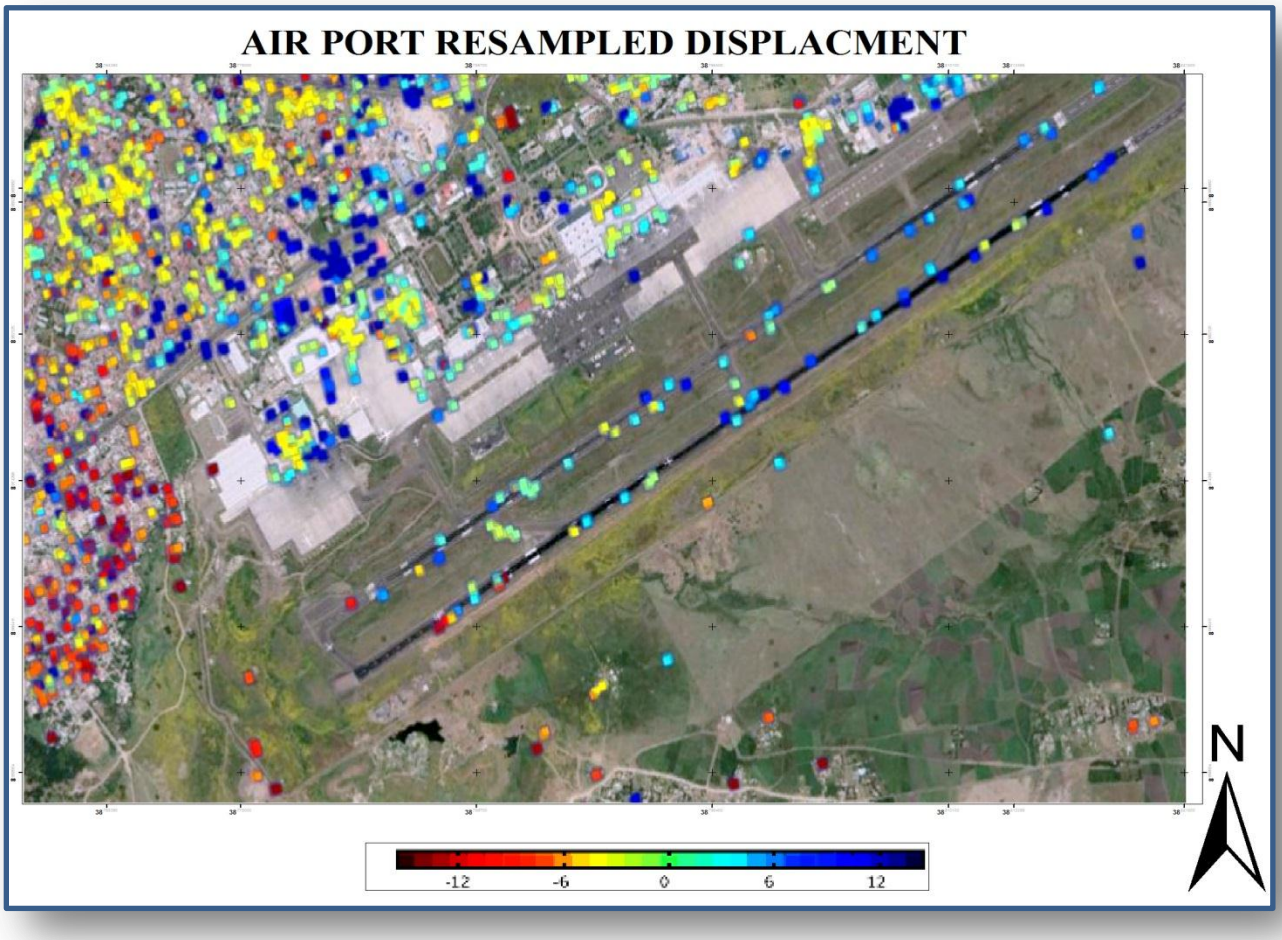


Fig 5.10 Test site 2 deformation map by interferogram approach the airport resampled displacement

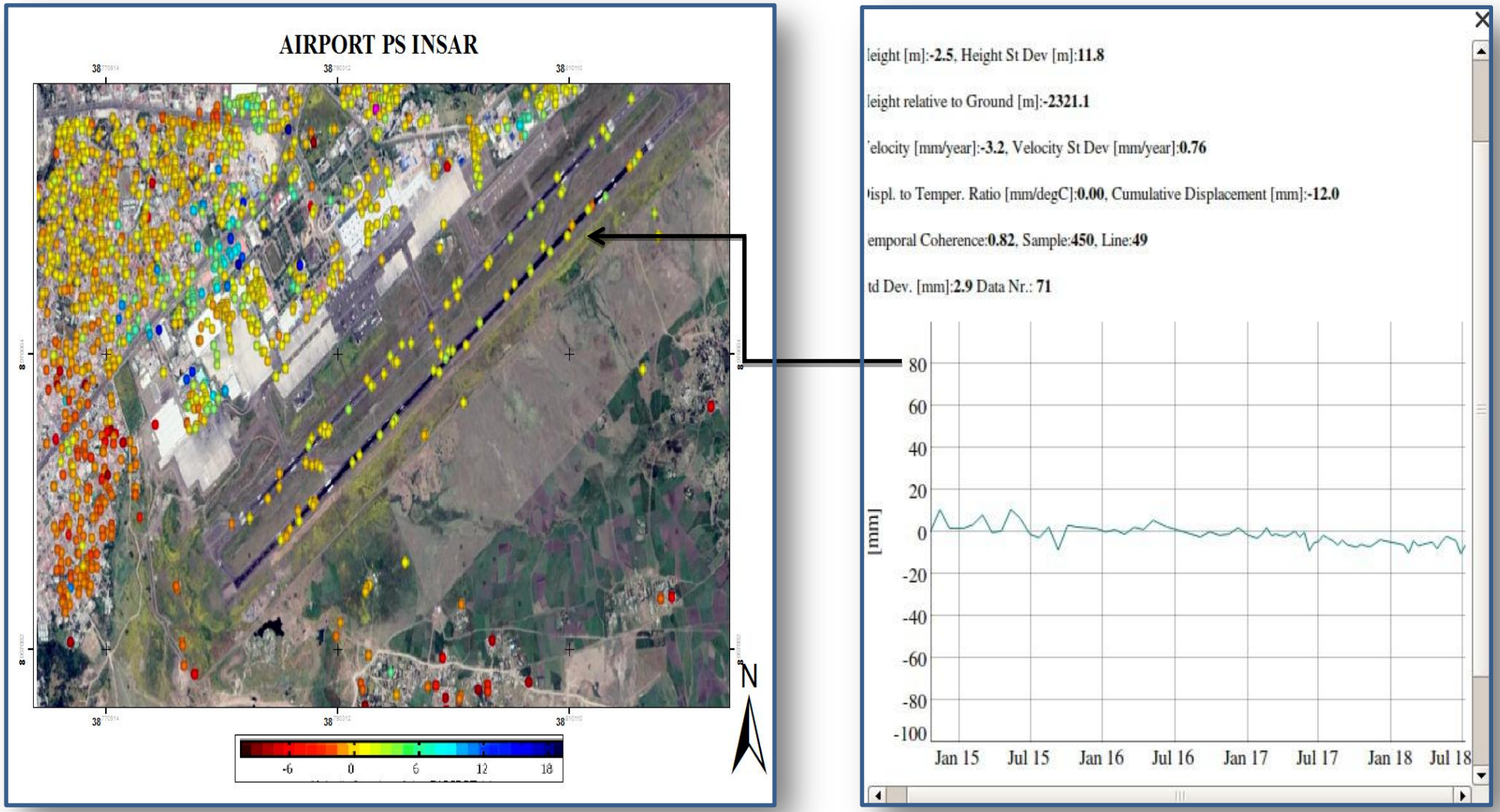


Fig 5.11 test site 2 deformation map and graph by PS approach of at Addis Ababa bole airport site

On these runway roads, we performed a deformation assessment throughout the PSI-based computation. then, as we can see in figure 5.11 there is a PS points lied on the runway roads and they indicate almost yellowish and some orange color the scale bar read as maximum PSI cumulative displacement -12 mm and minimum displacement 1.4mm. And also velocity of PSI is -3.2 mm/yr and 0.4mm/yr. Which means the runway is relatively severely subsidence and the structure are deformed trough time and also the graph shows not uniform level of deformation. But cross-compared these values with the surrounding bole area buildings the PS data show with red color that indicate crack pattern damages detected with 51mm cumulative displacement with PSI velocity level of estimated deformations and in some part of area the blue color indicated uplift area with maximum value 18 mm/yr.

## 5.5 VALIDATION

### 5.5.1 GPS Result

Like the above two test site studies in this validation site take small area demonstration using the previous methodology and can obtain relatively more stable ground motion and there is no structural instabilities occurred. The ps analysis show light blue bar and points which means in that specific location there is no uplifting or subsiding motion. But in some PS pointes relatively there is an earth science building PS velocity uplift 1.8 mm/yr and cumulative displacement 3.3 mm observed. So also in this area there is a contentious measurement GPS is install before 10 years ago and then we can compute a time series graph to validate the PS analysis in that location. Finally the result is shown at the figure 5.12 and 5.15 the time serious graph indicate easting and northing and up and down is at zero level which means there is no ground motion are done in that area.

Insar technique can catch an existing deformation moreover; deformation rate can be slightly different point to point in equi deformation area detected by insar .therefore the insar result must be validated through a more exact method such as GPS. In this study use one GPS station which is most effective surveying method for monitoring point wise deformation.

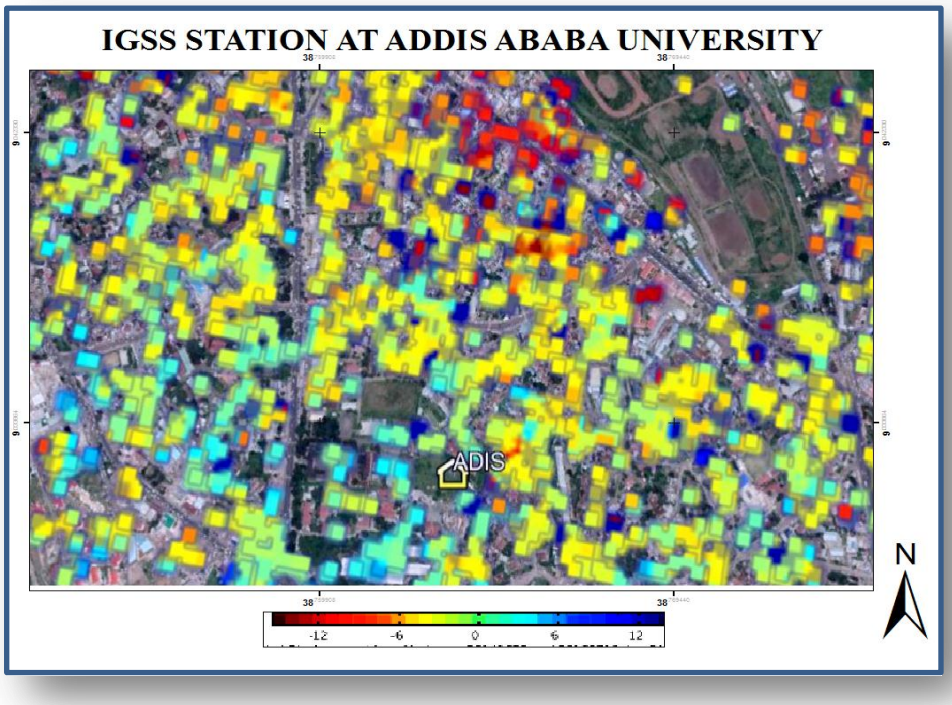


Fig 5.12 validation site deformation map by interferogram approach the IGSS station resampled displacement ascending way

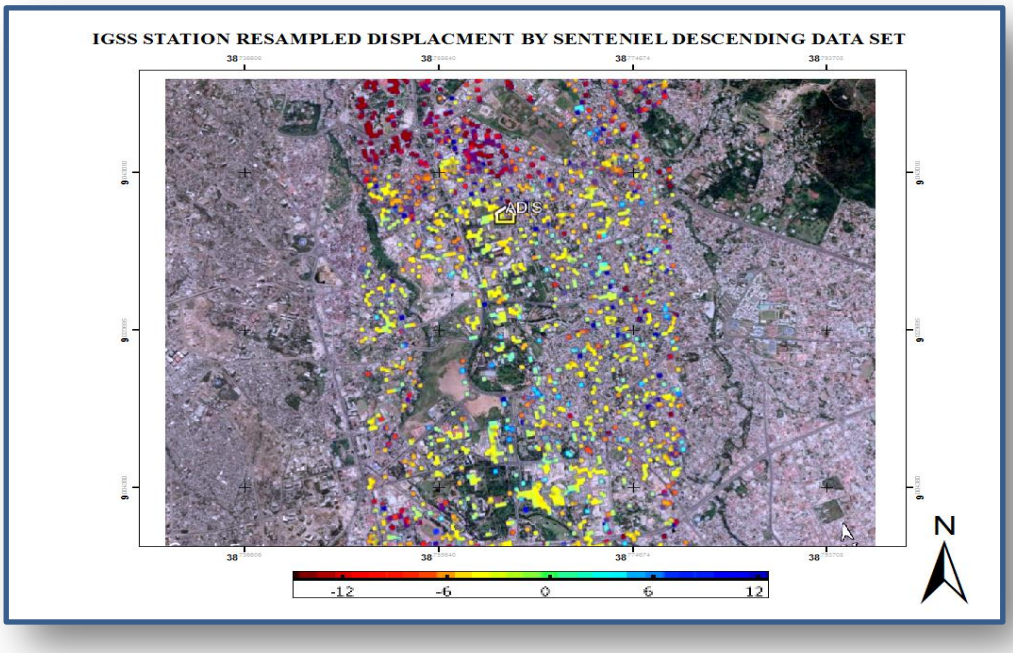


Fig 5. 13 validation site deformation map by interferogram approach the at IGSS resample displacement descending way

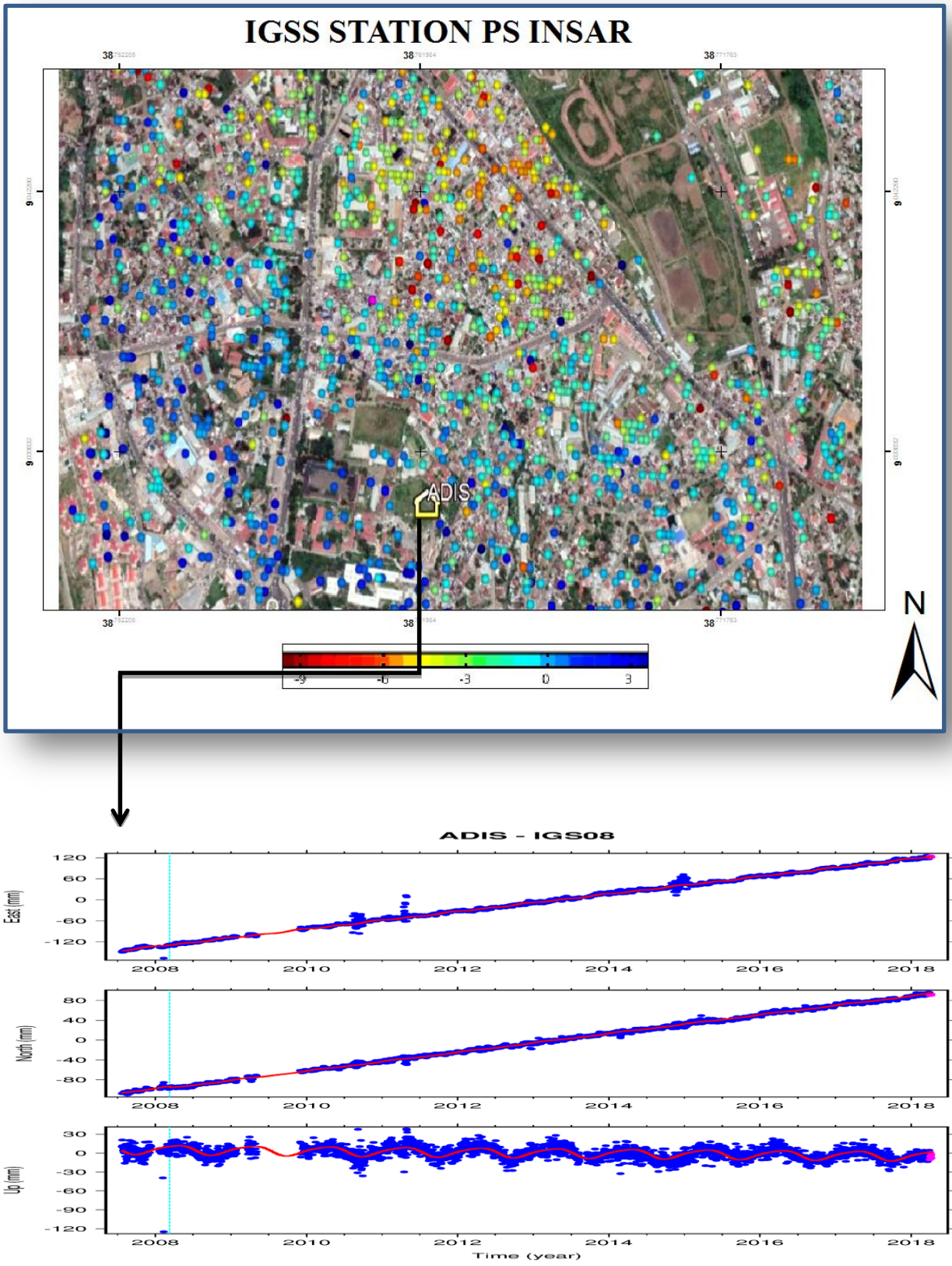


Fig 5.14 validation site deformation map and graph by PS approach of at Addis Ababa at IGSS station

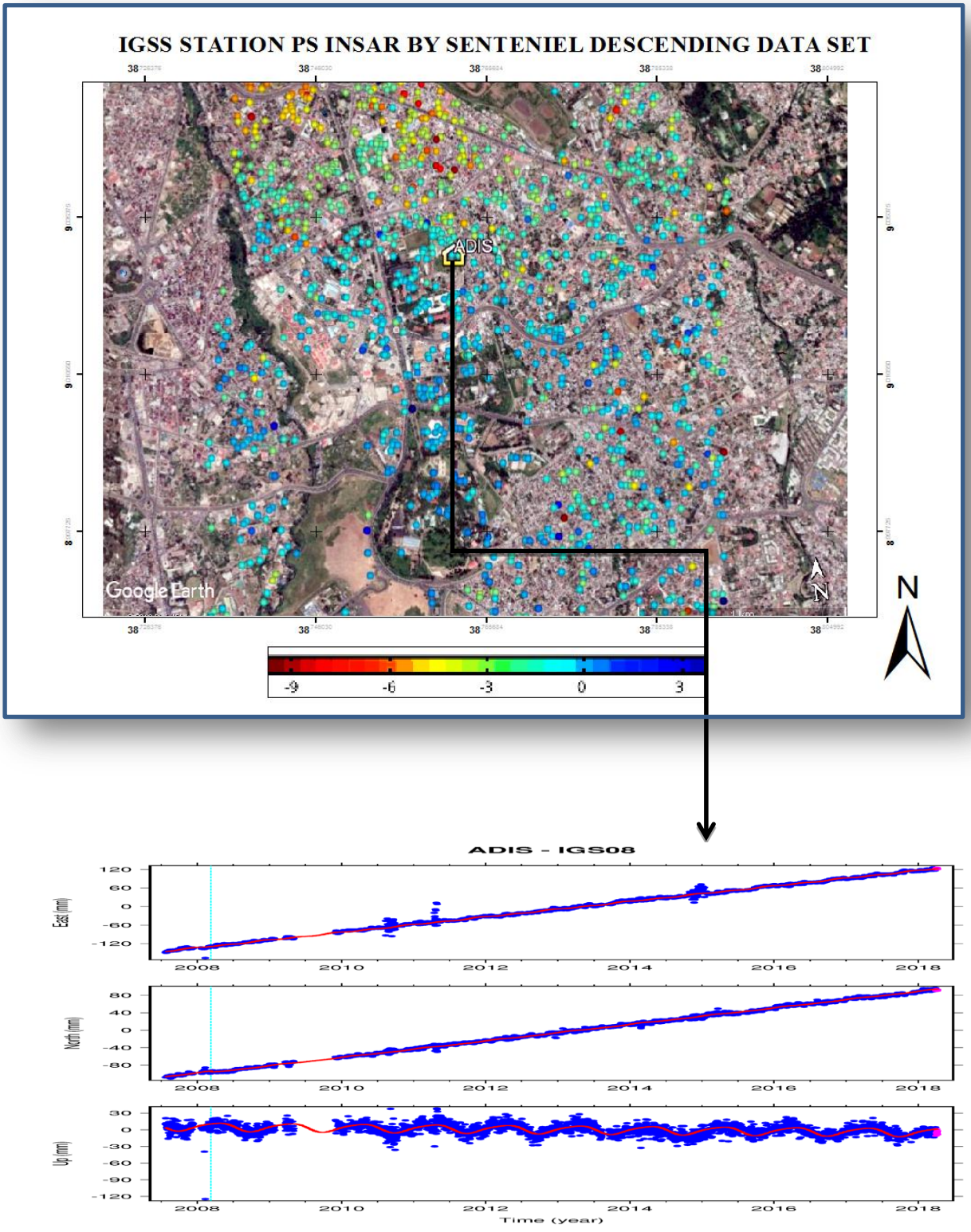


Fig 5.15 validation site deformation map and graph by PS approach of at Addis Ababa at IGSS station

### 5.5.2 Validation result

Results from the final analysis of displacement in the Addis Ababa University are presented in Table 4.For every year of the station GPS data; there are both cumulative displacements measured by the GPS and the displacement extracted from InSAR data. They were compared using OLS regression by using equation 3. Regression result between InSAR and GPS displacement of the at Addis Ababa campus is shown in Figure 5.16 The x-axis represents displacement from GPS, and the y-axis indicates displacement estimated by InSAR. The red line represents the linear regression result. The other points are some scatter and near this line, which shows that the regression equation y=56.099x- 6.830 fits these data closely. The linear correlation coefficient value r is 0.94 which means positive correlation and relative to close to the constant of 1, implying that the fit between InSAR measurements and GPS station is very high, meaning closely to the monitoring result. An analysis of the RMSE is 0.577, a value significantly lower than 1 indicating that the accuracy of InSAR reached the accuracy of near to ADIS GPS station.

Table 5.1 Detail analysis between GPS and INSAR five year displacement measurements

| year | GPS ADIS(DISPLACMENT) | INSAR(DISPLACMENT) |
|---|---|---|
| 2014 | 0.15 | 1.65 |
| 2015 | 0.14 | 0.45 |
| 2016 | 0.13 | 0.22 |
| 2017 | 0.13 | -2.13 |
| 2018 | 0.12 | -2.84 |

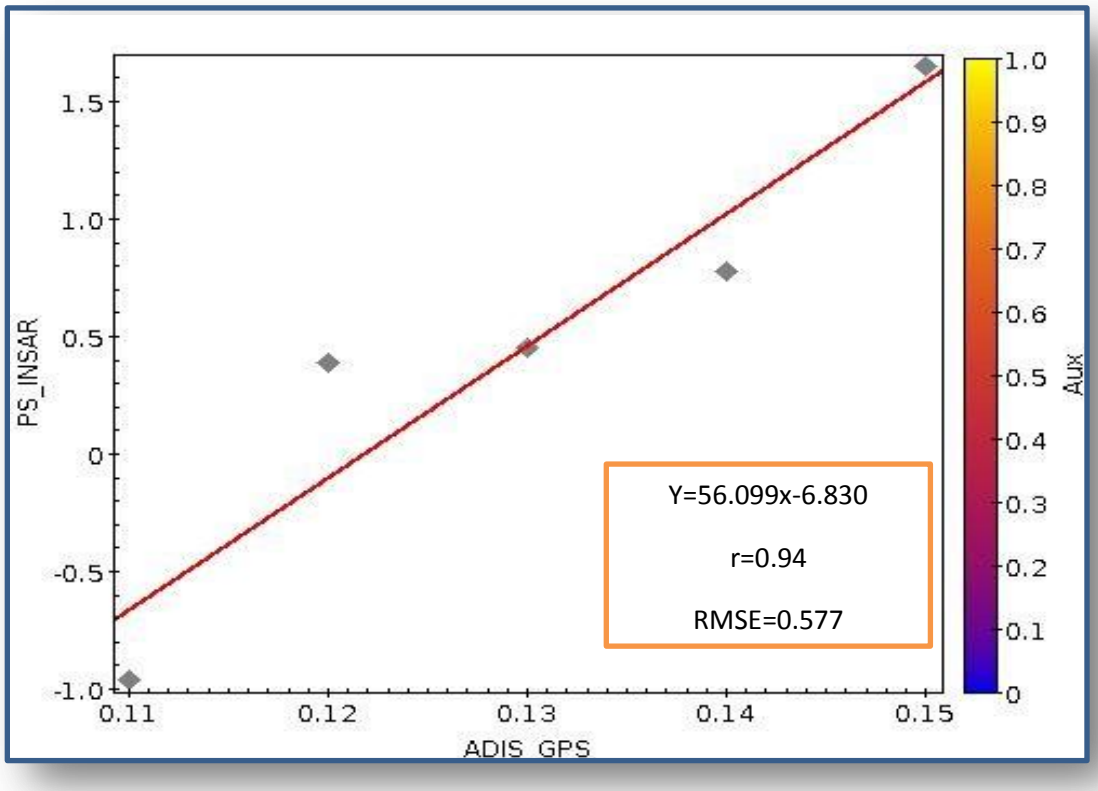


Fig 5.16 Validation result of ADIS GPS and PS_INSAR regression graph

An area presenting subsidence behavior was identified around presented subsiding behavior between 2014 and 2018 around 2 mm along and towards to -2.3mm the sensor LOS. Signs of noticeable displacements were not identified through the validation site. The GPS network designed using the InSAR velocity map is considered to be the most optimum one. An optimum GPS network is one including the minimum number of stations to minimize the costs while extracting the maximum information regarding the surface deformation. But in this study using one GPS station In order to evaluate the InSAR results, the GPS data can be used because of its high accuracy. The GPS data has the high temporal resolution while the InSAR measurements contain the high spatial resolution. As manmade structures are usually affected by phenomena such as thermal dilation, the behavior obtained through the PSI processing may be explained by the temperature causing the structure to dilate (going up or moving towards the sensor) Therefore, the joint use of the GPS and InSAR might be useful to interpret the deformation caused by the land subsidence. Nevertheless, the PSI technique proved to be useful to measure displacements on these infrastructures and may provide information for early warning systems.

# CHAPTER SIX

# 6. Conclusion and Recommendation

## 6.1 Conclusion

In this study the INSAR technique was used in order to determine the variation of structural deformation in the capital city of Addis Ababa caused by the land subsidence and some other factors. Our first finding of significance in this thesis was the discovery that large area and some test sites of small areas, in order to produce 22 descending image 10 interferogram between 2003-2010, 71 descending image 16 interferogram between 2014-2018 and 10 interferogram in ascending way in ENVISAT and SENTENEIL images respectively were used. The velocity map was then calculated using the stacking method. The minimum deformation rate uplift was 0 mm and the maximum deformation rate subsidence was estimated as -90mm for envisat, and finally minimum deformation rate was 3mm and maximum deformation rate was -9mm from sentinel data with in the study area the large area coverage. The other one is in this study the structural deformation yielded high quality INSAR data when processed using PSINSAR methods. PS-INSAR with high resolution SAR data allows a precise measurement of surface motions. Typically several PS point area found on a single building such a high PS density allows for an aggressive filtering of in coherent points. In dense urban environments, the number of PS points with multiple scattering centers is quite high however, movements detected on the surface by PSI data show the highest motion rates of the whole study area, reaching up to minimum velocity values of 3-4mm/yr and maximum displacement of about -9 up to -12 mm/yr at both data set with in large area coverage. As a result in the test site also found cumulative displacement -36.8mm and -10mm/yr that deformation was occurring in 2017 at koshe locations identified in test site1. This is a significant result in itself, when the city of Addis Ababa was monitor from the INSAR data. The result of INSAR analysis shows that the ground monitoring of an urban city can be performed with high precision. Moreover, detection of the parts where the collapse is expected to occur in the near future is also possible. The validation result of PSI and GPS station has a good agreement in vertical displacement with the correlation coefficient of 0.97 and RMSE error 0.577.The result here presented suggests that the INSAR technique can offer information useful to build up a monitoring and identification system. The reason of displacement in urban area, in this particular study area several factors can be considered to explain displacements. Among them, un stable huge amount of dump that is more fertilize the soil and subsurface structure, massive capacity of machine load and surface roughness, it should also be mentioned that the study area experiences. Therefore, using monitoring structural deformation observation and ground motion change can also be used for planning future. In these study area most part of the city is stable and no uplifting and subsidence are occurred, this

means that the city is suitable for huge project of infrastructure planning. But when we came to those test sites 1 and 2 there is severity of deformation may take place in the future.

## 6.2 RECOMMENDATION

The present study aims at structural monitoring of deformation using INSAR technique an approach of interferogram and time series PSINSAR. Considering the limitations in economics resources, importance of effective and reliable decision support tools that support the monitoring and management of infrastructure system cannot be over underlined. Therefore, radar satellite monitoring has the opportunity to increase the efficiency of such monitoring efforts. However, since radar technology has been emerging field in monitoring and management infrastructure, it is particularly important to investigate the potential of technology for highest benefits. Complexity of SAR image types and features require extra attention for evaluating the available and appropriate data sources for infrastructure monitoring. Besides the data selection, image processing should also be carried out carefully for accurate interpretation of resampled deformation and deformation velocities. INSAR based monitoring and data analysis end product might also be very helpful and cost saving for many other organization and agencies in the city. Therefore, cooperation and collaboration within and between organization and agencies will reduce the total cost of monitoring and INSAR data analysis efforts. As highlighted previously, although current methods and techniques are very practical for determining the location and severity at certain level of problems. But it needs further research and investigation, specifically on monitoring infrastructure. Such as:

1. Use to ground truth data sets observed from terrestrial methods, such as spirit leveling measurement and increase the availability of sufficient number of continuous measurement of GPS in order to validation of results.
2. In future for performing this kind of work increase number of datasets and improve quality of interferograms using different image pairs from different time span.
3. Make standardization on severity area by delineating and buffering zone for infrastructural activity.
4. Investigating the contribution of possible other products such as optical satellite imagery for improving the detection of location, severity and type of problems.
5. Evaluating these possibilities for different geological, surface structure and weather conditions

APPENDEX A .FIGURE

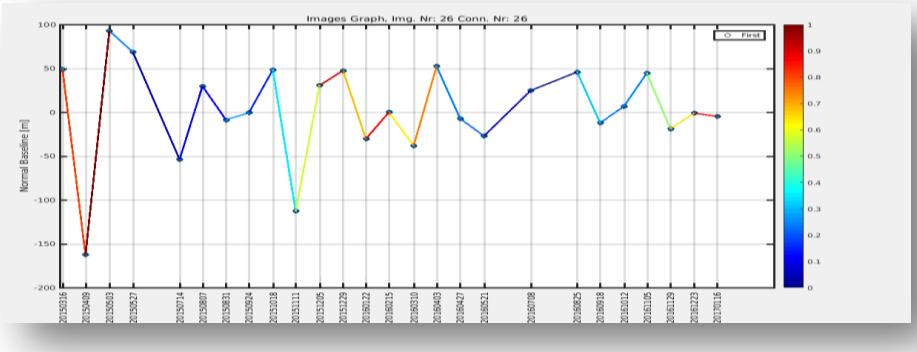


Figure A-1 sentinel ascending MST graph of with coherence value 26 image

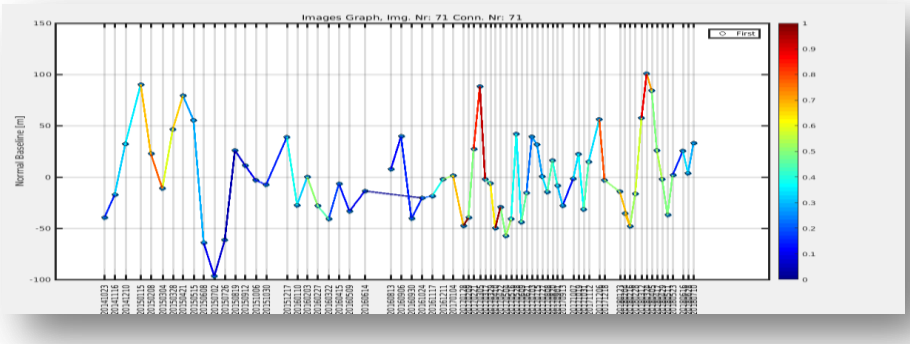


Figure A-2senteniel desending MST graph of with coherence value 71 image

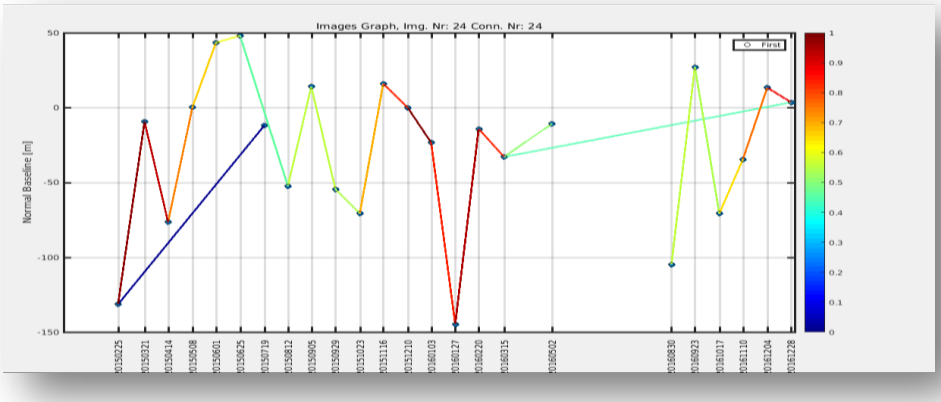


Figure A-3 sentinel ascending MST graph of with coherence value 24 image

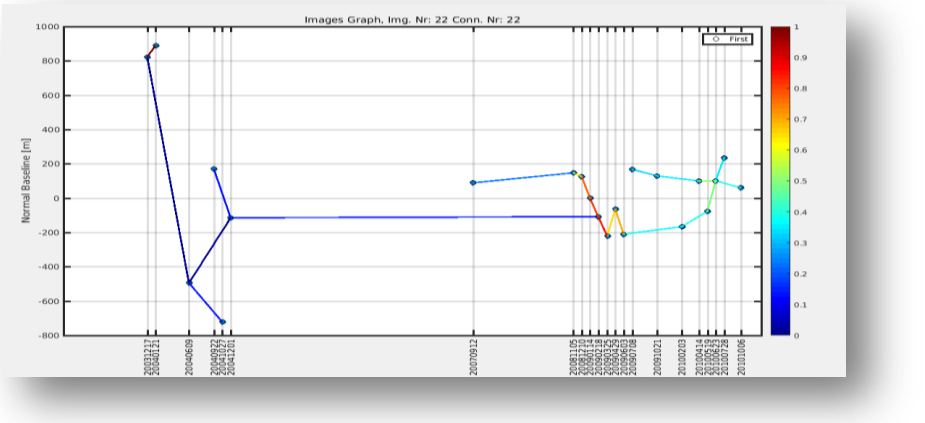


Figure A-4 ENVISAT descending MST graph of with coherence value 22 image

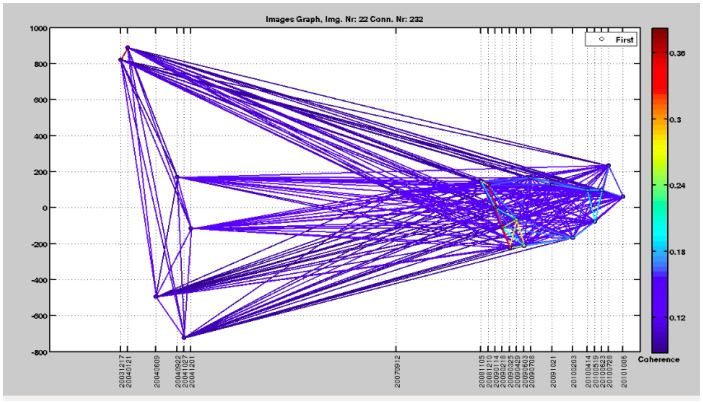


Figure A-5 Full graph of envisat no image 22 and each connect 222 image can create

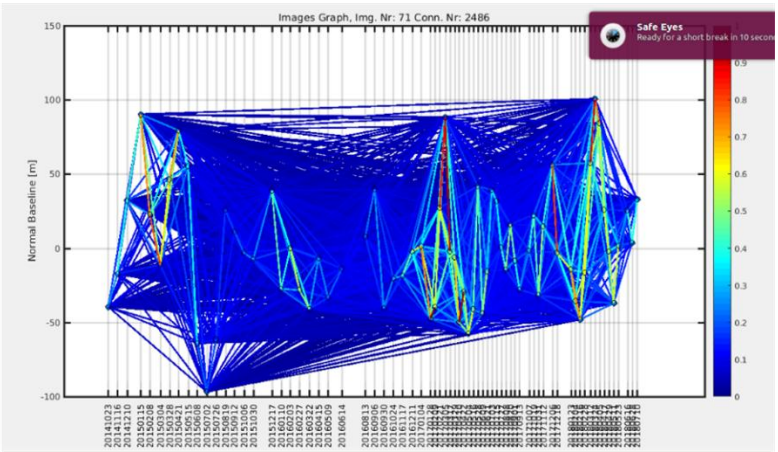


Figure A-6 Full graph of senteniel from descending no of image 71 and each connect 2486 image can create

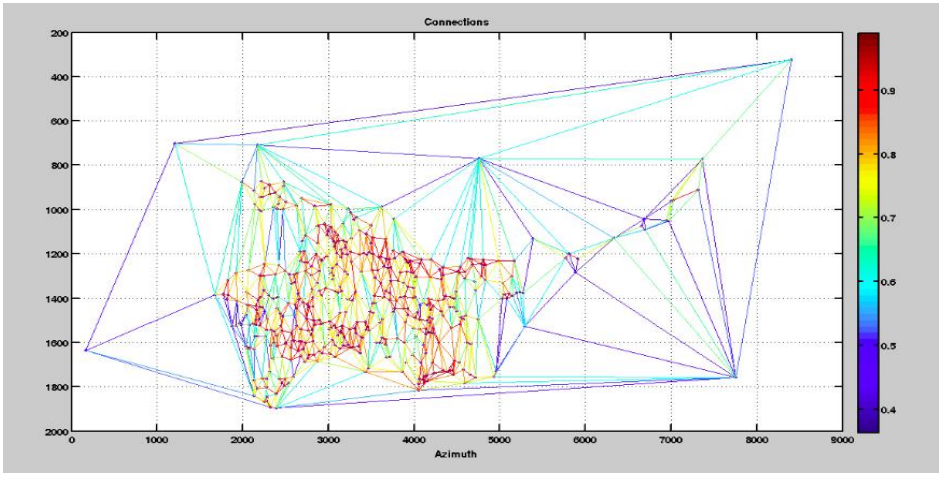


Figure A-7 Delunary graph of sentinel data set

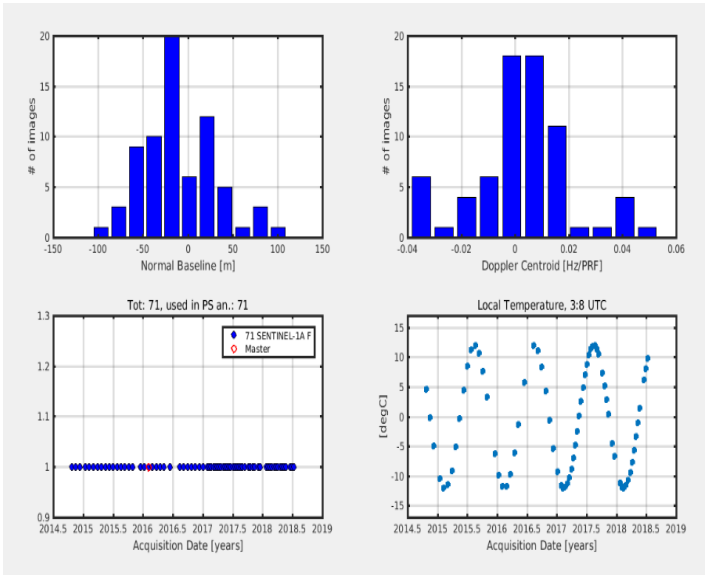


Figure A-8 Data statistics about sentinel dataset

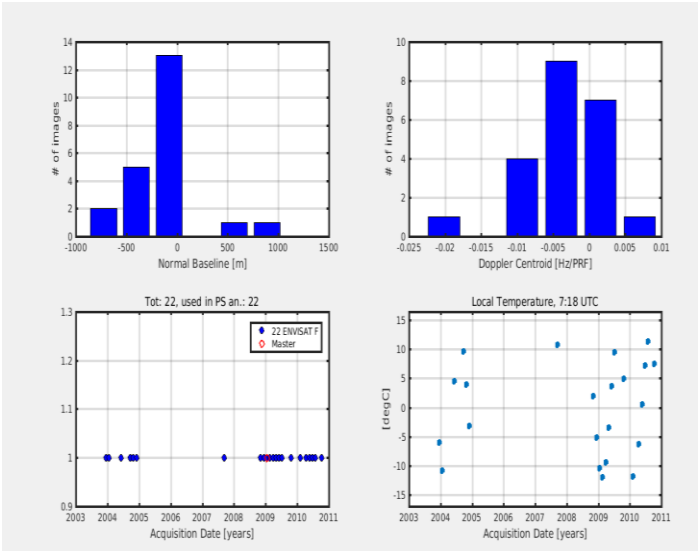


Figure A-9 Data statistics about envisat dataset

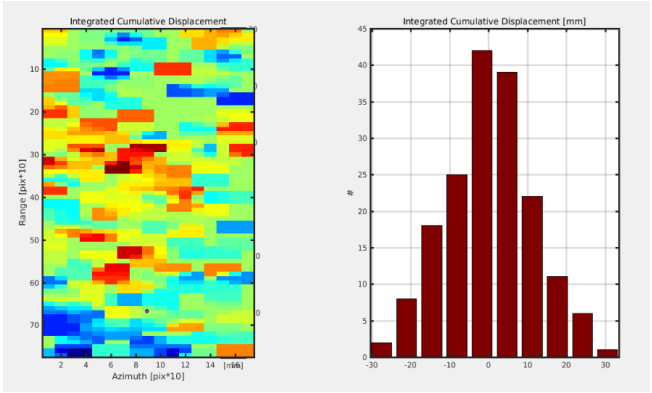


Figure A-10 APS removal in koshe test site integrated cumulative displacement in reference point at zero

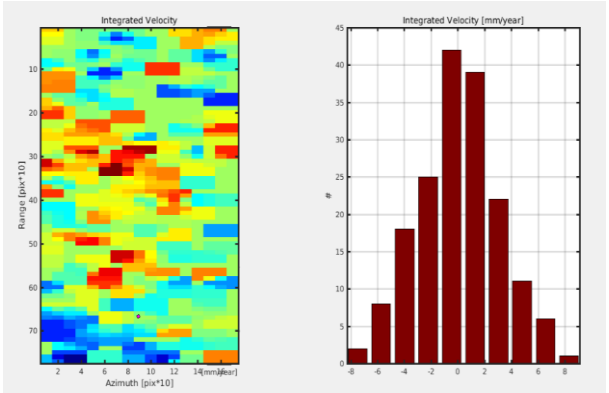


Figure A-11 APS removal in koshe test site integrated velocity in a reference point at zero

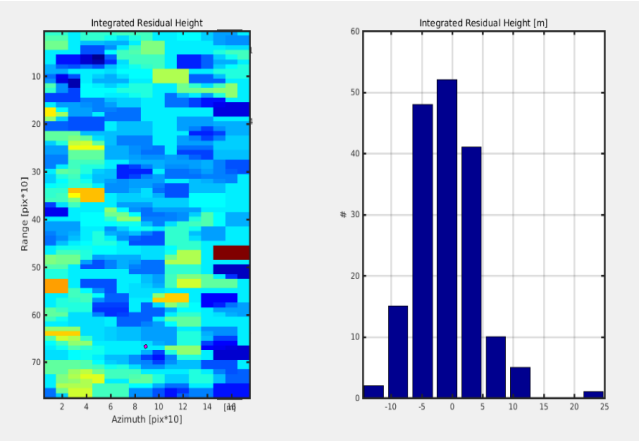


Figure A-12 APS removal at koshe test site

integrated hight at reference point at zero

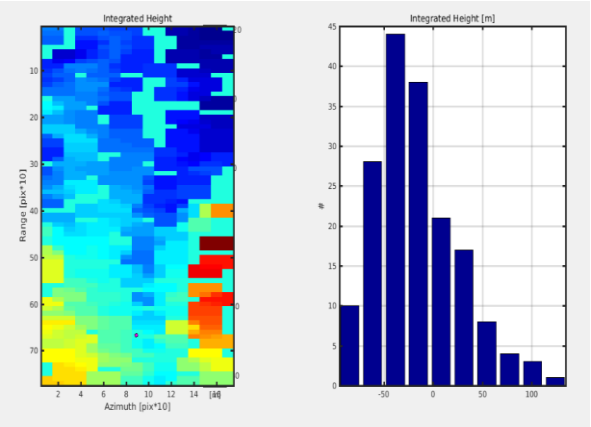


Figure A-13 APS removal in koshe test site

integrated residual height in reference point at zero

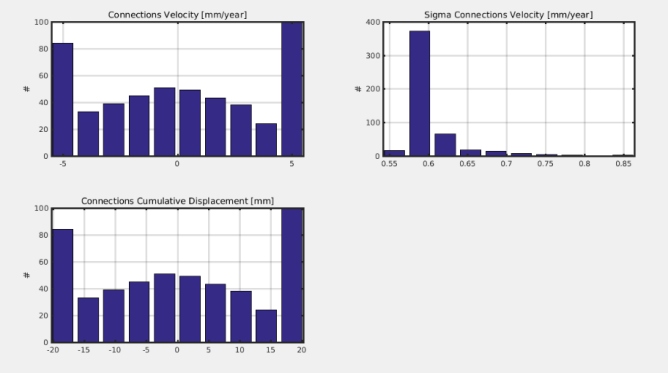


Figure A-14 APS removal in koshe test site connection velocity, sigma connection, connection cumulative at reference point

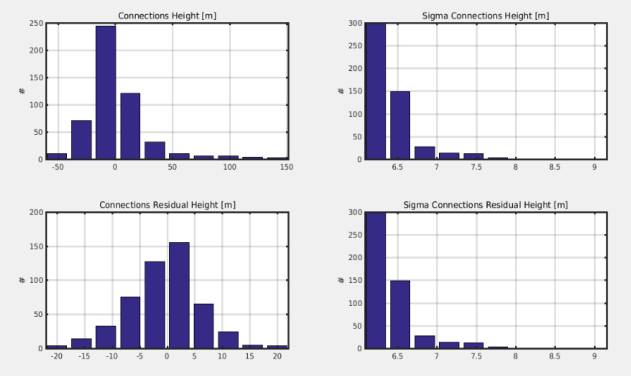


Figure A-15 APS removal in koshe test site connection height, sigma connection, connection residual and sigma connection residual height at reference point.

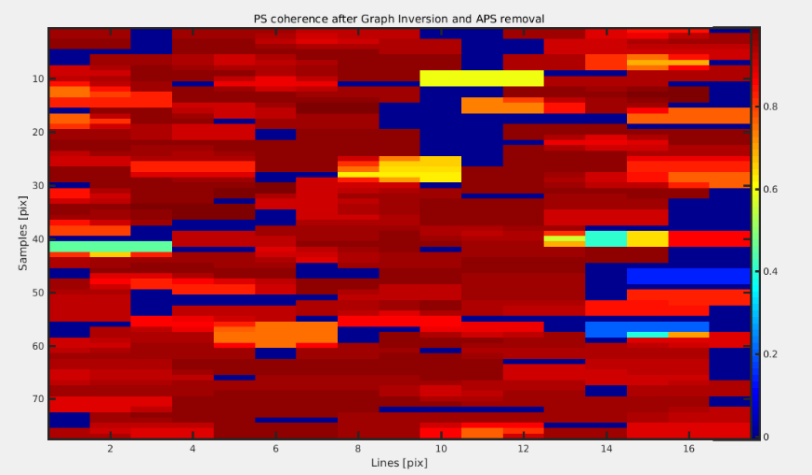


Figure A-16 The PS coherence after inversion and APS removal koshe test site

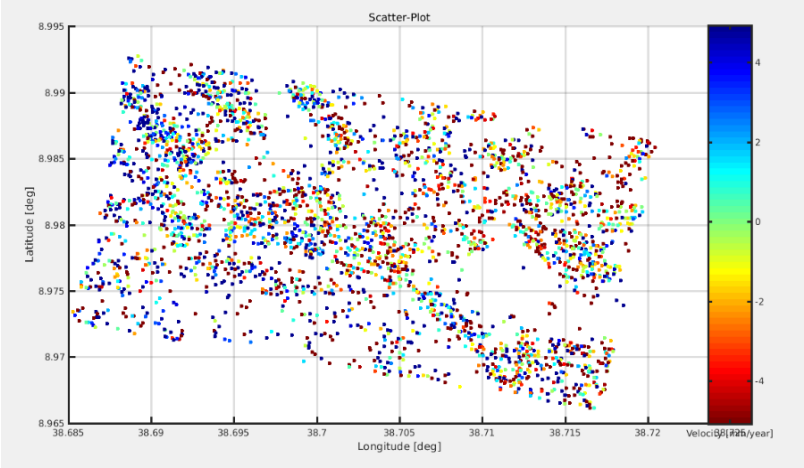


Figure A-17 PS candidate of scater plot of koshe test site

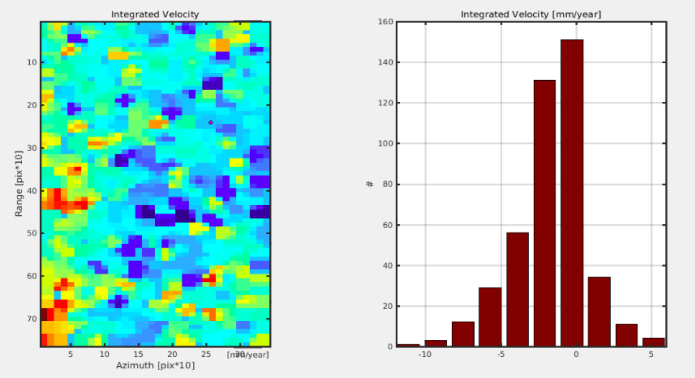


Figure A-18 APS removal at IGSS station integrated velocity reference point at zero

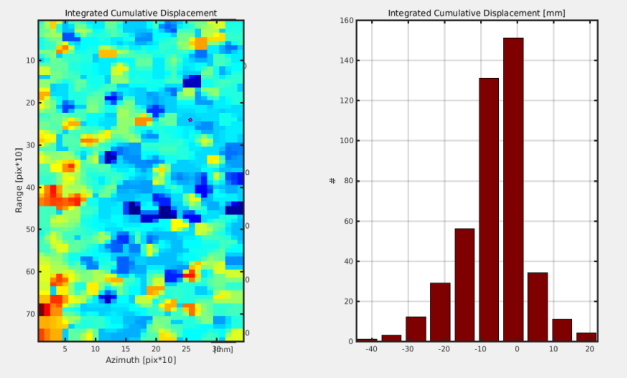


Figure A-19 APS removal at IGSS station integrated cumulative displacement reference point at zero.

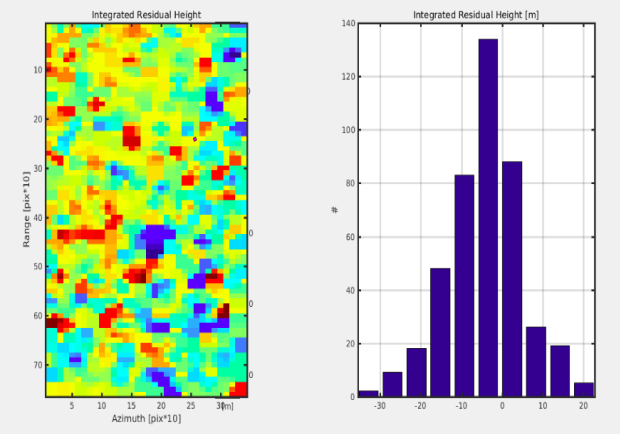


Figure A-20 APS removal at IGSS station integrated residual height reference point at zero

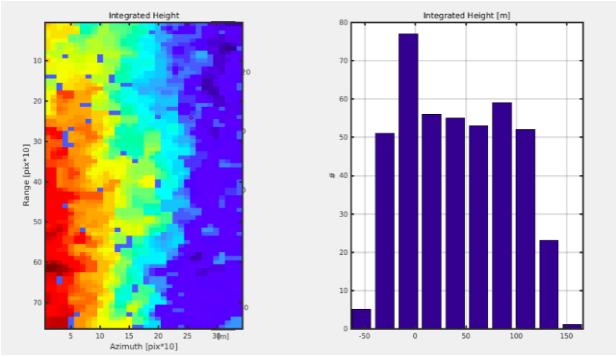


Figure A-21 APS removal at IGSS station integrated height reference point at zero

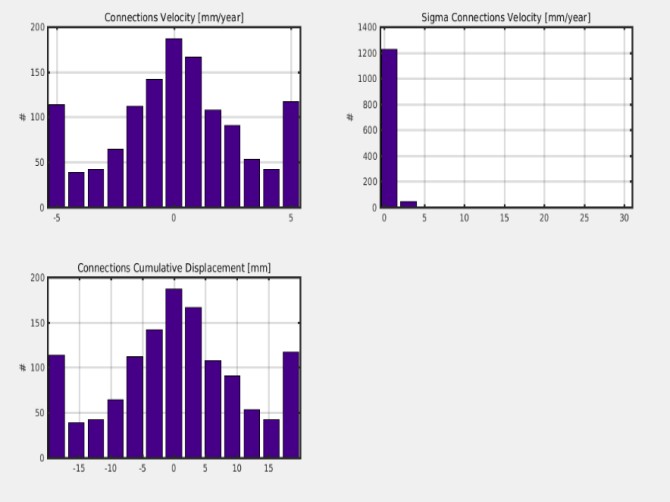


Figure A-22 APS removal at IGSS station connection velocity,sigma connection velocity and connection cumulative displacement reference point

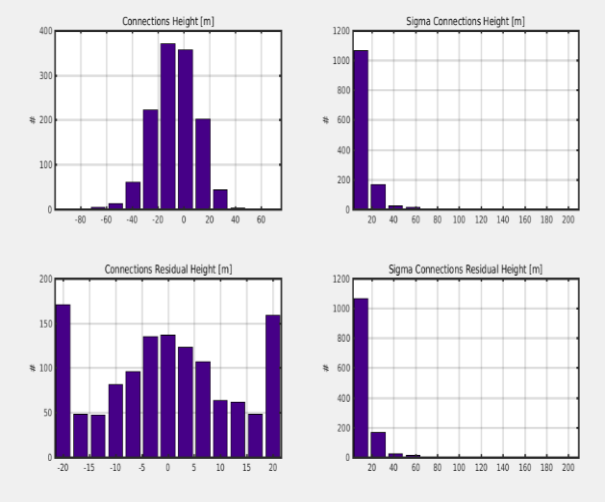


Figure A-23 APS removal at IGSS station Connection height, sigma connection height, connection residual height and sigma connection residual height reference point.

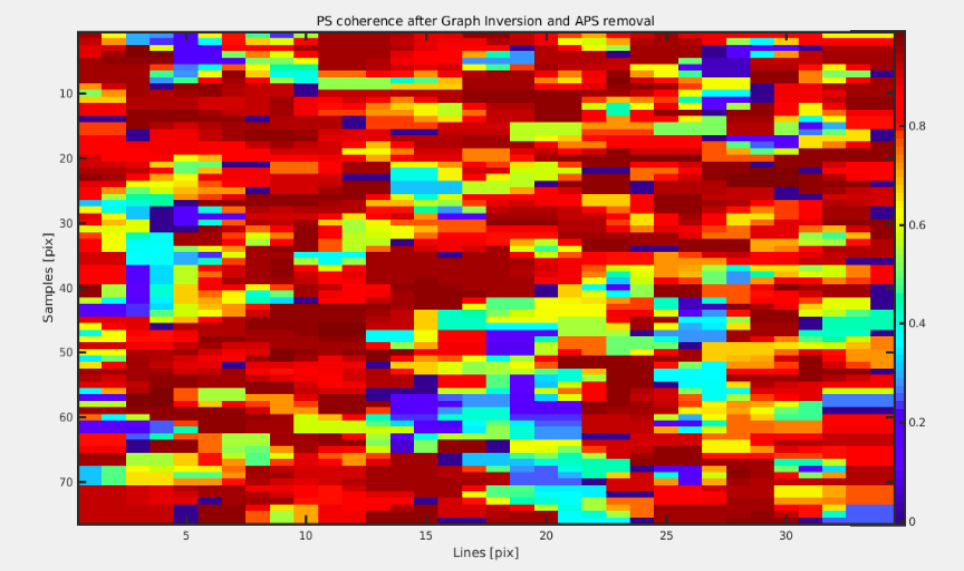


Figure A-24 The PS coherence after inversion and APS removal at IGSS station

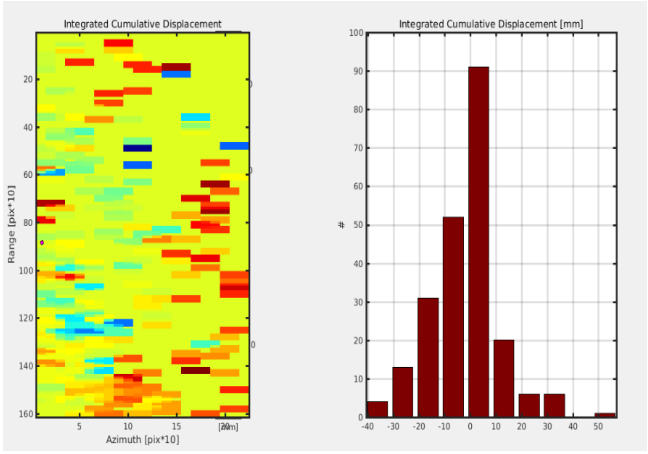


Figure A-25 APS removal at AIR PORT test siteintegrated site

cumulative displacement reference point at zero

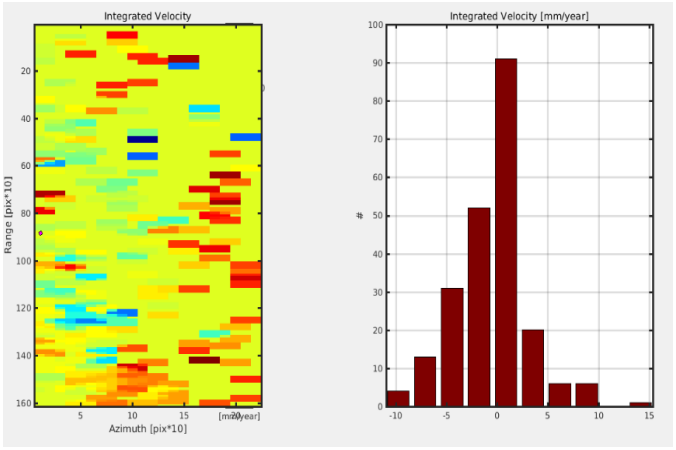


Figure A-26 APS removal at AIR PORT test

integrated velocity reference point at zero

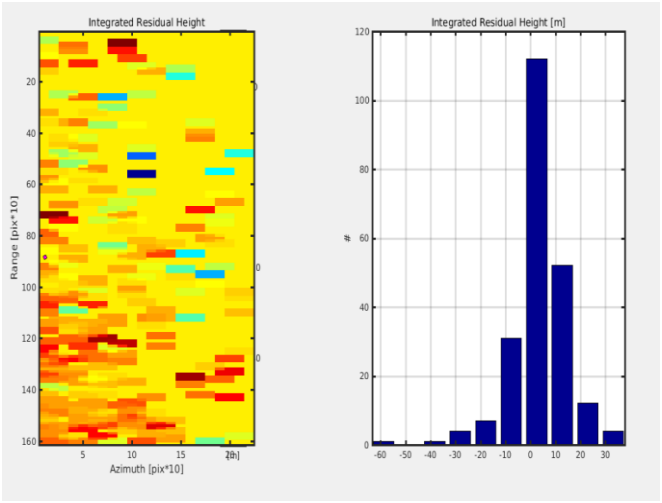


Figure A-27 APS removal at AIR PORT test site

integrated residual height reference point at zero

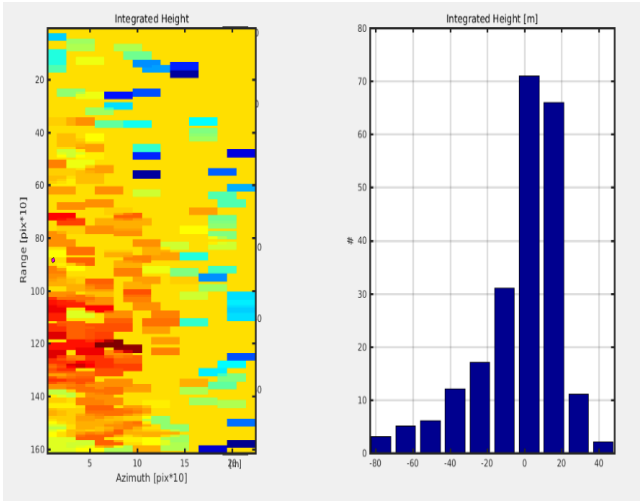


Figure A-28 APS removal at AIR PORT test site

integrated height reference point at zero

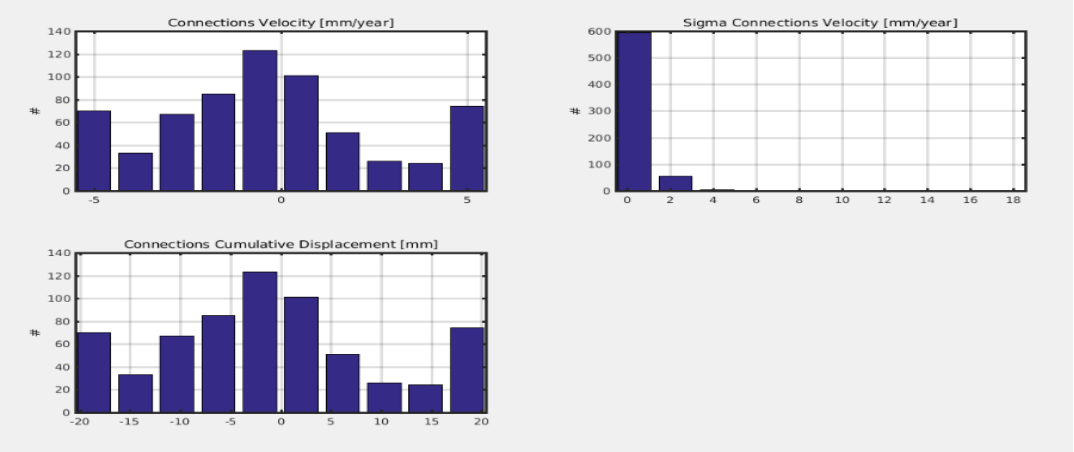


Figure A-29 APS removal at AIR PORT test site connection velocity, sigma connection velocity and connection cumulative displacement at reference point

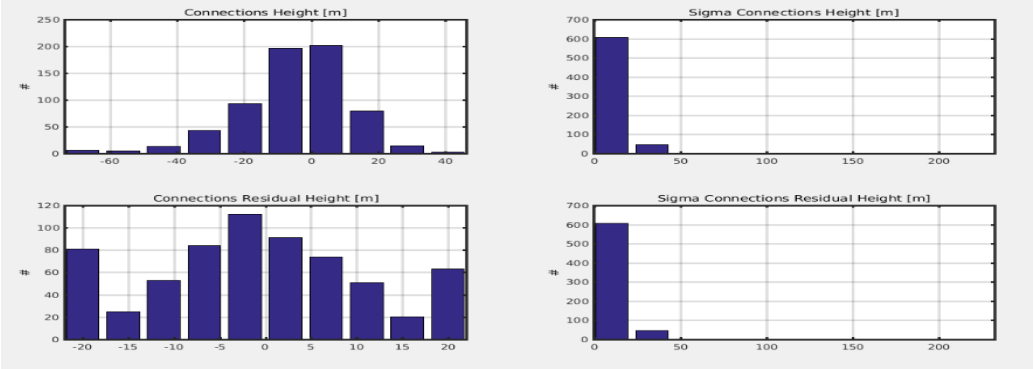


Figure A-30 APS removal at AIR PORT test site connection height, sigma connection height, connection residual height and sigma connection residual height reference point.

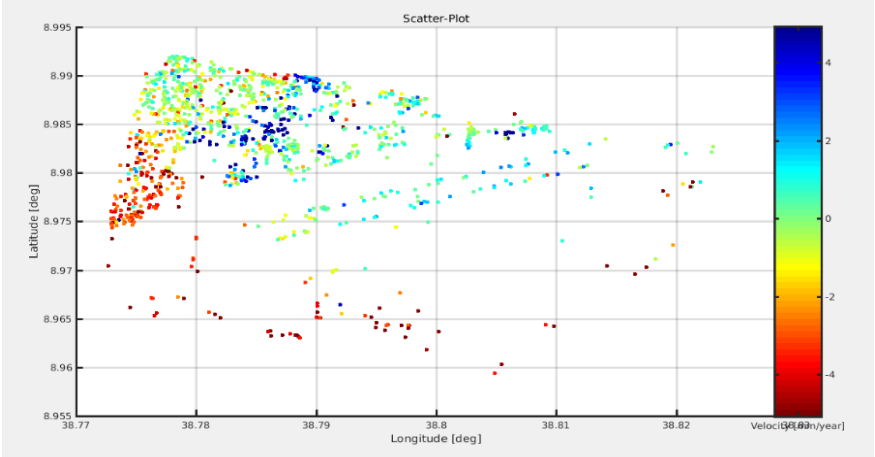


Figure A-31 PS candidate of scatter plot of AIR PORT test site

APPENDEX B TABLE

Dataset information on data acquisition sentinel Descending 71 image

| | Date | Polarization | B (Perpendicular base line) | T (Temporal base line) | $H_a$ (Height ambiguity) |
|---|---|---|---|---|---|
| 1 | 20141023 | VV | -39.470641 | -467.999974 | 0.028923 |
| 2 | 20141116 | VV | -17.309231 | -443.999980 | -0.034344 |
| 3 | 20141210 | VV | 32.072839 | -419.999992 | -0.041473 |
| 4 | 20150115 | VV | 90.234018 | -384.000005 | 0.020037 |
| 5 | 20150208 | VV | 22.597664 | -360.000011 | 0.118537 |
| 6 | 20150304 | VV | -11.150505 | -336.000010 | 0.022129 |
| 7 | 20150328 | VV | 46.293767 | -312.000004 | 0.030815 |
| 8 | 20150421 | VV | 79.318313 | -287.999995 | 0.035298 |
| 9 | 20150515 | VV | 55.324855 | -263.999981 | -0.025786 |
| 10 | 20150608 | VV | -64.209253 | -239.999958 | 0.099568 |
| 11 | 20150702 | VV | -96.832324 | -215.999953 | -0.030228 |
| 12 | 20150726 | VV | -61.673956 | -191.999937 | 0.030409 |
| 13 | 20150819 | VV | 25.951966 | -167.999922 | 0.044041 |
| 14 | 20150912 | VV | 11.288799 | -143.999911 | 0.074559 |
| 15 | 20151006 | VV | -3.094894 | -119.999905 | 0.051360 |
| 16 | 20151030 | VV | -7.537561 | -95.999906 | 0.026723 |
| 17 | 20151217 | VV | 38.807027 | -47.999986 | -0.005162 |
| 18 | 20160110 | VV | -27.407928 | -23.999930 | -0.002808 |
| 19 | 20160203 | VV | 0.000000 | 0.000000 | 0.028158 |
| 20 | 20160227 | VV | -28.170951 | 23.999997 | 0.004084 |
| 21 | 20160322 | VV | -40.929997 | 48.000002 | 0.013833 |
| 22 | 20160415 | VV | -6.670294 | 72.000012 | -0.025856 |
| 23 | 20160509 | VV | -33.338808 | 96.000025 | -0.029242 |
| 24 | 20160614 | VV | -13.754875 | 132.000081 | -0.013486 |
| 25 | 20160813 | VV | 7.604881 | 192.000118 | 0.058069 |
| 26 | 20160906 | VV | 39.563095 | 216.000130 | 0.049034 |
| 27 | 20160930 | VV | -40.651022 | 240.000108 | 0.056093 |
| 28 | 20161024 | VV | -20.502995 | 264.000108 | 0.053979 |
| 29 | 20161117 | VV | -18.462889 | 288.000104 | 0.027400 |
| 30 | 20161211 | VV | -2.370958 | 312.000097 | 0.058096 |
| 31 | 20170104 | VV | 1.403839 | 336.000074 | 0.042496 |
| 32 | 20170128 | VV | -47.593833 | 360.000067 | 0.022540 |
| 33 | 20170209 | VV | -39.743514 | 372.000193 | 0.125119 |
| 34 | 20170221 | VV | 27.225209 | 384.000190 | 0.126774 |
| 35 | 20170305 | VV | 88.402427 | 396.000189 | 0.116630 |
| 36 | 20170317 | VV | -2.165513 | 408.000192 | 0.067552 |
| 37 | 20170329 | VV | -6.268474 | 420.000195 | 0.042759 |
| 38 | 20170410 | VV | -49.885236 | 432.000201 | 0.030139 |
| 39 | 20170422 | VV | -29.179355 | 444.000208 | 0.071491 |
| 40 | 20170504 | VV | -57.590299 | 456.000215 | 0.055216 |
| 41 | 20170516 | VV | -41.035311 | 468.000222 | 0.030527 |
| 42 | 20170528 | VV | 41.824992 | 480.000228 | 0.034014 |

| | | | | | |
|---|---|---|---|---|---|
| 43 | 20170609 | VV | -44.199865 | 492.000238 | 0.033127 |
| 44 | 20170621 | VV | -15.436181 | 504.000246 | 0.008548 |
| 45 | 20170703 | VV | 39.118411 | 516.000253 | 0.024217 |
| 46 | 20170715 | VV | 31.541197 | 528.000261 | 0.036549 |
| 47 | 20170727 | VV | 0.396086 | 540.000270 | 0.064219 |
| 48 | 20170808 | VV | -14.480809 | 552.000277 | 0.033140 |
| 49 | 20170820 | VV | 16.123940 | 564.000284 | 0.052757 |
| 50 | 20170901 | VV | -8.351779 | 576.000290 | 0.049428 |
| 51 | 20170913 | VV | -27.839658 | 588.000295 | 0.124398 |
| 52 | 20171007 | VV | -1.570199 | 612.000302 | 0.054368 |
| 53 | 20171019 | VV | 22.495186 | 624.000304 | 0.040547 |
| 54 | 20171031 | VV | -31.743157 | 636.000305 | 0.069322 |
| 55 | 20171112 | VV | 14.959718 | 648.000301 | 0.071841 |
| 56 | 20171206 | VV | 56.200425 | 672.000292 | 0.044136 |
| 57 | 20171218 | VV | -3.050972 | 684.000289 | 0.041319 |
| 58 | 20180123 | VV | -14.437547 | 720.000273 | 0.044741 |
| 59 | 20180204 | VV | -35.687049 | 732.000269 | 0.028701 |
| 60 | 20180216 | VV | -48.197636 | 744.000267 | 0.086908 |
| 61 | 20180228 | VV | -16.441402 | 756.000266 | 0.064430 |
| 62 | 20180312 | VV | 57.423788 | 768.000267 | 0.060188 |
| 63 | 20180324 | VV | 100.721580 | 780.000268 | 0.046724 |
| 64 | 20180405 | VV | 84.261831 | 792.000271 | 0.071907 |
| 65 | 20180417 | VV | 26.018740 | 804.000277 | 0.070184 |
| 66 | 20180429 | VV | -2.205507 | 816.000284 | 0.058464 |
| 67 | 20180511 | VV | -37.079198 | 828.000291 | 0.066452 |
| 68 | 20180523 | VV | 1.985873 | 840.000299 | 0.056273 |
| 69 | 20180616 | VV | 25.268368 | 864.000316 | 0.021613 |
| 70 | 20180628 | VV | 3.797810 | 876.000324 | 0.044829 |
| 71 | 20180710 | VV | 32.989143 | 888.000330 | 0.041016 |

Table B-1 Dataset information sentinels descending on swath 1 their perpendicular and baseline information.

Dataset information on data acquisition sentinel ascending swath_3 27 image

| Date | Polarization | B (Perpendicular base line) | T (Temporal base line) | $H_a$ (Height ambiguity) |
|---|---|---|---|---|
| 1 | 20150316 | VV | 48.747706 | -336.000004 | 0.051935 |
| 2 | 20150409 | VV | -162.444940 | -312.000000 | 0.005550 |
| 3 | 20150503 | VV | 92.812254 | -287.999980 | 0.024161 |
| 4 | 20150527 | VV | 68.842749 | -263.999964 | 0.032500 |
| 5 | 20150714 | VV | -53.783950 | -215.999944 | 0.052750 |
| 6 | 20150807 | VV | 29.701572 | -191.999926 | 0.066663 |
| 7 | 20150831 | VV | -8.572228 | -167.999913 | -0.021126 |
| 8 | 20150924 | VV | -0.434116 | -143.999905 | -0.028454 |
| 9 | 20151018 | VV | 48.446279 | -119.999901 | 0.071570 |
| 10 | 20151111 | VV | -112.604103 | -95.999971 | 0.023211 |

| | | | | | |
|---|---|---|---|---|---|
| 11 | 20151205 | VV | 30.742599 | -71.999975 | 0.065709 |
| 12 | 20151229 | VV | 47.270646 | -47.999986 | 0.035700 |
| 14 | 20160122 | VV | -30.378792 | -23.999995 | 0.066657 |
| 15 | 20160215 | VV | 0.000000 | 0.000000 | 0.057220 |
| 16 | 20160310 | VV | -38.052947 | 23.999999 | -0.007836 |
| 17 | 20160403 | VV | 52.408785 | 48.000010 | -0.017865 |
| 18 | 20160427 | VV | -7.273218 | 72.000020 | 0.019461 |
| 19 | 20160521 | VV | -27.053676 | 96.000067 | -0.018496 |
| 20 | 20160708 | VV | 24.861974 | 144.000132 | 0.094693 |
| 21 | 20160825 | VV | 45.865912 | 192.000129 | 0.043048 |
| 22 | 20160918 | VV | -12.186163 | 216.000139 | 0.066004 |
| 23 | 20161012 | VV | 6.819149 | 240.000142 | 0.014944 |
| 24 | 20161105 | VV | 44.671930 | 264.000141 | -0.013160 |
| 25 | 20161129 | VV | -18.817604 | 288.000136 | 0.116471 |
| 26 | 20161223 | VV | -1.032724 | 312.000127 | 0.047942 |
| 27 | 20170116 | VV | -4.727721 | 336.000103 | 0.044896 |

Table B-2 Dataset information sentinels ascending on swath 3 their perpendicular and baseline information.

| Date | Polarization | | B (Perpendicular base line) | T (Temporal base line) | $H_a$ (Height ambiguity) |
|---|---|---|---|---|---|
| 1 | 20150225 | VV | -131.358447 | -288.000033 | 0.077908 |
| 2 | 20150321 | VV | -9.321145 | -264.000025 | 0.040270 |
| 3 | 20150414 | VV | -76.526754 | -240.000018 | 0.081038 |
| 4 | 20150508 | VV | 0.407096 | -216.000001 | 0.074635 |
| 5 | 20150601 | VV | 43.365037 | -191.999983 | -0.002775 |
| 6 | 20150625 | VV | 48.097862 | -167.999966 | 0.082222 |
| 7 | 20150719 | VV | -11.885068 | -143.999962 | 0.079870 |
| 8 | 20150812 | VV | -52.398901 | -119.999946 | 0.004967 |
| 9 | 20150905 | VV | 14.004605 | -95.999934 | -0.010683 |
| 10 | 20150929 | VV | -54.510388 | -71.999927 | -0.023231 |
| 11 | 20151023 | VV | -70.690412 | -47.999926 | 0.019506 |
| 12 | 20151116 | VV | 16.011235 | -23.999992 | 0.051144 |
| 13 | 20151210 | VV | 0.000000 | 0.000000 | 0.038818 |
| 14 | 20160103 | VV | -23.428948 | 24.000085 | 0.034859 |
| 15 | 20160127 | VV | -144.765903 | 47.999977 | 0.046609 |
| 16 | 20160220 | VV | -14.201965 | 71.999977 | 0.075929 |
| 17 | 20160315 | VV | -32.985205 | 95.999980 | 0.053639 |
| 18 | 20160502 | VV | -10.726129 | 144.000000 | 0.016307 |
| 19 | 20160830 | VV | -104.810184 | 264.000106 | 0.040258 |
| 20 | 20160923 | VV | 27.141207 | 288.000118 | 0.052477 |
| 21 | 20161017 | VV | -70.787888 | 312.000119 | 0.103384 |
| 22 | 20161110 | VV | -34.714954 | 336.000117 | 0.042086 |
| 23 | 20161204 | VV | 13.322737 | 360.000111 | 0.070458 |
| 24 | 20161228 | VV | 3.522284 | 384.000102 | 0.107944 |

Table B-3 Dataset information sentinels ascending on swath 1 their perpendicular and baseline information.

APPENDEX C websites

The following websites are listed here as a reference.

Alaska satellite facility vertex: http://www.asf.alaska.edu/sar-data/palsar/about-palsar/

ASAR Auxiliary Data Files: http://earth.esa.int/services/auxiliary_data/asar/

DEOS: http://www.deos.tudelft.nl/ers/precorbs/orbits/

EOLi: http://earth.esa.int/EOLi/EOLi.html

Sarproz licence: licensing@sarproz.com

UNISDR, 1999...study area: https://gprs.unops.org/pages/viewvacancy/VADetails.aspx?id=6060

## REFERENCE


Alem Tesfahunegn Construction and Building Design Enterprise – Ethiopia.

Alemayehu Teferra and Solomon Yohannes 1986 Investigations on the expansive soils of Addis Ababa.

Amy L.Parker, will E .Featherstone, Nigel T.penna, Mick S .Filmer and Mathew C.gathwaite. 2017 Practical consideration before installing ground based infrastructure for integrated InSAR and GNSS monitoring of Vertical land motion sensors, 17(8):1-20.

Amelung F.,D.L. Galloway J.W.Bell. A Zebker and R.J. Laczniak(1999). Sensing the ups and downs of Las Vegas : InSAR reveals structural control of land subsidence and aquifer system deformation, geology , 27(6),483-486.

Andrew Hooper 2008, A multi-temporal InSAR method incorporating both persistent scatterer and small baseline approaches.

Andrea Ciampalini,Federica Bardi, Silvia Bianchini, William Frodella, Chiara Del Ventisette, Sandro Moretti, and Nicola Casagli, Int J Appl Earth Obs Geoinf. 2014 Dec Analysis of building deformation in landslide area using multisensor PSInSAR™ technique, 33:166–180.doi: 10.1016/j.jag.2014.05.011

Alessandro Ferretti, Claudio Prati, and Fabio Rocca 2001, Permanent Scatterers in SAR Interferometry.

A Ferretti, D. Colombo, A. Fumagalli, F. Novali, and A. Rucci 2015, InSAR data for monitoring land subsidence.

Beth Ann Wisely and David Schmidt 2010, Deciphering vertical deformation and poroelastic parameters in a tectonically active fault-bound aquifer using InSAR and well level data, San Bernardino basin, California.

Buis, A. and J.D . Harrington ()2014 that sinking feeling , resenting JPL, Caltech no. 2014-073.

Burgmann, R,P.A. Rosen, and E.J. Fielding (2000), synthetic aperture radar interferometry to measure earth's surface topography and its deformation , annual review of earth and planetary science, 28(1),169-209.

C. Prati, A. Ferretti, D. Perissin 2011, Recent Advances on Surface Ground Deformation Measurement by means of Repeated Space-borne SAR Observations.

Cathleen E. Jones, Ph.D. 2017 Land subsidence measurements using airborne radar Impact to water conveyance infrastructure.

Carnec,c., and c. delacourt(2000), three years of mining subsidence monitored by SAR interferometry , near Garanne , France , jouranal of applied geophysics 43(1),43-54.

Cheng-sheng Yang ,Qin Zhang ,Qiang Xu ,Chao-ying Zhao ,Jian-bing Peng andLing-yun Ji Complex Deformation Monitoring over the Linfen–Yuncheng Basin (China) with Time Series InSAR Technology Remote Sens. 2016, *8*(4), 284.

Daniele Perissin Zhiying Wang Teng Wang, the SARPROZ InSAR tool for urban subsidence/manmade structure stability monitoring in China.

Davide Colombo, Tele-Rilevamento Europa TRE 2013, Measuring deformation from space. InSAR as an operational tool for mining sector.

Daniele Perissin and Teng Wang 2011 Time-Series InSAR Applications over Urban Areas in China. Zheyuan Du, Linlin Ge , Xiaojing Li and Alex Hay-Man Ng 2016 Subsidence Monitoring over the Southern Coalfield,Australia Using both L-Band and C-Band SAR Time Series Analysis.

Daniel Raucoules Parchiaridis I Denis Feurer Novalli FDeformation monitoring of the greater area of Thessaloniki (Northern Greece) using DInSAR techniques. Natural hazards and earth system sciences 8(4):779.

David U. Hooper, E. Carol Adair Andrew Gonzalez J. Emmett Duffy 2012 a global synthesis reveals biodiversity loss as a major driver of ecosystem change.

Davis P.M (1986)surface deformation due to inflation of an arbitrarily oriented triaxle ellipsoidal cavity in an elastic half space with reference to Kilauea volcano Hawaii, journal of geophysical research solid earth 91(B7),7429-7438.

Desmore J.,K. Ellett ,J.Howle ,M. Carpenter and M.Sneed(2010) Measuring land surface deformation on Bicycle Lake playa, Fort Irwin, California, USA .paper presented at land subsidence association.

Duncan E. E .J .S., Kuma and G .Avane(2010), surface deformation monitoring in the goldfields Ghana limited area, the electronic journal on information system in developing countries; 42(6),1-7

Duro J., D. Albiol, O. Mora, and B.Payas(2013), Application of advanced InSAR techniques for the measurement of vertical and horizontal ground motion in long wall mining, paper presented at coal operators conference.

Deodato Tapete Stefano Morelli, Riccardo Fanti Nicola Casagl 2015, Localising deformation along the elevation of linear structures: An experiment with space-borne InSAR and RTK GPS on the Roman Aqueducts in Rome, Italy.

Devin L. Galloway & Thomas J. 2011 Burbey Regional land subsidence accompanying groundwater extraction subsidence from Groundwater Use in California.

D. Roque E. Simonetto A.P. Falcão D. Perissin F. Durand L. Morel A.M. FonsecaL. Polidori 2016, AN ANALYSIS OF DISPLACEMENT MEASUREMENTS FOR LISBON, PORTUGAL, USING COMBINED INSAR AND GNSS DATA.

Dora ROQUE Daniele PERISSIN Ana Paula FALCÃO Rui GOMES António José ROQUE Ana Maria FONSECA 2016, Displacement Measurement Using SAR Interferometry An Application to the Lisbon Regional Outer Circular and Its Neighbourhood.

Estelle Chaussard , Shimon Wdowinski , Enrique Cabral-Cano , Falk Amelung 2014, Land subsidence in central Mexico detected by ALOS InSAR time-series.

Elliott 2009 Ecology of Marin Sediment: From Science to Manegment.

Fatma Canaslan Çomut Aydın Ustun Milan Lazecky Daniele Perissin 2016, Capability of detecting rapid subsidence with COSMO SKYMED and SENTINEL-1 dataset over konya city.

Farr et al., 2007 , The Shuttle Radar Topography Mission.

Francesca Cigna, Batuhan Osmanoğlu 1, Enrique Cabral-Cano, Timothy H. Dixon ,Jorge Alejandro Ávila-Olivera , Víctor Hugo Garduño-Monroy , Charles DeMets , Shimon Wdowinski,

Francesca Bozzano Carlo Esposito Stefania Franchi Paolo Mazzanti Daniele Perissin Alfredo Rocca Emanuele Romano 2015, Understanding the subsidence process of a quaternary plain by combining geological and hydrogeological modelling with satellite InSAR data: The Acque Albule Plain case study.

G.V Chilingar 1997 gas migration events preceding earthquakes.

Is. Parcharidis1, E. Lagios, V. Sakkas, D. Raucoules, D. Feurer, S. Le Mouelic, C. King, C. Carnec,F. Novali, A. Ferretti, R. Capes, and G. Cooksley, 2006 Subsidencemonitoring within the Athens Basin (Greece) using space radar interferometric techniques.

Ian JOUGHIN,Ben E. SMITH,Waleed ABDALATI 2010 Glaciological advances made with interferometric synthetic aperture radar.

James W. Borchers Michael Carpenter April 2014, Land Subsidence from ground water in California.

Joaquim J. M. de Sousa Milan Lazecky Ivana Hlavacova Matus Bakon Gloria Patricio and Daniele Perissin 2015**,** Satellite SAR interferometry for monitoring DAM deformation in Portugal.

Kui Yang, Li Yan, Guoman Huang, Chu Chen and Zhengpeng Wu 2016, Monitoring Building Deformation with InSAR:Experiments and Validation.

Jonathan C. L. Normand and Essam Heggy 2015 , InSAR Assessment of Surface Deformations in Urban Coastal Terrains Associated With Groundwater Dynamics.

John Mitchell , Jim Plume , Mark Tait, Peter Scuderi, Wayne Eastley 2012 National building information modelling imitative.

Le toan, T., et al.(2001), the biomass mission: mapping global forest biomass to better understand the terrestrial carbon cycle , remote sensing of environment, 115(11), 2850-2860.

Lillesand, T.M.,R.W.Kiefer, and J.W.Chipman(2008), remote sensing and image interpretation.

Lu, Zhong 2007 InSAR imaging of volcanic deformation over cloud-prone areas - Aleutian Islands.

Lu,N and W.J.Likos (2004),unsaturated soil mechanics,584pp, Wiley, Hoboken,NJ,USA.

Massonnet, D. & Feigl, K. L. Radar interferometry and its application to changes in the Earth's surface. Rev. Geophys. 36, 441-500

Matus bakon, juraj papco, daniele perissin, Joaquim j.sousa, milan lazecky October 5-7, 2016...Multi-sensor INSAR deformation monitoring over urban area of Bratislava (slovakia).

Maryam Dehghani, Mohammad Javad Valadan Zoej, Iman Entezam, Ali Mansourian and Sassan Saatchi, 2009 InSAR monitoring of progressive land subsidence in Neyshabour, northeast Iran.

M. Crosetto B. Crippa , E. Biescas O. Monserrat M. Agudo State of the art of land deformation monitoring using differential SAR interferometry.

M. Hosseini, M. J. Valadan Zoej , M.R. Mobasheri , M.Dehghani 2007 Land Subsidence Monitoring Using InSAR and GPS.

Minxue Zheng 1, Kaoru Fukuyama 1 and Kazadi Sanga-Ngoie, 2014 Application of InSAR and GIS Techniques to Ground Subsidence Assessment in the Nobi Plain, Central Japan.

Mohammad Ali Goudarzi 2010, Detection and measurement of land deformations caused by seismic events using InSAR, Sub-pixel correlation, and Inversion techniques.

Negin Fouladi Moghaddam, 2015 Investigation of the Subsurface Structural Behaviour in the Surat Basin using SAR Interferometry Deformation Maps.

Neeff, T., L.V. Dutra ,J.R. dos santos, C. d C. Freitas and L.S. Araujo(2005), T ropical forest measurement by interferometric height modeling and p-Band radar backscatter, forest science 51(6),585-594.

Ning Lu, ; and William J. Likos, 2006 Journal of Geotechnical and Geoenvironmental Engineering/Volume 132 Issue 2 - February 2006 Suction Stress Characteristic Curve for Unsaturated Soil.

Parcharidis et al. 2006; Raucoules et al. 2008, Subsidence in the Athens basin monitored by INSAR.

Perski, Z., R Hanssen,A.Wojicik, and T. Wojciechowski (2009), InSAR tool for terrain deformation near the Wileliczka salt mine,Poland, engineering geology,106(1-2),58-67.

P mazzant D perissin A.Rocca Structural Health Monitoring of Dams by Advanced Satellite SAR Interferometry: Investigation of Past Processes and Future Monitoring.

Pietro Milillo1, Roland Bürgmann2, Paul Lundgren1, Jacqueline Salzer3, Daniele Perissin4, Eric Fielding1, Filippo Biondi5 & Giovanni Milillo 2016 Space geodetic monitoring of engineered structures: The ongoing destabilization of the Mosul dam, Iraq.

Prats Iraola et al. 2015 Matteo Nannini Francesco De Zan Rolf ScheiberSentinel-1 Assessment of the Interferometric Wide-Swath Mode.

Qingli Luo, Daniele Perissin, Hui Lin, Yuanzhi Zhang, and Wei Wang 2013, Subsidence Monitoring of Tianjin Suburbs by TerraSAR-X Persistent Scatterers Interferometry.

Riadh ABDELFATTAH InSAR phase analysis: Phase unwrapping for noisy SAR interferograms.

Riccardo Lanari Paul Lundgren Mariarosaria Manzo Francesco CasuSatellite radar interferometry time series analysis of surface deformation for Los Angeles, California Geophysical Research Letters 31(23)

R S Chatterjee Shailaja Thapa K B Singh G Varunakumar and E V R Raju 2015 , Detecting, mapping and monitoring of land subsidence in Jharia Coalfield, Jharkhand, India by spaceborn edifferential interferometric SAR, GPS and precision levelling techniques.

R. Tomás, M. Cano, J. García-Barba, F. Vicente, G. Herrera, J. M. Lopez-Sanchez,J.J. Mallorquí 2013Monitoring an earthfill dam using differential SAR interferometry: La Pedrera dam, Alicante, Spain.

S. Erol B. Erol T. Ayan A General review of the deformation monitoring techniques and a case study: analyzing deformations using GPS/LEVELLING.

Silvia Bianchini Fabio Pratesi Teresa Nolesini and Nicola Casagli 2015, Building Deformation Assessment by Means of Persistent Scatterer Interferometry Analysis on a Landslide-Affected Area The Volterra (Italy) Case Study.

Shirvany, R.(2012), estimation of degree of polarization in polarimetric SAR imagery: principles and Applications, 116pp,

Stephen A. Nelson Sep 2015 deformation of rock.

Tsegaye Mekuria 2006, A multi-criteria analysis for solid waste disposal site selection using Remote sensing and GIS.

Teiloni E (2006) ground surface settlement due to underground works in geodetic deformation monitoring from geophysical to engineering role , edited by k.sanso and A .Gril pp 285-292 springer berlin Heidelberg.

Tianjin InSAR Land Subsidence Observation" Demonstration project Siddhartha bhaumick, 2013 land subsidence modeling by advanced D- insar techniques.

Timo Balz Lianhuan Wei Michael Jendryke Daniele Perissin Mingsheng Liao 2012 TomoSAR and PS-INSAR analysis of high-rise building in Berlin.

World bank 2015, Addis Ababa, Ethiopia Enhancing Urban Resilience.

Yongqi CHEN, Guobao ZHANG, Xiaoli DING and Zhilin LI Monitoring Earth Surface Deformations with InSAR Technology: Principle and Some critical Issues.

Zegeye Cherenet, Helawi Sewnet 2012 Building Ethiopia: Sustainability and Innovation in Architecture and Design.

Zhou, Zhiwei (2013). The applications of InSAR time series analysis for monitoring long-term surface change in peatlands.

Zheyuan Du, Linlin Ge , Xiaojing Li and Alex Hay-Man Ng 2016 Subsidence Monitoring over the Southern Coalfield,Australia Using both L-Band and C-Band SAR Time Series Analysis.